LULEÅ UNIVERSITY OF TECHNOLOGY

DOCTORAL THESIS

Laser Welding

Energy Redistribution and Weld Geometry

CONNY LAMPA

Department of Materials and Manufacturing Engineering
Division of Materials Processing

1997:33 • ISSN: 1402 - 1544 • ISRN: LTU - DT - - 1997:33 - - SE

Laser Welding; Energy Redistribution and Weld Geometry

av

Conny Lampa

Akademisk avhandling

som med vederbörligt tillstånd av Tekniska Fakultetsnämnden vid Luleå tekniska universitet för avläggande av teknologie doktorsexamen kommer att offentligt försvaras i Luleå tekniska universitetets sal E 246, fredagen den 16 januari 1998 kl 10.00.

Handledare: Professor Claes Magnusson.

Fakultetsopponent: Dr. William O'Neill, Department of Industrial Studies, University of Liverpool, England.

1997:33

Laser Welding

Energy Redistribution and Weld Geometry

CONNY LAMPA

Department of Materials and Manufacturing Engineering
Division of Materials Processing

1997:33 • ISSN: 1402 - 1544 • ISRN: LTU - DT - - 1997:33 - - SE

Everything should be made as simple as possible, but not simpler

Albert Einstein

This thesis is dedicated
to my parents

Alvar and Birgitta

PREFACE

Since December 1992 I have had the pleasure of conducting experimental and theoretical research in the field of high power laser welding at the Department of Materials and Manufacturing Engineering, Luleå University of Technology. This thesis is the result of investigations into the nature of the deep penetration CO_2 laser welding process with emphasis on the weld shape and energy redistribution.

Several people have been important in completion of this work. I sincerely thank my supervisor Professor Claes Magnusson for his constant support and encouragement during this work, Dr. John Powell from whom I have received invaluable guidance, Dr. Anders Ivarson for support and advice and Dr. Alexander Kaplan for inspiring discussions and support during my stay in Vienna. I also want to thank all my colleagues and friends, especially at the Department of Materials and Manufacturing Engineering, for helping me and creating an excellent working atmosphere.

Luleå, November 1997

Conny Lampa

ABSTRACT

Over the past few years laser welding has developed into a process which has a wide range of application over a number of industries. Industrial growth in this area has been stimulated by improvements in production rates and quality but technologically the process is still not fully understood. This work aims to contribute to the understanding of deep penetration laser welding with emphasis on energy redistribution and weld geometry.

The seven papers which make up the thesis investigate various aspects of the absorption and redistribution of energy during laser welding. Theoretical and experimental methods have been used to analyse the effects of process parameters on the geometry of the resultant welds. Considerable success has been achieved in matching theoretical predictions to actual results.

This work has helped to clarify a number of features of the laser welding process including the following;

1. The effect of process parameters on the efficiency of laser welding.
2. The mechanisms of energy absorption which result in a weld.
3. The effect of an increased external pressure on the laser-material interaction.
4. The effect of thermocapillary flow and how it can be taken advantage of in industrial applications.

Keywords: laser, welding, efficiency, hyperbaric, point-source, line-source, thermocapillary, Marangoni, flow, steel, copper.

LIST OF PAPERS

This dissertation consists of the following seven papers:

I. Lampa, C., Powell, J., Ivarson, A. and Magnusson, C. (1995) Factors Affecting the Efficiency of Laser Welding. Lasers in Engineering (4). pp. 73-83.

II. Lampa, C., Powell, J., Ivarson, A., Runnemalm, H. and Magnusson, C. (1996) The Influence of Gap Width on Laser Welding. Proceedings of the Laser Materials Processing Conference, ICALEO'95. Nov. 13-16 1995, San Diego CA, USA. pp. 504-512.

III. Ducharme, R., Kapadia, P., Lampa, C., Ivarson, A., Powell, J. and Magnusson, C. (1996) A Point and Line Source Analysis of the Laser Material Interaction in Hyperbaric Keyhole Laser Welding. Proceedings of the Laser Materials Processing Conference, ICALEO'95. Nov. 13-16 1995, San Diego CA, USA. pp. 1018-1027.

IV. Ducharme, R., Kapadia, P., Lampa, C., Ivarson, A., Powell, J. and Magnusson, C. (1997) Effects of Different Shielding Gas Composition on the Process of CW CO_2 Laser Welding in the Hyperbaric Range. SPIE Proceedings of the XI International Symposium on Gas Flow and Chemical Lasers and High-Power Laser Conference, GCL/HPL'96. Aug. 25-30 1996, Edinburgh, UK. pp 530-533.

V. Lampa, C., Kaplan, A.F.H., Powell, J. and Magnusson, C. (1997) An analytical thermodynamic model of laser welding. Journal of Physics D: Applied Physics (30). pp. 1293-1299.

VI. Lampa, C., Powell, J. and Magnusson, C. Laser Welding of Copper to Stainless Steel. Presented at the Laser Material Processing Conference, ICALEO'97. Nov. 17-20 1997, San Diego CA, USA. Submitted for publication.

VII. Lampa, C., Kaplan, A.F.H., Powell, J. and Magnusson, C. The Effect of Process Speed on Energy Redistribution in Deep Penetration CO_2 Laser Welding. Submitted for publication in Journal of Lasers Applications.

CONTENTS

Introduction

INTRODUCTION

This thesis is the result of experimental and theoretical research into the nature of the deep penetration CO_2 laser welding process with emphasis on the weld shape. The main body of the work is divided up into seven papers which follow this introduction. The introduction itself is divided into the following parts:

- General notes
- Laser welding mechanisms
- Executive summary of the appended papers

General notes

Over the last decade the technique of laser welding has become a widely accepted joining method which offers manufacturing possibilities hitherto difficult or impossible by other joining methods. The growth of laser welding as an industrial tool has been accelerated because of its advantages compared to other, conventional joining techniques. Some of these advantages include:

- Low thermal distortion of the workpiece due to low heat input.
- Deep and narrow welds can be produced with high metallurgical quality (General rule: 1 kW of laser power at a welding speed of 1 m/min gives approximately 1.5 mm penetration in steels).
- The heat affected zone is narrow which reduces metallurgical damage and also allows welds to be made close to heat sensitive components.
- High welding speeds can be accomplished, up to several meters per minute.
- It is a flexible process: One laser can be shared by several workstations performing laser welding as well as other processes such as cutting and heat treatment.

- Laser welding is suited to automation and can also operate in conjunction with robots.

- Most applications do not require filler materials or other welding consumables other than shielding gases.

- Post-weld treatment is not normally required.

- Welds can be performed in difficult geometries and where access is limited.

- Complex joint configurations and dissimilar material thickness can be welded.

It is important to note that despite these positive points laser welding does not supersede other welding techniques but serves as a complement in applications which can take advantage of the above mentioned opportunities. One example of an area where laser welding is of great interest is the automotive industry. General Motors, Volvo and BMW are companies which utilise laser welding in their production lines, for example the new 5-series of BMW has approximately 11 metres of laser weld on each car body [1].

Laser welding mechanisms

Laser welding is a fusion welding process, i.e. material is joined by melting. In this section the laser welding mechanisms will be described in simple terms. For the purpose of this discussion the laser itself can be simply considered to be a heating device.

Laser welding can be carried out by one of two mechanisms [2].

(i) Conduction limited welding, where the laser acts like a point source of energy moving across the surface of the sheet. Welds formed by this process are roughly semi-circular in cross section.

(ii) Keyhole welding, where the laser acts as a line source of energy penetrating into the body of the material. This line source travels across the sheet producing welds which are narrow and deep.

Conduction limited welding

The principle of conduction limited welding is simple. The laser beam irradiates the material surface and heat is conducted radially away from the laser-material interaction zone. The molten pool thus established has a semi-circular type cross section as shown in figure 1. The depth to width ratio of welds of this sort gives them a higher tolerance to poor fit up than keyhole type welds. As a joining process however, conduction limited welding is far less efficient than keyhole welding in terms of energy consumed per unit area of join.

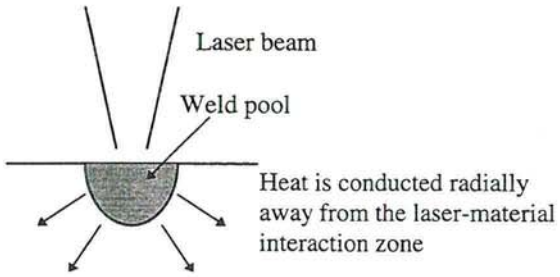

Figure 1. Conduction limited welding.

Deep penetration keyhole welding

When deep penetration welds are produced the laser acts as a line source of energy throughout the depth of the material rather than a point source acting from the top surface only. This line source welding mechanism is made possible by the generation of a *keyhole* which penetrates into the material. The keyhole takes the form of a narrow, deep, vapour filled cavity surrounded by molten metal. As this zone is traversed across a metal sheet the liquid metal flows around the cavity and solidifies behind it. The keyhole is produced only at high power densities ($\geq 10^6$ W cm^{-2}) by the following mechanism: Initially a conduction limited weld pool similar to that shown in figure 1 is produced. At high power densities a dimple is formed in the centre of this melt pool as a result of vaporisation of the melt and thermocapillary or Marangoni stirring. This stirring action is driven by surface tension gradients in the melt which result from the severe thermal gradients (the melt is boiling in the centre and only just melting at the edges which are only a millimetre or so away).

The stirring action drives liquid away from the centre of the melt and thus a centre dimple is formed, see figure 2a. The dimple absorbs the incident beam more efficiently than the previously undimpled melt surface. This increased absorption results in more central boiling and accelerated Marangoni flow both of which act to deepen the central dimple until a keyhole is formed, see figure 2b. The superheated, partially ionised vapour which fills and covers the keyhole is called a plasma and, as we shall see, it has an important part to play in how the laser energy is transferred to the workpiece.

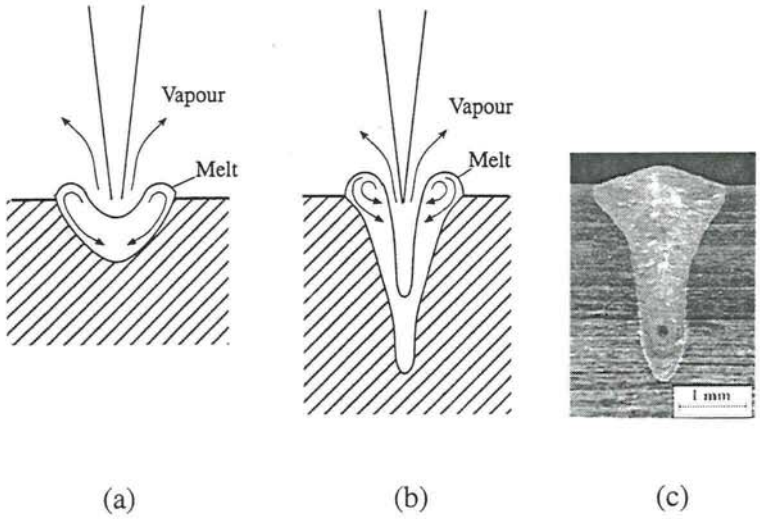

Figure 2. The creation of a keyhole. (a) At high power densities vaporisation and thermocapillary stirring act together to create a dimple in the centre of the melt. (b) The dimple absorbs the laser energy more effectively and deepens to create a keyhole. (c) A typical micrograph of a keyhole weld.

Power absorption in deep penetration keyhole welding

The plasma associated with the keyhole absorbs a proportion of the laser light. The light which is absorbed by the plasma cloud above the keyhole is re-radiated in all directions and only a portion of it reaches the workpiece surface. Energy which is absorbed by the plasma inside the keyhole is eventually re-radiated and conducted onto the keyhole sides and assists the melting process. The majority of the laser energy is absorbed directly by the walls of the keyhole as a result of Fresnel absorption [3].

Fresnel absorption always involves a certain amount of reflection of the incident laser beam. The reflected beam continues to propagate into the keyhole by multiple reflections at the keyhole wall (see figure 3). During each reflection of the laser beam, laser power is partly absorbed by the keyhole wall and partly by the keyhole plasma. The remaining laser power which is not absorbed by the plasma or by Fresnel absorption is reflected out of the keyhole and is lost to the welding process.

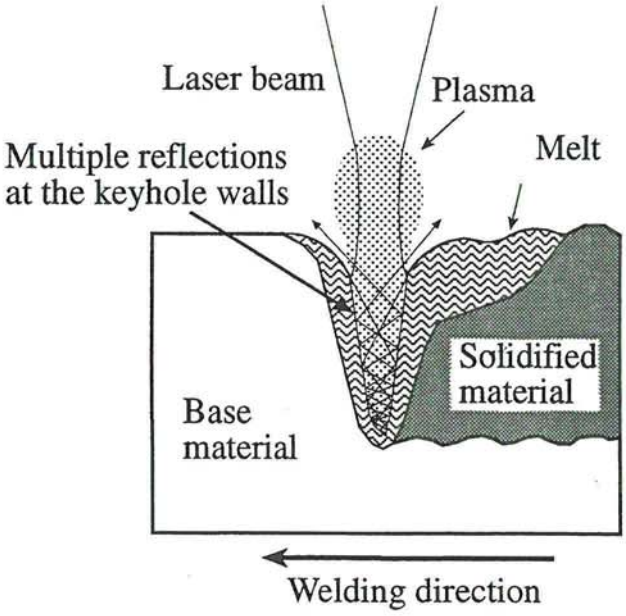

Figure 3. Schematic of the deep penetration laser welding process.

The Fresnel absorption coefficient is dependent on the angle between the incoming laser light and the keyhole wall [3], see figure 4 for steel.

Light passing through the plasma in the keyhole is absorbed as a result of the inverse Bremsstrahlung mechanism (i.e. photons are absorbed by electrons) which is significant at laser wavelengths greater than 5 μm [4] (CO_2 lasers radiate at 10.6 μm). The absorption can be described by Beer-Lambert's law [5]:

$$P_a = P_0(1-\exp(-\alpha_{iB}z)) \tag{1}$$

where P_a is the laser power (W) absorbed when passing through a path length z (m), P_0 is the incident laser power and α_{iB} is the plasma absorption coefficient due to inverse Bremsstrahlung (m^{-1}).

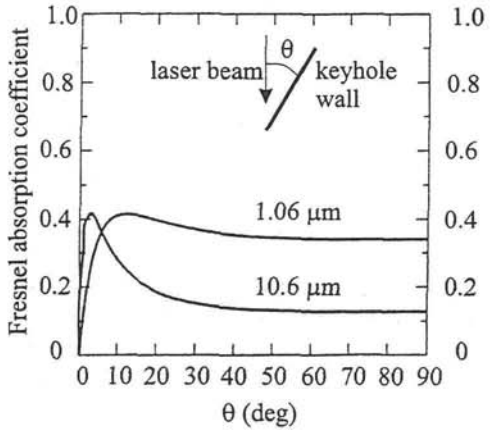

Figure 4. Fresnel absorption as a function of the angle of the keyhole wall. Circular polarised laser light of 10.6 μm and 1.06 μm wavelength. Material: steel [4].

The temperature dependence of the plasma absorption is shown in figure 5 [6] for various mixtures of iron plasma and the helium shielding gas. For pure iron plasma there is a maximum peak in absorption around 13 000 K which is explained by the following: The laser light interacts mainly with free electrons and the absorption coefficient increases with temperature because of the increased degree of ionisation. However at increasing temperatures, reaching the level of almost complete first ionisation, the overall density of the plasma decreases more rapidly than the electron density increases. Inert gases such as helium reduce the level of ionisation and resultant absorption because they have a high ionisation energy.

The temperature field inside the keyhole has been calculated by Kaplan [4] and shown to experience high temperature gradients. This lead to large variations in local plasma absorption coefficients. The temperature near the keyhole wall is too low to give any detectable absorption. The central zone of the keyhole also has a low absorption coefficient, in this case because of the high temperature and related low overall plasma density. In between these two zones there is a relatively thin layer with a high absorption coefficient. It has been shown [7] that in the keyhole the absorption reaches values in the range of 50-200 m^{-1} for steels interacting with CO_2 laser light with an average value of the order of $100m^{-1}$.

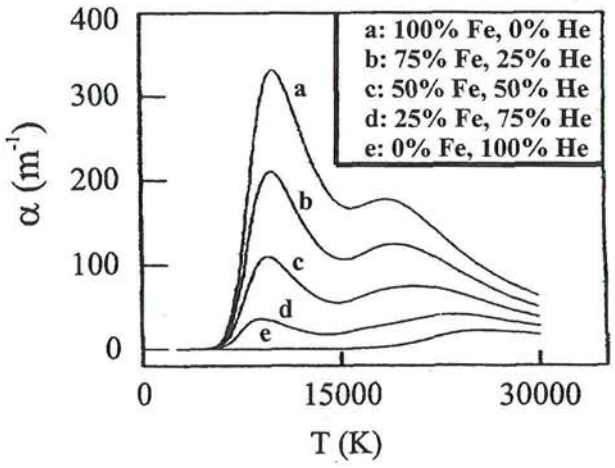

Figure 5. Plasma absorption coefficient as a function of temperature for different iron-helium plasma mixtures: a) 100% Fe, 0 % He, b) 75% Fe, 25% He, c) 50% Fe, 50% He, d) 25% Fe, 75% He, e) 0% Fe, 100% He [6].

The moving point and line source

The concept of using moving point and moving line sources of power in welding applications was first derived by Rosenthal [8]. The moving point source relates to cases when a power source which is approximated as a point moves with constant velocity over the surface of a thick plate. The moving line source on the other hand, assumes that the power is distributed uniformly along a line in the depth direction of a thin plate.

The concept of using the moving line source in modelling the power distribution to the workpiece via a keyhole was successfully used by Swift-Hook and Gick [9]. This model however only describes a parallel sided liquid region and not the widening at the top of the weld pool which is typical for deep penetration laser welding (see figure 2c). Steen et.al. [10] used the combination of a moving line source and moving point source in order to describe this top part of the weld region. A schematic of the combined point and line source model is shown in figure 6.

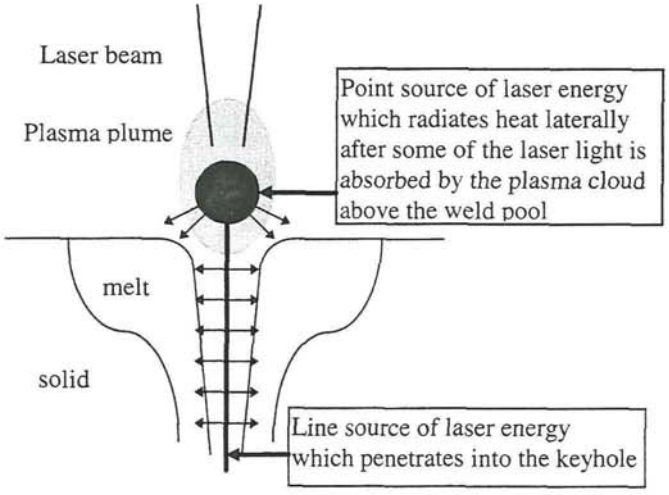

Figure 6. A schematic demonstrating the combined point and line source model of laser welding.

This model is used in *Paper III* and *Paper IV* for the analysis of laser welding at pressures greater than atmospheric. The concept of combining the moving line and point sources gives simple and useful analytical solutions concerning the weld pool shapes. There are however some restrictions to it as the shape of the weld pool is not entirely parallel sided. Kaplan [7] successfully developed a model where the line source strength varied in magnitude with the depth of penetration in order to predict the actual shape of the weld.

Thermocapillary flow in deep penetration laser welding

The concept of using a point source in calculating the geometry of the top part of the weld is useful but does not give a physical explanation of the broadening of the weld pool. This broadening is actually the result of thermocapillary stirring (figure 7).

The driving forces for thermocapillary flow in weld pools can be described by three phenomena [11]:

(i) Surface tension force

(ii) Buoyancy force

(iii) Electromagnetic force

In laser welding however, the electromagnetic force can be neglected due to the fact that no electrical current is used.

Surface tension forces

In general the surface tension of a melt decreases with temperature. In the case of laser welding this means that the surface tension will be at a maximum at the edges of the weld pool and a minimum in the centre. This surface tension gradient creates a stirring action which acts outwards from the centre of the weld pool (In certain cases this flow pattern can be reversed by surface active agents such as sulphur or oxygen in steel [12]).

Buoyancy forces

The density of liquid metals decreases with temperature. Thus the hotter melt towards the centre of the weld pool will tend to rise whilst the cooler material at the edges will tend to sink. This action reinforces the surface tension stirring effect.

The convection stirring induced by these two forces increases the lateral thermal transport in the melt pool. This tends to widen the top of the weld profile to give it its distinctive shape (see figure 2c). In *Paper V* this broadening of the top of the weld pool is accommodated by introducing an enhanced thermal conductivity towards the top of the weld pool.

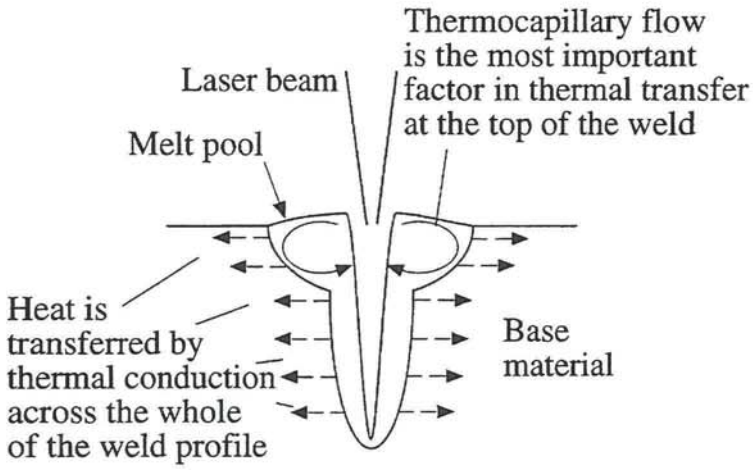

Figure 7. Thermocapillary or Marangoni flow which generates a vigorous stirring action in the melt.

Executive summary of the appended papers

In this section the papers which make up the remainder of the thesis are summarised. The seven papers are:

Paper I: Factors Affecting the Efficiency of Laser Welding.

Paper II: The Influence of Gap Width on Laser Welding.

Paper III: A Point and Line Source Analysis of the Laser Material Interaction in Hyperbaric Keyhole Laser Welding.

Paper IV: Effects of Different Shielding Gas Composition on the Process of CW CO_2 Laser Welding in the Hyperbaric Range.

Paper V: An Analytical Thermodynamic Model of Laser Welding.

Paper VI: Laser Welding of Copper to Stainless Steel.

Paper VII: The Effect of Process Speed on Energy Redistribution in Deep Penetration CO_2 Laser Welding.

The absorbed power in the workpiece as a function of welding speed is experimentally defined in *Paper I*. The efficiency expressed as a function of the joining rate is shown to rise with increasing welding speed. In *Paper II* an inter-workpiece gap was introduced. In order to reduce the sensitivity for weld drop out, geometrical modifications of the weld zone are suggested. *Paper III* and *Paper IV* deal with hyperbaric laser welding (welding at pressures above atmospheric). The experimental results are explained by using a point and line source approach for the energy transport. In *Paper V* the point source is substituted by an enhanced thermal conductivity to account for the weld top broadening caused by thermocapillary stirring. The thermocapillary stirring can be taken advantage of in applications where lateral thermal transport is important in the production of a weld. This is demonstrated in *Paper VI* where stainless steel is welded to copper. *Paper VII* explains the different absorption and loss mechanisms in deep penetration laser welding and how they change in nature with welding speed.

Paper I: Factors Affecting the Efficiency of Laser Welding.

This paper examines the factors which affect the efficiency of laser welding using theoretical and experimental results. The redistribution of power which takes place during the welding process is investigated and the proportion of the original laser output power which contributes to the welding process identified. The change of weld cross section geometry as a function of welding speed is discussed and an increase of welding efficiency has been found as the weld speed increases.

Conclusions

The results of this experimental program demonstrated that during laser welding the laser output power was divided into three approximately equal parts:

1. Power used in melting.
2. Power absorbed by the workpiece but not used in melting.
3. Power which either never reached the workpiece or left it after interaction.

The proportion of the power involved in the melting process increased with welding speed and, more importantly, the aspect ratio of the weld cross section changed to give much higher joining rates. This rise in welding efficiency with increasing processing speed is the result of a reduction in lateral convective stirring in the melt. This reduction in stirring is made possible because, at higher speeds, the melt has a shorter lifetime in any one place along the weld line.

In most cases of real welding applications the depth of penetration is fixed and the process parameters are altered accordingly. The three most important process parameters are:

1. The lens or mirror focal length.
2. The laser power.
3. The welding speed.

From the point of view of process efficiency it is clear from our earlier discussion that the process speed should be set at the maximum possible value. This will generally entail the use of maximum laser power. This combination will give the greatest joining rate and narrowest welds at the maximum welding efficiency.

***Paper II*: The Influence of Gap Width on Laser Welding.**

This paper investigates the effects that inter-workpiece gaps can have on the laser welding process. The work demonstrates theoretically and experimentally that the process can accommodate and may even be improved by small gaps. As the gap reaches a limiting value however, the welding mechanism collapses. Larger gaps can be accommodated if the geometry of the cut edges is suitably altered.

Conclusions

1. Very small gaps (less than 0.1 mm) can result in welds with flatter profiles than can be achieved when producing bead on plate welds. This may have positive effects on the fatigue life of welded components.
2. As the gap increase in size, the amount of laser light leaving the bottom of the weld zone increases in an exponential manner.
3. As the gap reaches a critical size, the available melt cannot bridge it and the welding process collapses.
4. The geometry of the laser-material interaction zone can be modified to improve the gap sensitivity of the process.

***Paper III*: A Point and Line Source Analysis of the Laser Material Interaction in Hyperbaric Keyhole Laser Welding.**

Summary

This paper presents the results of a theoretical and experimental research program investigating laser welding at pressures above atmospheric. Experimentally it was discovered that the welding mechanism rapidly collapsed in pressures in excess of atmospheric if argon or nitrogen were used as the shield gas. In the case of helium however the depth of penetration of the welds decreased gradually as the pressure was increased from 0.1 to 0.8 MPa.

A theoretical model using a combination point and line source of energy was used to examine the welding interaction. The point source of energy represented the laser absorption in the plasma plume above the keyhole. The line source represented the absorption of energy in the keyhole.

Experimental and theoretical results both agreed that as the pressure of the helium increased the point source grew in magnitude and the line source diminished which explains the gradual reduction in weld penetration depth.

Paper IV: Effects of Different Shielding Gas Composition on the Process of CW CO_2 Laser Welding in the Hyperbaric Range.

Summary

This paper presents the results of an investigation of laser welding with different shield gas mixtures at pressures above atmospheric. Earlier work (*Paper III*) identified trends in weld pool geometry using helium at hyperbaric pressures and showed that the deep penetration welding process was not possible at these pressures when using argon or nitrogen as the shield gas.

The present work concentrated on the effect of using mixtures of helium and argon. Once again a combined line and point source energy transfer model was employed to analyse the results. The charge in proportion of the line and point sources was calculated for different atmospheres and pressures and this gave a close agreement with the experimental results. The effect of changing the F-number of the welding optics was also analysed.

***Paper V*: An Analytical Thermodynamic Model of Laser Welding.**

An earlier model of deep-penetration laser welding has been simplified in order to provide a useful model of process analysis. This work involves the modelling of the various energy-absorption mechanisms which determine the keyhole shape and thus the dimensions of the melt pool. The penetration depth and weld width (top and bottom) predicted by the model are shown to be in close agreement with experimental results. The widening of the top of the weld seam as a result of Marangoni flow is accurately modelled by introducing an artificially enhanced value for the workpiece's thermal conductivity towards the top of the weld. The model allows analysis of the dependence of the weld profile on the process parameters.

Conclusions

A simplified version of an earlier model [1] can predict weld-bead dimensions with an accuracy of greater than 90 %. The width of the bottom of the weld (w_b) is calculated using standard values for the workpiece conductivity, λ_1. The width of the top of the weld (w_t), which is widened by thermocapillary flow, is calculated using an artificially high value for the thermal conductivity, λ_2. A suitable relationship between the two conductivities is $\lambda_2 = 2.5\ \lambda_1$. The penetration depth (d) is calculated by dividing the total power absorbed in the keyhole by the average line-source strength of the incident laser beam.

***Paper VI*: Laser Welding of Copper to Stainless Steel.**

This paper investigates the possibility of CO_2 laser welding austenitic stainless steel to copper. The experimental results show that solidification cracking may be the greatest problem in this application. It is suggested that the cracks are generated in three ways:

- Liquid metal embrittlement, due to the presence of copper in the solidifying steel grain boundaries.
- Stresses generated during solidification due to fixturing and differences in the thermal properties of the materials involved.
- A solidification mode change due to the rapid weld solidification involved in laser welding of austenitic stainless steel.

To overcome these problems the fixturing and specimen edge preparation have to be optimised to minimise the amount of copper in the fusion zone, to reduce the stresses, and to minimise the cooling rate during solidification. These factors were taken into account and the resulting welds were of high integrity with the same strength as the original copper being welded. The role of thermocapillary or Marangoni flow in transferring heat to the copper side of the weld is also discussed.

Conclusions

1) Laser welding copper to stainless steel components is technically and commercially feasible.
2) Laser-interface misalignment must be optimised to produce a complete weld without excessive dilution of the melt with copper.
3) Thermocapillary or Marangoni flow is responsible for the lateral spread of the stainless steel melt and the eventual contact melting of the copper.
4) Argon is the preferred weld shroud gas. Helium does not ionise sufficiently in the plasma above the weld and hence aids the production of a narrow weld with insufficient Marangoni flow. Nitrogen may increase the susceptibility to solidification cracking in laser welding of austenitic stainless steels as it suppresses the formation of delta ferrite.

***Paper VII*: The Effect of Process Speed on Energy Redistribution in Deep Penetration CO_2 Laser Welding.**

This work discusses energy absorption mechanisms in CO_2 laser welding and how they are affected by changes in the process speed. Two main energy absorption processes govern the welding interaction:

i) Fresnel absorption at the keyhole walls.

ii) Absorption by the partially ionised metal vapour (or plasma) in the keyhole (laser energy absorbed in this way is re-radiated or conducted to the keyhole walls).

A theoretical model of these absorption mechanisms has been developed and shown to agree closely with experimental results. Fresnel absorption has been identified as being dominant over plasma absorption and becomes even more influential as welding speeds are increased.

Conclusions

i) Fresnel absorption at the walls of the keyhole is the dominant energy transfer mechanism in laser welding. Energy absorption by this method is optimised when the keyhole walls are close to the Brewster angle with respect to the incident beam. As speeds increase the keyhole wall will become more inclined and absorption will be reduced.

ii) Plasma absorption plays a more minor role which diminishes in importance as welding speeds are increased.

iii) An increasing amount of incident power is lost to the welding process as speeds are increased. Although plasma plume absorption decreases with speed this is more than compensated for by increases in workpiece surface and keyhole reflection effects.

References

1. Larsson, J.K. (1997) Automotive Laser World - The Use of Lasers in Car Body Manufacturing. Proceedings of the 6th Nordic Laser Materials Processing Conference, NOLAMP 6. Aug. 27-29, 1997, Luleå, Sweden. pp. 76-94.
2. Lampa, C., Sarady, I., Powell, J., Mattson, J. and Magnusson, C. (1993) Laser Welding of Dissimilar Metals. Conf. Proc. of 4th Conf on Laser Materials Processing in the Nordic Countries, NOLAMP 4. Aug. 16-18, 1993, Sønderborg, Denmark. pp. 215-224.
3. Beyer, E. (1995) Scweißen mit Laser (Berlin: Springer).
4. Kaplan, A. (1994) Modellrechnung und numerische Simulation von Absorption, Wärmeleitung und Strömung des Laser-Tiefschweißens. Dissertation, Technical University of Vienna, Austria.
5. Steen, W.M. (1991) Laser Materials Processing (Berlin: Springer).
6. Beck, M., Kern, M., Berger, P. and Hügel, H. (1996) Einfluß der Plasmawolke auf Einkopplung und Prozeßstabilität beim Lasertiefschweißen mit CO_2-Lasern. Laser und Optoelektronik (28). pp. 72-78.
7. Kaplan, A. (1994) A model of deep penetration laser welding based on calculation of the keyhole profile. Journal of Physics D: Applied Physics (27). pp. 1805-1814.
8. Rosenthal, D. (1941) Mathematical Theory of Heat Distribution During Cutting and Welding. Welding Journal (20). pp. 220s-234s.
9. Swift-Hook, D.T and Gick, A.E.F. (1973) Penetration Welding with Lasers. Welding Journal (52). pp. 492s-499s.
10. Steen, W.M., Dowden, J., Davis, M. and Kapadia P. (1988) A point and line source model of laser welding. Journal of Physics D: Applied Physics (21). pp. 1255-1260.
11. Wang, Y.H. and Kou, S. (1986) Driving forces for convection in weld pools. Proceedings of the International Conference on Trends in Welding Research. May 18-22, 1986, Gatlinburg, TE, USA. pp. 65-69.
12. Kou S. (1987) Welding Metallurgy. (New York: Wiley).

Paper I

Factors Affecting the Efficiency of Laser Welding

Factors Affecting the Efficiency of Laser Welding

C. Lampa [*], J. Powell [*+], A. Ivarson [*], C. Magnusson [*]

[*] Division of Materials Processing
Luleå University of Technology
SE-97187 Luleå, Sweden

[+] Laser Expertise Ltd.
Harrimans Lane, Dunkirk
Nottingham NG7 2TR, UK

ABSTRACT

This paper examines the factors which affect the efficiency of laser welding using theoretical and experimental results. The redistribution of power which takes place during the welding process is investigated and the proportion of the original laser output power which contributes to the welding process identified. The change of weld cross section geometry as a function of welding speed is discussed and an increase of welding efficiency has been found as the weld speed increases.

1. INTRODUCTION

When discussing the efficiency of a welding process it is, of course, very important to define what is meant by that efficiency. As the whole point of welding is to join item A to item B, the efficiency must be related to the joining rate at a given power input level. The welding efficiency can therefore be expressed as: vd/P where P is the input power, v is the welding speed, and d the depth of penetration. This approach is the one used during the following discussion although it must be borne in mind that in practice there is usually a requirement for a minimum penetration depth for a given weld. Another point to consider is the weld cross sectional area. If welding efficiency is being discussed this area should be a minimum for a given depth of penetration as extra melting would indicate a decrease in efficiency. In practice however it is sometimes desirable to have a larger than minimum weld cross section for fit-up and/or metallurgical reasons.

This paper discusses the efficiency of laser welding expressed as a func tion of joining rate. Various process parameters have a direct influence on this rate, particularly the speed of the welding process [1]. It will be demonstrated that as the welding speed increases the penetration depth decreases but the joining efficiency rises.

2. THEORETICAL DISCUSSION

It was mentioned earlier that the efficiency of the welding process can be determined from:

$$\varepsilon_{weld} = vd/P \qquad (1)$$

where:

ε_{weld} = the welding efficiency of the joining process (m^2/J).
P = the incident laser power (W).
v = the welding speed (m/s).
d = the depth of penetration of the weld (m).

It is clear that this efficiency is related to the effectiveness of the laser power in producing a deep keyhole during welding. In this paper the input power P is divided into useful and wasted components during the interaction:

$$P = P_k + P_l \qquad (2)$$

where:

P_k = power used to melt the workpiece.
P_l = power dissipated from the interaction zone by conduction, convection etc.

P_k and P_l are complex interrelated variables because, for example, a proportion of the heat "lost" by conduction away from the weld zone acts to preheat the next part of the weld. It is nevertheless true that a high conductivity material will be welded with less efficiency than a low conductivity one.

The factors P_k and P_l can be expanded to further clarify the distribution of the input power:

$$P_k = P_d + P_w \qquad (3)$$

where:

P_d = the proportion of the power contributing to the depth of the penetration of the weld.

P_w = the proportion of the power contributing to lateral melting of the workpiece.

$$P_l = P_a + P_b + P_c + P_e + P_f + P_g \quad (4)$$

where:

P_a = conducted losses from the melt zone (Watts).

P_b = power used in boiling the workpiece and in ionising that vapour.

P_c = power prevented from interacting with the workpiece as a result of absorption by, or reflection off the plasma cloud.

P_e = convective thermal losses from the weld zone.

P_f = radiative thermal losses from the weld zone.

P_g = reflected losses from the weld zone.

Figure 1 is a visual representation of equations (3) and (4).

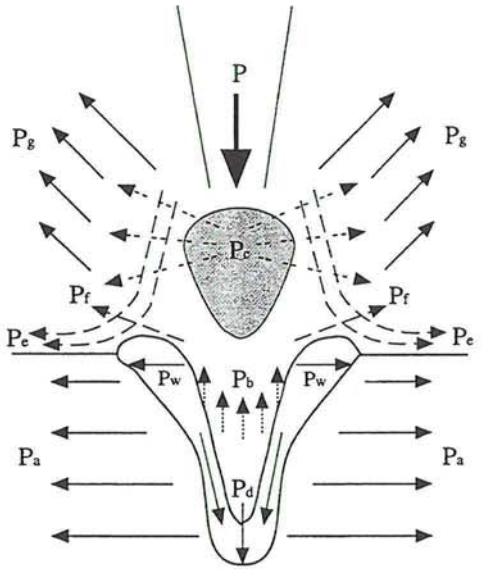

Figure 1. The redistribution of power during the welding process.

From this description of the welding interaction it is clear that the welding efficiency will be maximised if the amount of input power P converted to P_d is a maximum, i.e.:

$$\varepsilon_{weld} \propto P_d/P \tag{5}$$

Using this qualitative approach it is also possible to identify the influence of certain material properties on the welding efficiency:

$$\varepsilon_{weld} \propto 1/(\lambda T_m T_b L_f L_v \rho c_p) \tag{6}$$

where:

λ = thermal conductivity (W/m K).
T_m = melting point (K).
T_b = boiling point (K).
c_p = specific heat capacity (J/kg K).
L_f = Latent heat of fusion (J/kg).
L_v = Latent heat of vaporisation (J/kg).
ρ = density (kg/m^3).

As well as these material property variables there is one process parameter which has a profound effect on the welding efficiency. This parameter is the welding speed itself. As the following sections will show, the depth of penetration does not decrease in inverse proportion to a rise in welding speed (i.e. if the welding speed is doubled then the depth of penetration is greater than the half value which might be expected).

3. EXPERIMENTAL WORK AND DISCUSSION

In order to investigate the influence of welding speed on the efficiency of the process a number of bead-on-plate welds were carried out under the following conditions:

Laser model: Rofin-Sinar 6000
Laser power: 1400 W
Welding speed: 0.5 - 4 m/min
Focusing mirror focal length: 270 mm
Shielding gas: Helium (45 l/min)
Nozzle diameter: 5 mm
Nozzle-material stand-off: 8 mm
Workpiece material: Stainless steel 5 mm thick (SS 2333)

Table 1. Stainless steel composition

	Fe	Cr	Ni	Mo	S	P	Mn	Si	C
wt(%)	65.875	18.0	10.5	2.5	0.03	0.045	2.0	1.0	0.05
At(%)	65.21	19.12	9.89	1.44	0.05	0.08	2.01	1.97	0.23

Cross sections of the welds produced are shown in figure 2.

3.1. The redistribution of laser energy during welding

During production of the welds shown in figure 2, a water calorimeter was used to establish how much power was absorbed by the workpieces during welding. The technique is very simple: The samples were immersed in water a few seconds after completion of the weld and the temperature rise of the water was measured. From this energy measurement, the power absorbed could be calculated. The results of this investigation are given in figure 3, which clearly indicates that the absorbed power remained almost constant at approximately 940 Watts.

This figure includes all the power absorbed, $P_{(absorbed)}$, by the workpieces, i.e.:

$$P_{(absorbed)} = P_k + P_a = 940 \text{ W} \qquad (7)$$

See equations (2) and (4) for explanations of P_k and P_a.

This constitutes only two thirds of the output power of the laser and so the other 460 Watts must have been either;

a) prevented from entering the weld zone by interaction with the plasma (P_c), or
b) lost from the weld zone as a result of boiling (P_b), convection (P_e), radiation (P_f), or reflection (P_g).

The distribution of $P_{(absorbed)}$ into P_k and P_a can be investigated by finding how much material was melted per unit time for each welding speed. This is calculated by multiplying the cross sectional area of the welds (figure 4) by the welding speed. The results are given in figure 5.

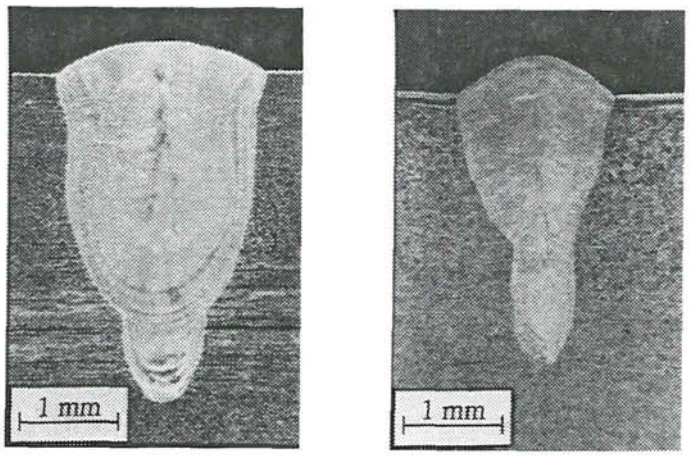

a) v = 0.5 m/min b) v = 1.0 m/min

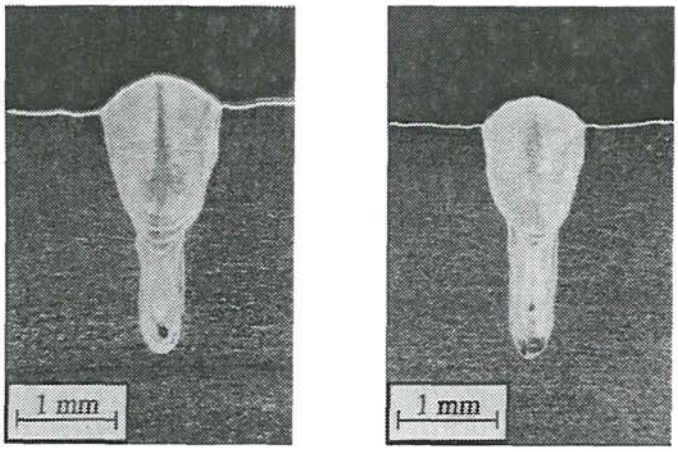

c) v = 1.5 m/min d) v = 2.0 m/min

Figure 2 a-d. The cross sections of the welds produced at different speeds (laser power 1400 W, mirror focal length 270 mm, helium assist gas).

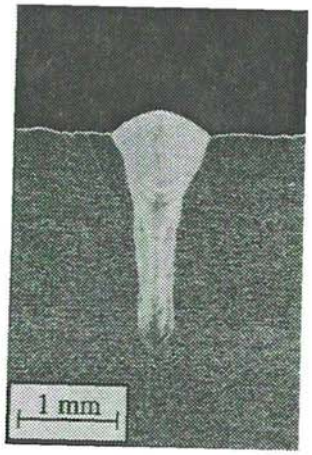

e) v = 2.5 m/min

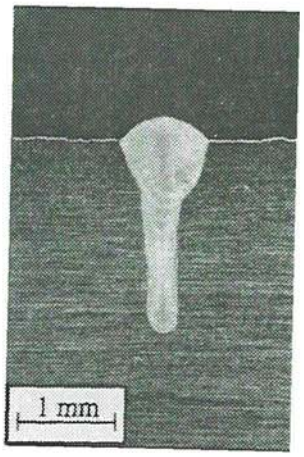

f) v = 3.0 m/min

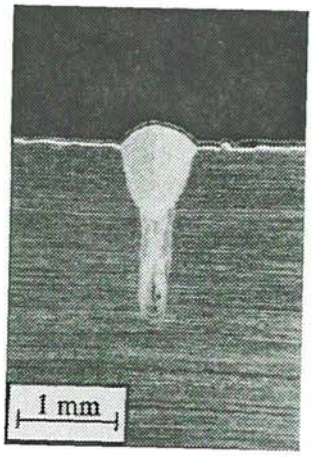

g) v = 3.5 m/min

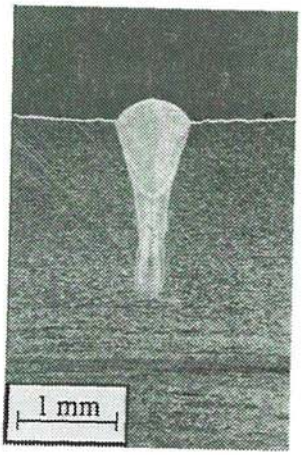

h) v = 4.0 m/min

Figure 2 e-h. The cross sections of the welds produced at different speeds (laser power 1400 W, mirror focal length 270 mm, helium assist gas).

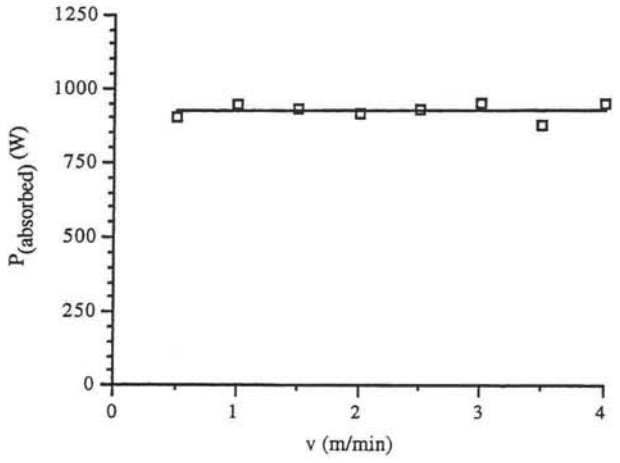

Figure 3. The variation of laser power absorbed during welding as a function of welding speed.

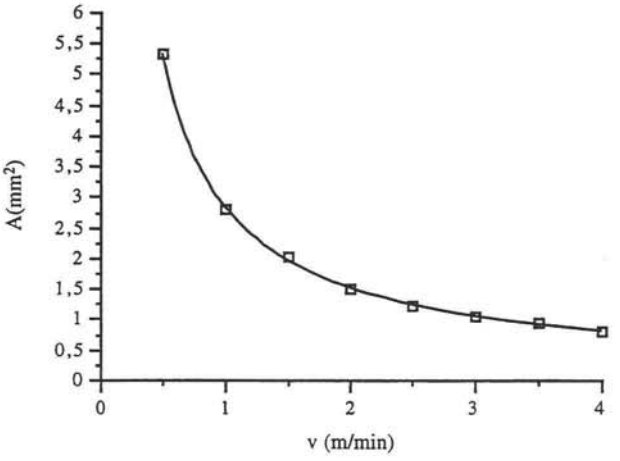

Figure 4. The variation of weld cross sectional area with welding speed.

As a first approximation the power (P_k) needed to melt the material involved in each case can be calculated from the following formula [2]:

$$P_k = Av\rho(c_p\Delta T+L_f) \quad (8)$$

where:

P_k = Power involved in melting material.
A = Weld cross section area (m^2).
v = Welding speed (m/s).
ρ = Density (8020 kg/m^3) [3].
c_p = Heat capacity of solid (500 J/kg K) [4].
ΔT = Difference between the average weld melt temperature and the room temperature ($\approx$2000 K).
L_f = Latent heat of fusion (300 kJ/kg) [4].

The temperature rise of 2000 K was estimated from the consideration that the outer surface of the weld melt is boiling (T_b = 3073 K) and the liquid / solid interface is at the melting point (T_m = 1673 K). The average of these two temperatures is approximately 2000 K above ambient.

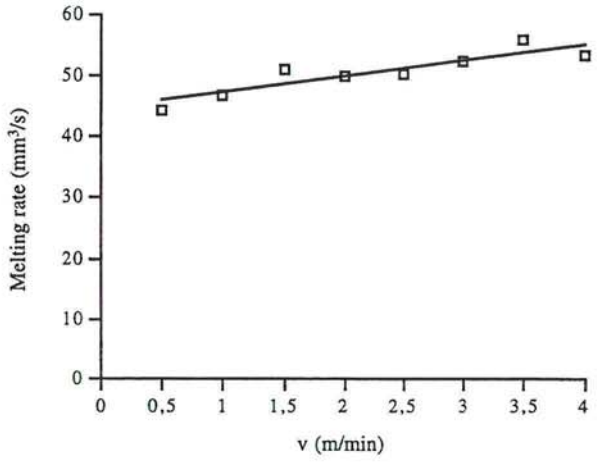

Figure 5. Material melted per unit time as a function of the welding speed.

Figure 5 demonstrates that the volume of melt generated per second rises from 44 mm^3 to 53 mm^3 as the welding speed rises from 0.5 to 4 m/min. Using equation (8) the power used in melting can be shown to rise from approximately 450 W to 550 W over the same range.

We are now beginning to identify the magnitude of the components of the redistributed laser input power expressed in equations (2), (3), and (4): i.e. from equation (8) and figure 5:

$$P_k = 500 \text{ W } (\pm 10\%) \tag{9}$$

from equation (2):

$$1400 \text{ W} = \approx 500 \text{ W} + P_l \tag{10}$$

$$P_l = \approx 900 \text{ W} \tag{11}$$

from equations (7) and (9):

$$\approx 500 \text{ W} + P_a = 940 \text{ W} \tag{12}$$

$$P_a = \approx 440 \text{ W} \tag{13}$$

Substituting values for P_l and P_a into equation (4):

$$\approx 500 \text{ W} = P_b + P_c + P_e + P_f + P_g \tag{14}$$

Table 2 Summarises the important points from these results.

Table 2. Summary of the redistributed laser input power

Description	Symbol	Watts	% of P
Laser output power	P	1400 W	100 %
Total power absorbed	$P_{(absorbed)}$	940 W	67 %
Power used in melting	P_k	500 W	36 %
Power lost by conduction from the weld zone	P_a	440 W	31 %

For the laser-material interactions examined here the power absorbed by the workpiece was approximately two thirds of the output power of the laser. Approximately half of this absorbed power was utilised in melting the workpiece and the other half was lost by conduction from the weld zone. The one third of the laser output power not absorbed by the workpiece can be divided into two types:

a) Power which reaches the workpiece and then leaves it (P_b, P_e, P_f, and P_g).
b) Power which never reaches the workpiece (P_c).

By direct observation we know that some boiling and ionisation of the vapour generated takes place. The level of boiling was shown to be very low during this experimental run by the simple method of weighing the samples before and after the welding process. The results showed negligible weight loss even at the lowest speeds where the amount of material melted was at a maximum. This boiling and ionisation process will be the subject of future work by the present authors as will the values of $P_{b,c,e,f,g}$. However, the focus of this work is on the relationship between P and P_d.

3.2. Joining rate and depth of penetration

Figure 6 shows the variation of the depth of penetration at different welding speeds, and figure 7 gives the joining rate by multiplying the penetration depth by the welding speed in each case.

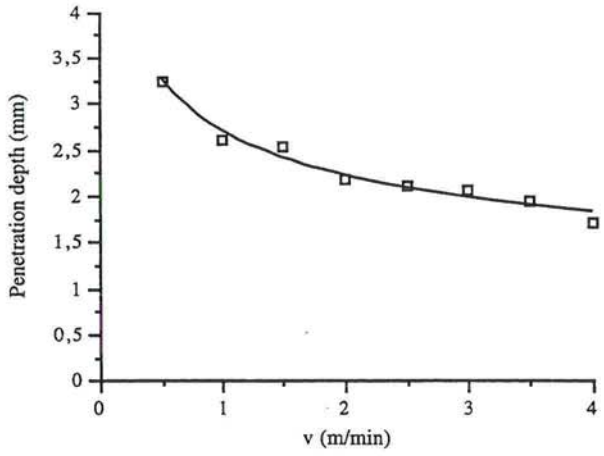

Figure 6. The variation in weld penetration depth as a function of welding speed.

It is clear from figure 7 that the joining rate (and therefore the welding efficiency) increases with the welding speed. This rapid growth of joining rate may seem surprising when it is considered that the increase in melting rate is comparatively insignificant (see figure 5). The disproportionate rise in joining rate is a result of the change in weld cross section geometry as the speeds are increased (see figure 2). To understand this change it is necessary to analyse the mechanisms which govern the weld geometry. For a given optical arrangement with a set focal spot size the two most influential process parameters are the laser power (P) and the welding speed (v). At low values of P/v (i.e. at low laser powers or high speeds) the cross section of the weld produced (if any) will be semi circular. This is because the heat from the laser penetrates radially into the material from the surface. Such welds are known as conduction limited (none of the welds produced during this experimental run were of this type). As P/v is increased by reducing the welding speed or increasing the laser power, the weld type changes from conduction limited to the "keyhole" type.

Figure 8 shows in schematic form, the development of a keyhole from an initial laser generated surface melt. As the melt becomes rapidly heated by the laser, a severe thermal gradient is set up. The centre of the melt approaches the boiling point and the edge, which is in contact with solid material, remains at the melting point. This thermal gradient is associated with a surface tension gradient as demonstrated in figure 8a. The higher surface tension at the relatively cool edges of the melt acts to pull the liquid away from the centre which causes the geometry of the melt to change (figure 8b).

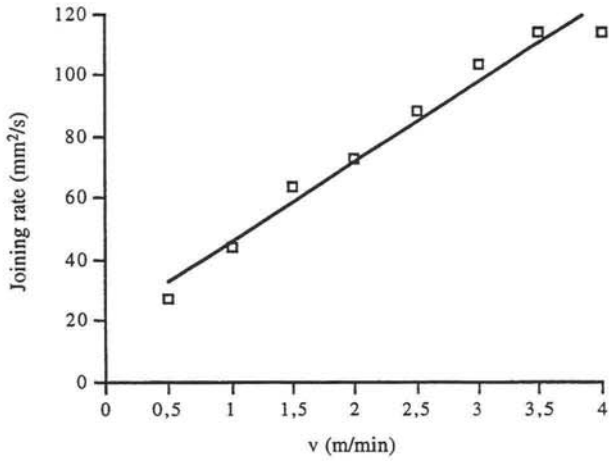

Figure 7. Joining rate as a function of the welding speed.

The shape of the melt improves the absorbtivity in that area and this causes temperatures to rise further. This increase in central temperature amplifies the depth of central depression by a combination of surface tension effects and the initiation of surface boiling which increases the pressure on the centre of the melt. This depression depth amplification continues until a keyhole is formed (figure 8c). This narrow deep hole is prevented from collapsing by the vapour pressure of the boiling liquid surrounding it.
Although the surface tension driven convective flow is helpful in producing a keyhole it becomes counter productive at higher values of P/v. At low welding speeds the convective flow becomes a dominant heat transfer mechanism and causes lateral growth of the melt by continuously supplying heat to the liquid/solid interface (see figure 9). The lateral spread of the melt demonstrated in figure 9 is encouraged at lower processing speeds because the laser-material interaction time at any point along the weld line (v/d) is large. This increase in interaction time allows the relatively slow convection currents time to circulate more often and thus transport energy sideways. This lateral distribution of laser power at lower speeds effectively increases the value of P_w (see equation (3)) and thus reduces the ratio P_d/P which is proportional to the efficiency (equation (5)).

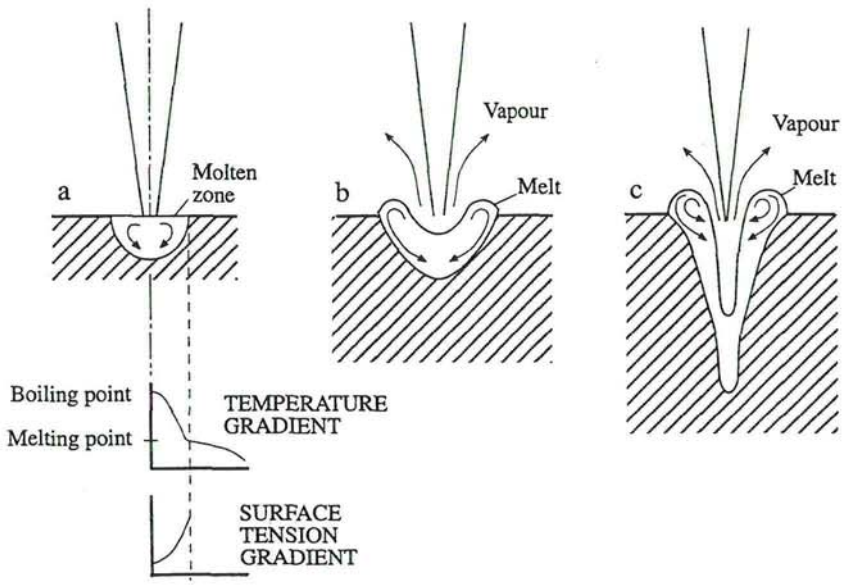

Figure 8. The creation of a keyhole type weld pool.

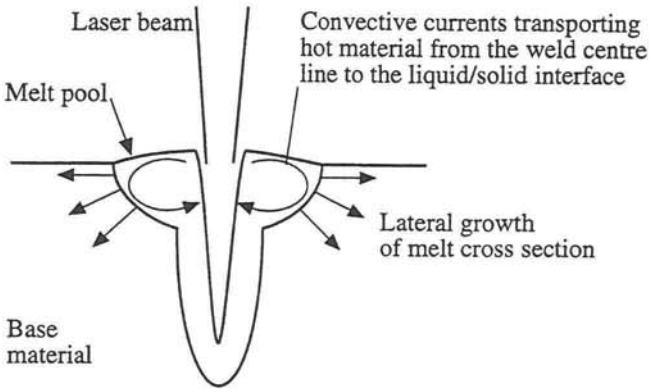

Figure 9. A schematic of the role of convective stirring in spreading the weld cross section.

4. SUMMARY AND CONCLUSIONS

The results of this experimental program demonstrated that during laser welding the laser output power was divided into three approximately equal parts:

1. Power used in melting.
2. Power absorbed by the workpiece but not used in melting.
3. Power which either never reached the workpiece or left it after interaction.

The proportion of the power involved in the melting process increased with welding speed and, more importantly, the aspect ratio of the weld cross section changed to give much higher joining rates. This rise in welding efficiency with increasing processing speed is the result of a reduction in lateral convective stirring in the melt. This reduction in stirring is made possible because, at higher speeds, the melt has a shorter lifetime in any one place along the weld line.

In most cases of real welding applications the depth of penetration is fixed and the process parameters are altered accordingly. The three most important process parameters are:

1. The lens or mirror focal length.
2. The laser power.
3. The welding speed.

From the point of view of process efficiency it is clear from our earlier discussion that the process speed should be set at the maximum possible value. This will generally entail the use of maximum laser power. This combination will give the greatest joining rate and narrowest welds at the maximum welding efficiency.

5. ACKNOWLEDGEMENTS

The authors would like to thank Mr. Göran Åberg for his help in the laser laboratory and the Swedish Research Council for Engineering (TFR) for providing funding for this work.

6. REFERENCES

1. Metzbower, E.A. (1993) Penetration Depth in Laser Beam Welding Proceedings of the Laser Materials Processing Symposium ICALEO'92. Oct. 25-29 1992, Orlando FL, USA. pp 163-175.
2. Luxon, J.T. and Parker, D.E. (1992) Industrial Lasers and Their Applications. 2nd edition (New Jersey: Prentice-Hall). ISBN: 0 13 459538 6.
3. Chemical Rubber Company Inc. CRC Handbook of Chemistry and Physics. 72nd edition 1991-1992. Lide, D.R. (editor).
4. Steen, W.M. (1991) Laser Materials Processing. (Berlin: Springer). ISBN: 3 540 19670 6.

Paper II

The Influence of Gap Width on Laser Welding

The Influence of Gap Width on Laser Welding

C. Lampa [*], J. Powell [*#], A Ivarson [*], H. Runnemalm [#], C. Magnusson [*]

[*] Division of Materials Processing
[#] Department of Mechanical Engineering
Luleå University of Technology
SE-97187 Luleå, Sweden

[+] Laser Expertise Ltd.
Harrimans Lane, Dunkirk
Nottingham NG7 2TR, UK

ABSTRACT

This paper investigates the effects that interworkpiece gaps can have on the laser welding process. The work demonstrates theoretically and experimentally that the process can accommodate and may even be improved by small gaps. As the gap reaches a limiting value however, the welding mechanism collapses. Larger gaps can be accommodated if the geometry of the cut edges is suitably altered.

1. INTRODUCTION

The use of filler wires and powder during laser welding has been investigated [1, 2] but it is far more common to use lasers for autogenous welding applications. The lack of any filler material requires that the parts to be welded are either in contact or very close to one and other. This excellent fit up is sometimes difficult to achieve in practice and it is the aim of this paper to analyse the sensitivity of the process to gaps between the workpieces. It will be demonstrated by a combined theoretical and experimental approach that the weld quality is fairly stable over a limited range of inter workpiece gap, but falls off rapidly if this range is exceeded. The paper ends with guidelines for geometrical changes in the weld zone which make the process less gap sensitive.

2. THEORETICAL DISCUSSION

Lampa et. al [3] stated that the laser input power P can be divided into useful and wasted components during the welding interaction:

$$P = P_k + P_l \quad (1)$$

where:

P_k = power used to melt the workpiece.
P_l = power dissipated from the interaction zone by conduction, convection etc.

P_k and P_l can be expanded to clarify the distribution of the input power:

$$P_k = P_d + P_w \quad (2)$$

where:

P_d = the proportion of the power contributing to the depth of the penetration of the weld.
P_w = the proportion of the power contributing to lateral melting of the workpiece.

$$P_l = P_a + P_b + P_c + P_e + P_f + P_g + P_r \quad (3)$$

where:

P_a = conducted losses from the melt zone (Watts).
P_b = power used in boiling the workpiece and ionising the vapour
P_c = power prevented from interacting with the workpiece as a result of absorption by, or reflection off the plasma cloud.
P_e = convective thermal losses from the weld zone
P_f = radiative thermal losses from the weld zone
P_g = reflected losses from the weld zone
P_r = power radiated through the material

P_r is a new parameter with respect to previous investigation [3].

Figure 1 is a visual representation of equations (2) and (3).

This present investigation is primarily concerned with the influence of P_r on equation (1). It will be clearly demonstrated that an increase in gap width will increase P_r dramatically with a consequent drop in P_k. As P_k reduces, less material is melted and eventually the gap between the workpieces cannot be bridged. At this point the welding process fails. The experimental method used involved the direct measurement of P_r and $P_{(absorbed)}$ where:

$$P_{(absorbed)} = P_k + P_a \tag{4}$$

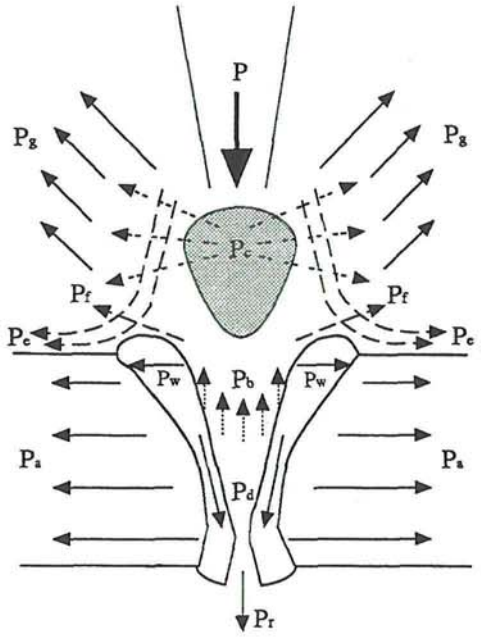

Figure 1. The redistribution of power during the welding process.

3. EXPERIMENTAL RESULTS

In order to investigate the influence of gap width on the process a number of welds were carried out under the following conditions:

Table 1. Process parameters used

Laser Model: Rofin-Sinar 6000
Laser Power: 1375 W (TEM_{00} mode) and 2700 W (multimode)
Welding speed: 1.7 m/min (1375 W) and 2.7 m/min (2700 W)
Focusing mirror focal length: 270 mm
Shielding gas: Helium (50 l/min)
Nozzle diameter: 5 mm
Nozzle-material standoff: 10 mm
Workpiece material: Stainless steel 2 mm thick
Gap width: Bead on plate - 0.3 mm

Table 2 gives details of the workpiece material used.

Table 2. Stainless steel composition

	Fe	Cr	Ni	Mo	S	P	Mn	Si	C
wt(%)	65.875	18.0	10.5	2.5	0.03	0.045	2.0	1.0	0.05
At(%)	65.21	19.12	9.89	1.44	0.05	0.08	2.01	1.97	0.23

Figure 2 presents the etched micrographic cross sections of selected welds from the series.

The power absorbed by the material, $P_{(absorbed)}$, was measured by a simple technique using a water calorimeter. The samples were immersed in a known volume of water a few seconds after completion of the weld and the temperature rise of the water was measured. From this measurement, the power absorbed can be calculated. The results of this experiment are shown in figure 3.

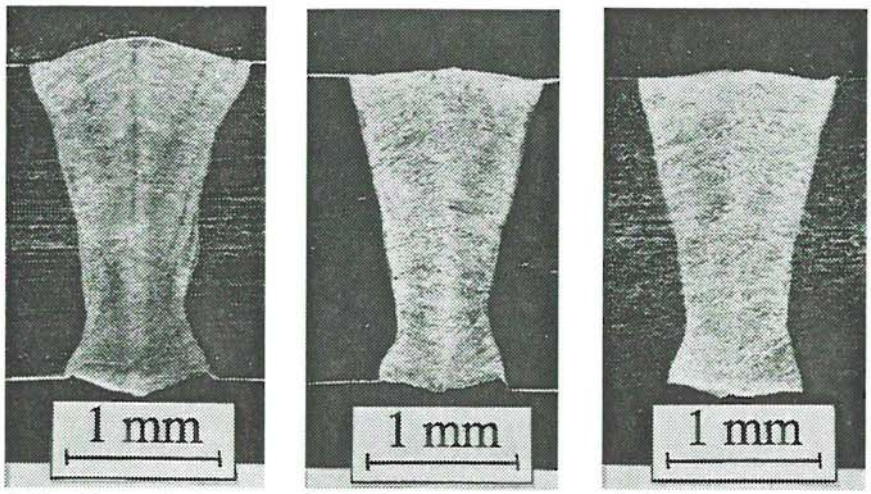

a) Bead on plate b) 0.00 mm c) 0.06 mm

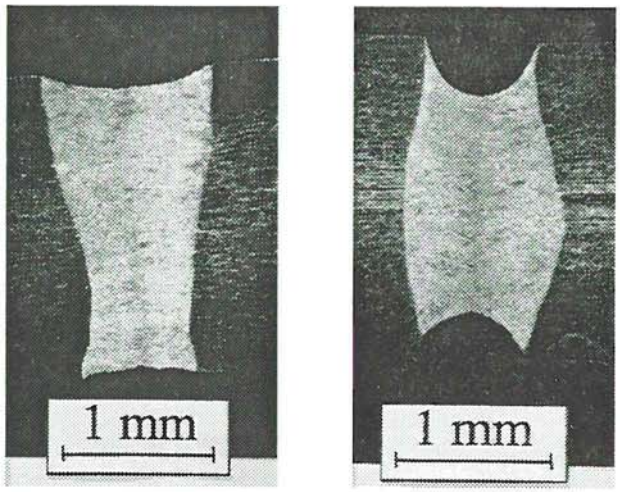

d) 0.16 mm e) 0.26 mm

Figure 2 a-e. Cross sections of welds made with different gap widths at a laser power of 2700 Watts. The lower power welds show a similar trend but are generally 20 % narrower, and the maximum gap welded was 0.20 mm rather than 0.26.

The laser power radiated through the workpiece P_r was measured by using it to evaporate a block of acrylic positioned below the workpiece. The acrylic block was weighed before and after the operation, the amount of acrylic vaporised being a measure of the power transmitted through the workpiece (3000 J of CO_2 laser light will evaporate 1 cm^3 acrylic [4]). The results of this investigation are shown in figure 4.

Optical measurements of the molten zone cross section can be used to generate a graph showing the change in melting rate with gap width, as shown in figure 5.

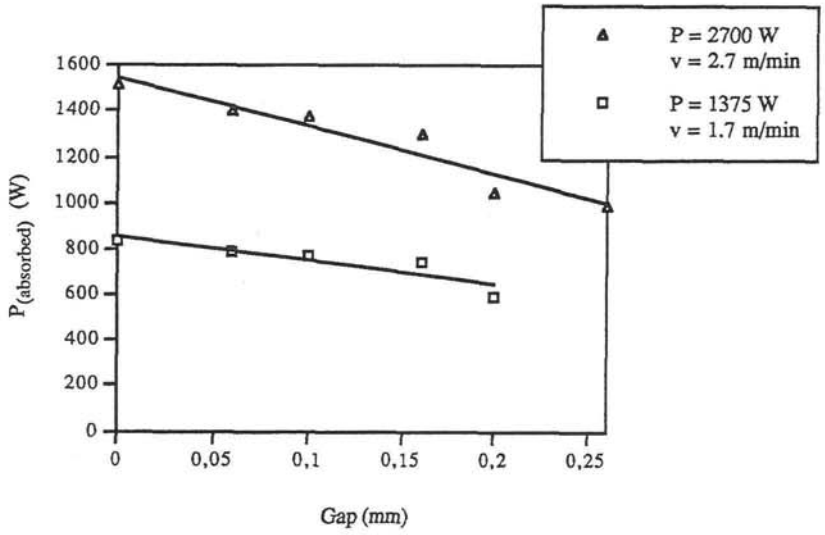

Figure 3. Power absorbed by the workpiece ($P_{(absorbed)}$) as a function of gap width. The welding process collapsed at gap widths above those shown here.

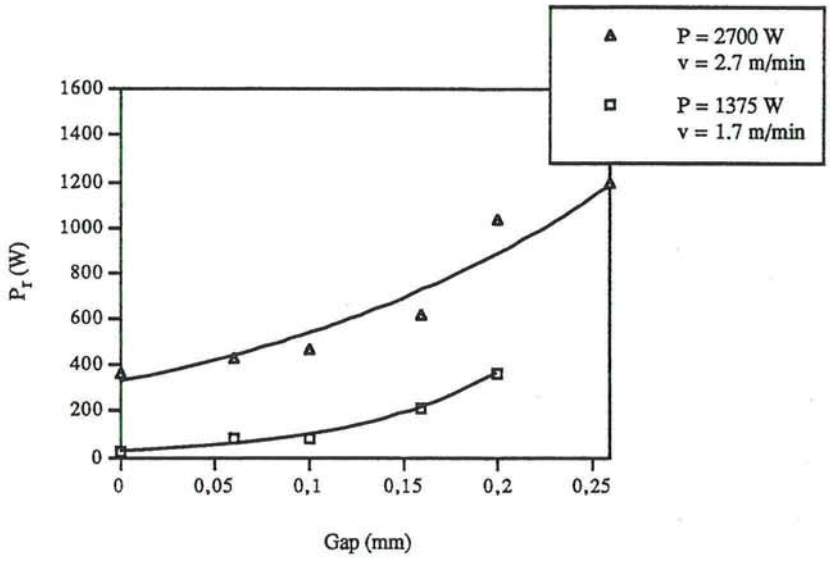

Figure 4. Power radiated through the workpiece (P_r) as a function of gap width.

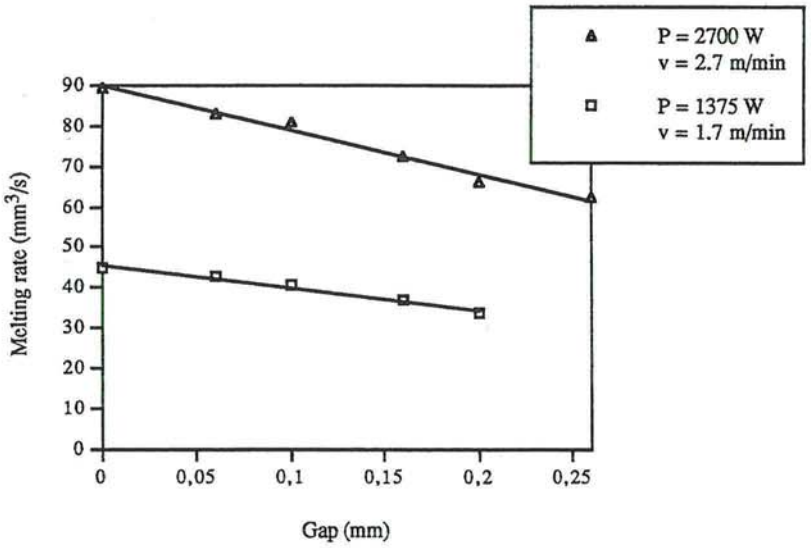

Figure 5. The material melting rate involved in generating the welds as a function of gap width.

4. DISCUSSION

The results clearly show that as the gap width increases, the power absorbed by the workpiece and the material melting rate both decrease. This reduction in melting rate eventually leads to failure of the process as a diminishing amount of melt is attempting to bridge an increasing gap. This point is demonstrated by figure 2. Figure 2 also demonstrates two other interesting points, i.e. :

a) A bead on plate (BOP) weld does not respond in the same way as a zero gap weld. This is clearly because, in most cases, zero gap actually means contact between two non-flat edges. There is therefore enough of an air gap along the interface to allow the weld to assume flatter profile than a BOP weld.
b) When the inter-workpiece gap is small, the flatness of the top and bottom of the weld can be optimised. This effect may due to capillary action down the narrow gap and may have positive effects on the fatigue strength of the welded component.

The linear decrease in melting rate shown in figure 5 is clearly related to a linear decrease in material available to the melting process as the gap increases. As the gap width rises above a limiting value (0.2 and 0.26 mm in these cases) the material melting rate will drop rapidly towards zero as the melt no longer bridges the gap. Under these conditions the workpieces will experience only minor edge surface melting. This dramatic drop off in performance is clearly indicated by the curves in figure 4, which demonstrate that the amount of light passing through the gap increases in an exponential manner.

The power absorbed by the workpiece, figure 3, decreases in a linear rather than an exponential manner. This is probably because of a change in the geometry of the plasma plume surrounding the weld zone. If bead on plate welds are being produced, this plume fills the weld pool cavity and the space immediately between it and the incoming laser beam. As the geometry of the weld zone changes with increasing gap width, this plume may descend into the gap. If this happens, the efficiency of the welding process will change. This efficiency change is due to the fact that a plasma above the weld partially blocks the incoming light. A hot plasma inside the gap however will help to transfer heat to the workpiece edges. This hypothesis is in keeping with the findings of Beyer [5], who discovered a reduction in the levels of over weld plasma with increasing gap width. As the welding process collapses above a certain limiting gap width this linear decrease in power absorbed changes by a step function because there is no longer any absorbing weld pool bridging the gap

4.1. Geometrical factors of the weld zone

It is clear that a number of geometrical factors affect the response of the welding process to gap between the workpieces. These parameters include:

- The gap width
- The material thickness
- The focal diameter of the laser beam
- The focal depth of the laser beam

Obviously any gap will have an effect on the cross sectional geometry of the solidified weld, which will affect its mechanical properties. On the other hand a large number of laser welds are used for hermetic sealing and these merely require continuous bridging of the inter workpiece gap. This being the case it is important to identify ways of minimising the gap sensitivity of the process.
This sensitivity can be reduced in the following ways:

1. Increase the material thickness. This will of course, necessitate the alteration of the process parameters as well e.g. a reduction in welding speed or an increase in laser power. The broader welds produced and the deeper interface will however mean that the process will be able to cope with larger gaps.

2. Change the beam/workpiece geometry. Figure 6 demonstrates two methods of changing the geometry of the interaction zone to make it less gap sensitive. Figure 7 proves the effectiveness of this technique if, for example, a gap width of 0.4 mm is encountered.

3. Increase the focal diameter and depth of the laser beam by increasing the focal length of the focusing lens or mirror. This will, of course, need a reduction in welding speed or an increase in laser power because enlarging the focal spot reduces the intensity of the beam.

One final geometrical aspect of gap sensitivity needs to be borne in mind: If a laser beam is moving along a line of varying gap width, the maximum gap width allowed is larger when moving from a narrow to a wider gap. This is because of the ability of the existing melt to bridge the gap.

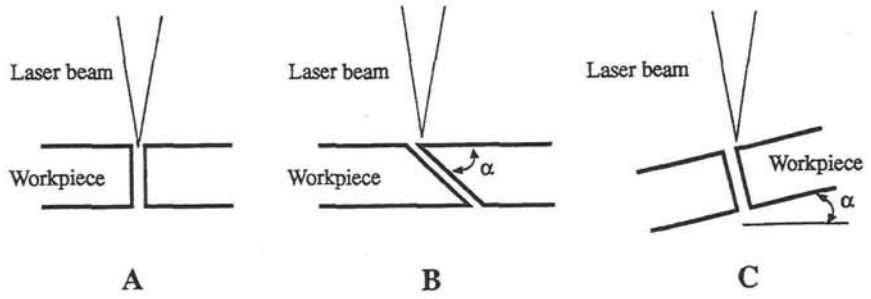

Figure 6. Changing the beam/workpiece geometry from A to B or C will reduce gap sensitivity (see figure 7) although processing speeds may need to be reduced.

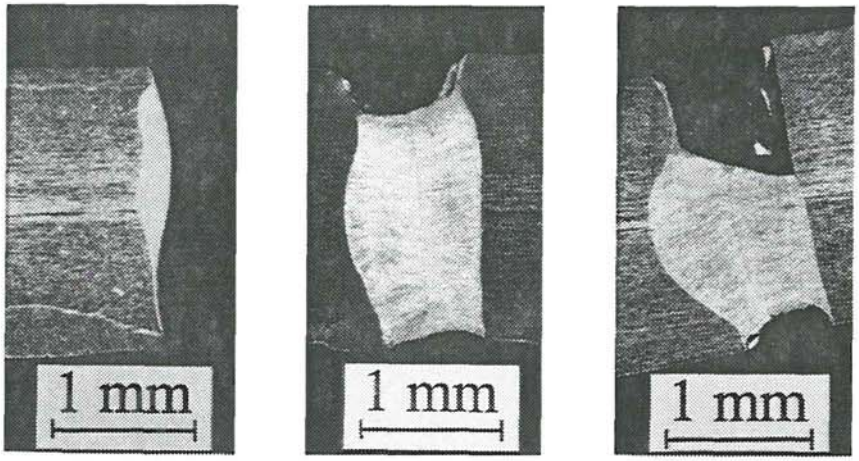

Figure 7. Practical results of using the geometrical modification shown in figure 6 at a gap width of 0.4 mm. A) One side of a fig 6A type "weld". No weld produced. Both edges experienced only surface melting. B) A weld made with the same gap width but with the preweld edge preparation shown in figure 6B ($\alpha = 60°$). Successful hermetic seal weld produced. C) A weld made with the same gap width but with the preweld geometry shown in figure 6C ($\alpha = 10°$). Successful hermetic seal weld produced.

5. CONCLUSIONS

1. Very small gaps (less than 0.1 mm) can result in welds with flatter profiles than can be achieved when producing bead on plate welds. This may have positive effects on the fatigue life of welded components.
2. As the gap increase in size, the amount of laser light leaving the bottom of the weld zone increases in an exponential manner.
3. As the gap reaches a critical size, the available melt cannot bridge it and the welding process collapses.
4. The geometry of the laser-material interaction zone can be modified to improve the gap sensitivity of the process.

6. ACKNOWLEDGEMENTS

The authors would like to thank Mr. Göran Åberg for his help in the laser laboratory and Mr. Åke Wesselheim for his help with the experimental preparation. The funding for this work was provided by the Swedish Research Council for Engineering Science (TFR).

7. REFERENCES

1. Lampa, C., Sarady, I., Powell, J., Mattson, J. and Magnusson, C. (1993) Laser Welding of Dissimilar Metals. Conf. Proc. of 4th Conf on Laser Materials Processing in the Nordic Countries, NOLAMP 4. Aug. 16-18, 1993, Sønderborg, Denmark. pp. 215-224. ISBN: 87 984641 0 8.
2. Salminen, A.S., Kujanpää, V.P. and Moisio, T.J.I. (1993) Beam-wire interaction during laser welding with filler wire. Conf. Proc. of 4th Conf on Laser Materials Processing in the Nordic Countries, NOLAMP 4. Aug. 16-18, 1993, Sønderborg, Denmark. pp. 185-190. ISBN: 87 984641 0 8.
3. Lampa, C., Powell, J., Ivarson, A. and Magnusson, C. (1995) Factors Affecting the Efficiency of Laser Welding. Lasers in Engineering (4), pp. 73-83. ISSN: 0898 1507.
4. Miyamoto, I., Maruo, H. and Arata, Y. (1985) Intensity Profile Measurement of Focused CO_2 Beam using PMMA. Conf. Proc. of Materials Processing Symposium, ICALEO'84. Nov. 12-15 1984, Boston MA, USA. pp. 313-320. ISBN: 0 912035 26 9.
5. Beyer, E. (1993) Process Monitoring and Quality Control. Module 2: Systems and Safety, EuroLaser Academy (ELA). Oct. 11th - Nov. 6th 1993, Aachen, Germany.

Paper III

A Point and Line Source Analysis of the Laser Material Interaction in Hyperbaric Keyhole Laser Welding

A Point and Line Source Analysis of the Laser Material Interaction in Hyperbaric Keyhole Laser Welding

R. Ducharme [*], P. Kapadia [*],
C. Lampa [+], A. Ivarson [+], J. Powell [+#], C. Magnusson [+]

[*] Physics Department
University of Essex, Colchester
Essex CO4 3SQ, UK

[+] Division of Materials Processing
Luleå University of Technology
SE-97187 Luleå, Sweden

[#] Laser Expertise Ltd.
Harrimans Lane, Dunkirk
Nottingham NG7 2TR, UK

ABSTRACT

A continuous CO_2 laser of 1.35 kW has been used to study the welding of 5 mm thick stainless steel for a range of external pressures (0.1 to 0.8 MPa) in shielding gas environments of pure helium, argon and nitrogen. It was found that keyhole laser welding could not be carried out for pressures significantly in excess of atmospheric pressure using argon and nitrogen shielding gases, but that the process was possible over the whole range of pressures using helium as a shielding gas.

The data using helium is summarised in the form of weld pool profiles for a series of values of the external pressure in increments of 0.05 MPa over the entire range of pressures. The interaction of the laser light with the weld specimen is analysed using the concept of a point and line source representing the strength of the laser coupling to the material. The line source of heat represents the net effect of absorption processes in the keyhole and the point source represents the absorption of heat from the laser in the plume. The differential equation for steady state heat conduction is solved using these point and line sources and their strengths are adjusted until the calculated weld pool profile matches that provided by the results of the experiment.

It was found that as the external pressure was increased above atmospheric pressure, the strength of the line source decreased monotonically and that the point source increased. The increasing strength of the point source is due to enhanced inverse Bremsstrahlung absorption in the plume with rising pressure. The effect attenuates the available power in the laser beam and is responsible for the declining strength of the line source with increasing external pressure. The analysis points to the crucial part played by the plume and that of the shielding gas employed in the hyperbaric welding processes.

1. INTRODUCTION

The experimental configuration employed in studying hyperbaric laser welding using a continuous CO_2 laser of 1.35 kW power is described. The process is studied using argon, nitrogen and helium as shielding gases. The results are summarised in graphs and photographs of the weld profile over a range of pressures from 0.1 to 0.8 MPa for weld specimens of 5 mm thickness of steel.

The analysis of the experimental data was carried out by using the point and line source approach. In the laser welding of metals the incident laser energy on the material is absorbed by complicated processes in the plume above the keyhole as well as in the laser generated keyhole. The variation of the energy absorption with depth in the weld piece can be represented by a point and line source. This general concept was developed mathematically in two previous papers [1, 2]. It is intended, in this paper, to present an analysis of the experimental data for hyperbaric laser welding based on the application of these ideas. Here the method has been simplified and used to generate a computer code capable of handling a large number of welds in a single run.

Measurements of the maximum weld width, the parallel-sided part of the weld and the penetration depth are fed into the program which then yields the point and line source strength. This method of analysis clearly displays the increasingly dominant part played by the point source as the pressure increases and the resulting decline of the line source which, at sufficiently high pressures, should culminate in a purely conduction type weld being produced.

The fact that the increase in pressure did not produce any increase in the line source strength in the keyhole strongly suggests that inverse Bremsstrahlung absorption may not be playing a significant part in the keyhole at all values of the pressure over the entire range of pressures. This observa-

tion has important implications for the mathematical modelling of the laser welding of materials and will be discussed further elsewhere.

2. EXPERIMENTAL CONFIGURATION

A continuous CO_2 laser beam of 1.35 kW was used to study the welding of 5 mm thick stainless steel sheets for a range of external pressures from 0.1 to 0.8 MPa in shielding gas environments of pure helium, argon and nitrogen. The experimental configuration is illustrated in figure 1.

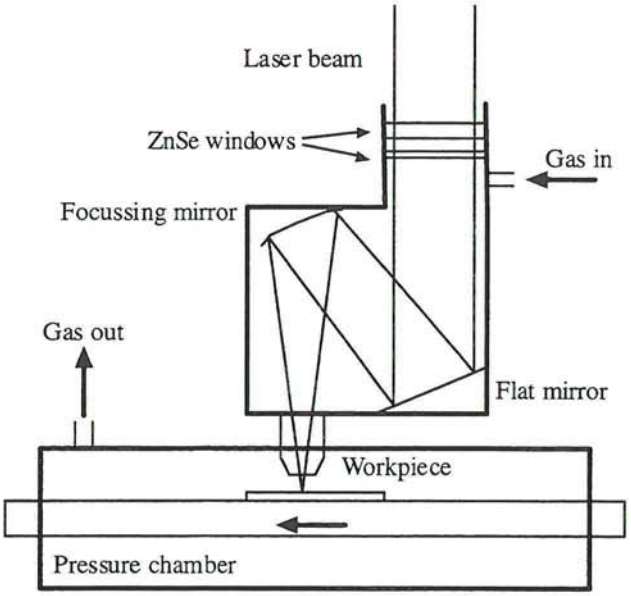

Figure 1. Experimental set-up.

The CO_2 laser beam of 10.6 micrometer wavelength is admitted into the hyperbaric chamber through Zinc-Selenide (Zn-Se) windows and is incident on the weld by a system of reflecting and focusing mirrors. The apparatus is designed to minimise distortion of the Zn-Se windows and the focusing characteristics as a result of high pressures in the chamber. The 20 mm diameter laser beam is first admitted through a 5 mm thick Zn-Se window and then passes through a second Zn-Se window of 3 mm thickness. The shielding gas is admitted into the chamber below this window. The laser beam is reflected off a plane mirror onto a focusing mirror of 180 mm focal length perpendicularly onto the specimen which is free to translate. This gave a focused spot diameter for the near Gaussian beam of 0.27 mm.

The laser beam travels through a nozzle which has a stand-off distance of 10 mm from the surface of the specimen in the hyperbaric chamber. The pressure was varied from 0.1 to 0.8 MPa in increments of 0.05 MPa. To minimise gas dynamic effects in the weld zone the gas flow through the chamber was kept constant for the range of gases and pressures used at a value of 550 g/h. The welding speed throughout the trials was 2.5 m/min and the stainless steel test pieces were all of the same dimensions i.e. 160 x 20 x 5 mm.

It was found that keyhole laser welding could not occur for pressures significantly in excess of atmospheric pressures for argon and nitrogen shielding gases. Using helium as the shielding gas, however, the welding process was possible over the whole range of pressures.

3. POINT AND LINE SOURCE METHOD

The concept of the line source originates in a solution of the heat conduction equation obtained by Rosenthal (1941) [3]. The work of Swift-Hook and Gick (1973) [4] made use of this idea of a line source to describe the absorption of laser light in the keyhole. The concept of a line source is useful in modelling the parallel-sided part of the liquid region of the weld, but does not describe the semi-circular part of the weld at the top. This work was accordingly extended by the group at the University of Essex to produce a point and line source model of laser welding [1, 2]. The steady state heat conduction equation with a temperature distribution T in $z \geq 0$ is:

$$K\nabla^2 T = U\frac{\partial T}{\partial x} \tag{1}$$

where K is the thermal diffusivity of the material and U is the translation speed of the specimen. Rosenthal showed that this equation possesses two fundamental solutions the first of which is:

$$T - T_0 = q_p \frac{\exp\left\{\frac{1}{2}Ux / K - \frac{1}{2}U\left[x^2 + y^2 + (z-c)^2\right]^{\frac{1}{2}} / K\right\}}{4\pi k\left[x^2 + y^2 + (z-c)^2\right]^{\frac{1}{2}}} \tag{2}$$

The point source of heat has strength q_p and is located at (0, 0, c) in a medium whose temperature far from the souce is T_0. The second solution corresponds to a line source of strength q_l per unit length on the z axis and is:

$$T - T_0 = q_l K_0 \left[\frac{1}{2} U \left(x^2 + y^2 \right)^{\frac{1}{2}} / K \right] \exp\left(\frac{1}{2} Ux / K \right) / 2\pi k \qquad (3)$$

Here k is the thermal conductivity of the specimen and K_0 is a modified Bessel function. In the extension of the line source to include the point source it was noted in [1] that further solutions to the heat conduction equation could be obtained by using linear combinations of the two solutions. In fact, the line source solution can be derived from the point source solution by integration over all values of c. If we assume that relatively little heat is lost by cooling from the surface of the workpiece at $z = 0$ then the boundary conditions to be satisfied there is:

$$\frac{\partial T}{\partial z} = 0 \qquad \text{at } z = 0 \qquad (4)$$

This was described in [1] using the method of images where a point and line source description was developed. The weld widths and weld profile were also calculated there and compared with experimental welds. In [2] the model was modified to extend it to deal with specimens of finite thickness and was compared with the results of experiment. This point and line source description was used here with the objective of constructing a computer code capable of rapidly analysing a large number of welds to yield an empirical map encompassing the broadest possible conditions including hyperbaric welding. With this end in view it was found that dropping the introduction of image charges was found to produce negligible practical effects so that after suitable numerical checks were made these terms were omitted simplifying the computer program. The fact that the penetration of the specimen was partial and not close to the thickness of the specimen (which was 5 mm in thickness) could explain the insensitivity of the calculation to the presence of image terms.

To apply the method, the maximum weld width was measured at the top of the nail head shaped weld profile. The stem width of the parallel-sided part of the weld was measured and the average value was found. Thirdly the penetration depth in the weld piece was also measured. The line source strength was evaluated next until the maximum calculated weld width of the weld profile matched the observed stem width from the weld profile data. The strength of the point source was determined by varying its strength until the maximum calculated width of the weld matched the measured weld width. The total line source contribution of the absorbed power is the power per unit depth due to the line source multiplied by the depth of the weld.

4. RESULTS AND DISCUSSION

Figure 2 shows polished and etched cross-sections of welds produced in an atmosphere of helium at pressures of 0.1, 0.3, 0.5 and 0.8 MPa.

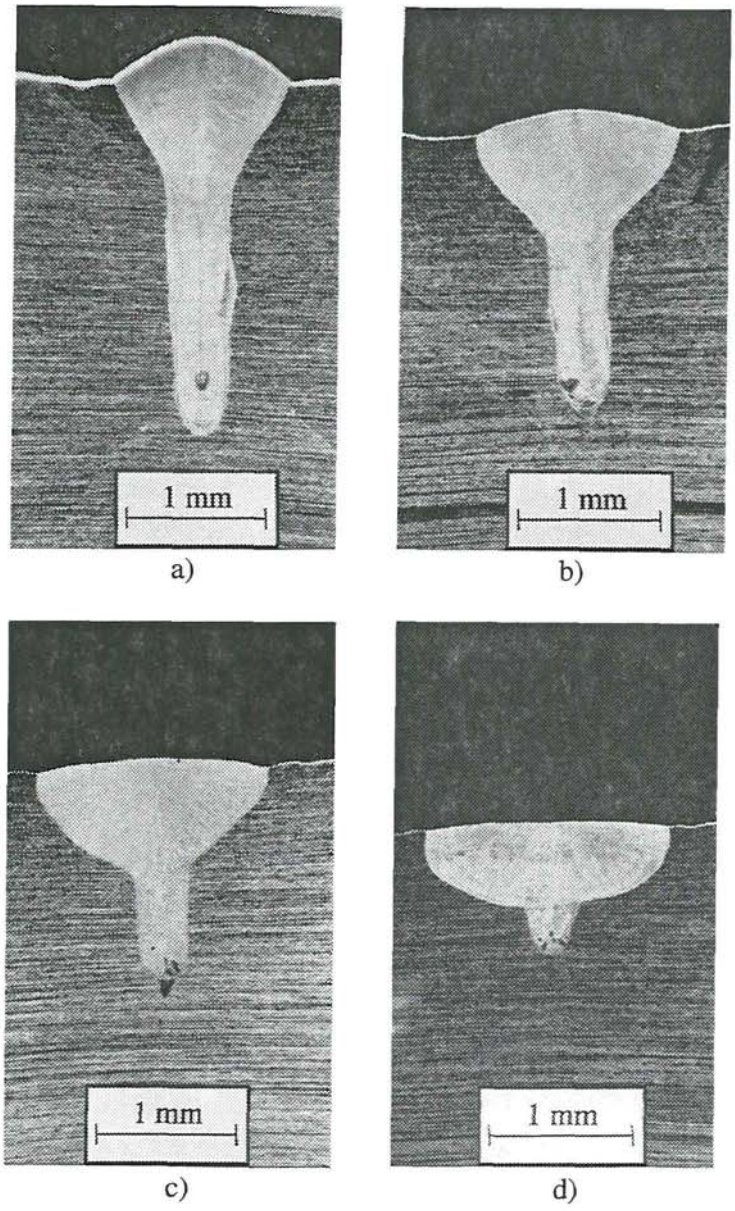

Figure 2. Polished and etched cross-sections of welds produced in an atmosphere of helium at pressures of a) 0.1 MPa, b) 0.3 MPa, c) 0.5 MPa and d) 0.8 MPa.

A gradual decrease in penetration depth and an increase in the weld bead width can be clearly seen and these effects are produced graphically in figures 3 and 4.

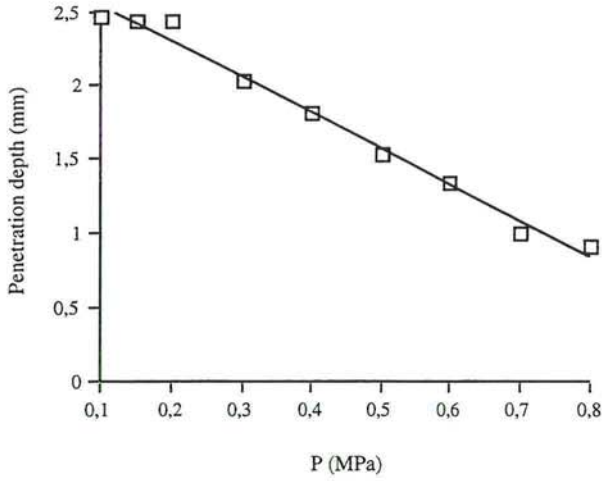

Figure 3. Penetration depth as a function of ambient pressure in an atmosphere of helium.

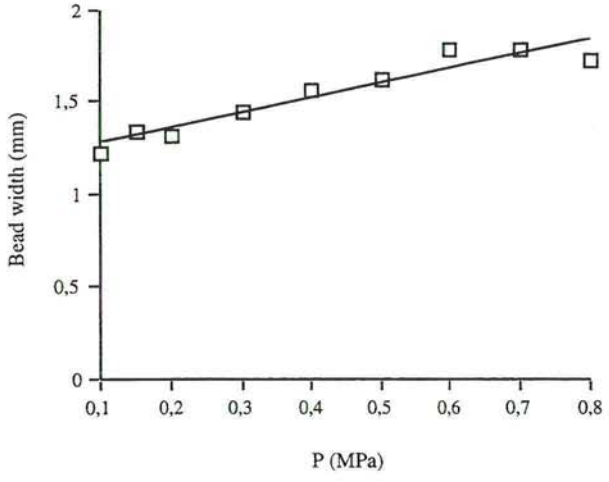

Figure 4. Weld bead width as a function of ambient pressure in an atmosphere of helium.

Figures 5 and 6 show graphs for weld produced in an atmosphere of nitrogen. These results show that the welding process fails in nitrogen for all pressures greater than approximately 0.16 MPa. Argon has also been used as the shielding gas and has been found to produce similar results to nitrogen. It is suggested that the use of argon and nitrogen shielding gases leads to much larger and uncontrollable plumes than if helium is used.

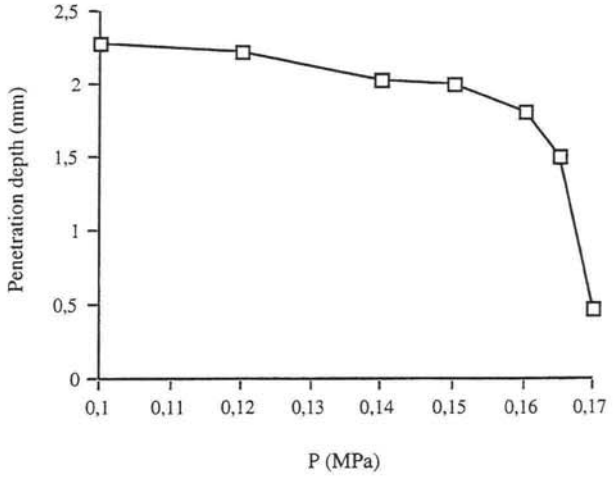

Figure 5. Penetration depth as a function of ambient pressure in an atmosphere of nitrogen.

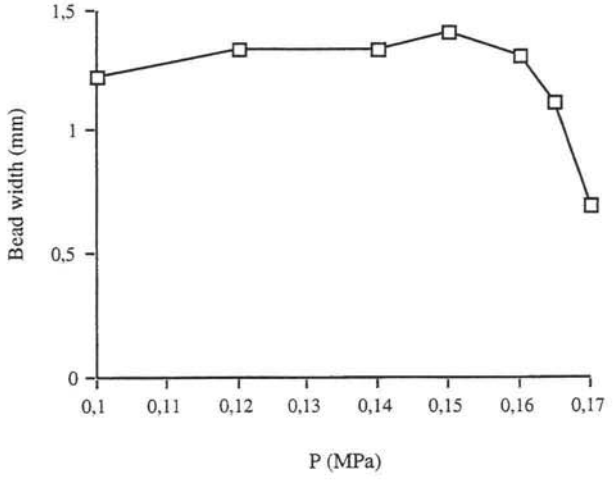

Figure 6. Weld bead width as a function of ambient pressure in an atmosphere of nitrogen.

The plume absorbs the laser light through inverse Bremsstrahlung processes and defocuses it as a result of spatial variations in the refractive index of the plasma. If the plume is large enough then it can completely block the beam causing the welding process to fail. A further important feature of the problem is that the plume has a much lower mass density than the cooler shielding gas surrounding it. It is therefore prone to becoming detached from the weld piece and floating in the path of the laser beam. The absorption coefficient of the plume due to inverse Bremsstrahlung processes rises as the pressure increases producing subsequent increases in the size and buoyancy of the plume. Both the problems of the blocking of the laser light and detachment therefore become more serious under hyperbaric conditions.

Table 1 shows the point and line source strengths characterising 12 welds at range of different pressures between 0.1 and 0.8 MPa. These results have been calculated using the point and line source method described in the previous section.

Table 1. Point and line source strengths for welds at different pressures. The line total is equal to the product of the line source strength and the weld penetration depth. The power loss is calculated as the difference between the incident power in the laser beam and the total power that is absorbed in the weld piece

pressure MPa	point source W	line source W/mm	line total W	power loss W
1.0	290	315	820	238
1.5	329	282	641	324
2.0	364	309	665	321
3.0	438	282	578	333
3.5	495	304	618	235
4.0	652	266	480	217
4,5	675	248	508	167
5.0	675	266	427	248
5.5	675	258	387	287
6.0	675	266	373	301
6.5	675	252	327	347
7.5	675	258	323	352
8.0	675	268	321	353

Figure 7 shows a comparison of the experimental weld pool cross-section at 0.1 MPa to a computed weld pool cross-section based on the point and line source strengths given in table 1, for the same weld. The calculation has been performed using the finite volume method to solve the three dimensional heat conduction equation for the temperature distribution in the weld piece. The weld pool has been assumed to be bounded by an isothermal surface at the melting point of the metal.

Dowden et al [5] has shown that the absorption coefficient of a plasma due to inverse Bremsstrahlung increases approximately as the square of the pressure. The experimental data, however, shows that the line source strength decreases slightly with increasing pressure, but the depth of the keyhole decreases more significantly. At a pressure of 0.1 MPa the penetration depth is 2.6 mm and at 0.8 MPa it decreases to 1.2 mm whereas the line source strength decreases from 315 W/mm to 268 W/mm. These results show that there is increased inverse Bremsstrahlung absorption in the plume as the pressure increases and appears to indicate the absence of inverse Bremsstrahlung in the keyhole. If significant inverse Bremsstrahlung absorption were taking place in the keyhole, as the pressure increases inverse Bremsstrahlung absorption would increase and this would be reflected in an increasing line source strength.

Mathematical models of the laser welding process with plasmas in the keyhole absorbing laser radiation by inverse Bremsstrahlung have been constructed by Dowden et al [5], by Ducharme et al [6] as well as by Tix and Simon [7]. All these models point to high keyhole temperatures and neglect radiation losses from metallic plasmas. Reintroducing these radiation losses following the method of Cram et al [8] indicate that radiation losses from metallic plasmas are several magnitudes greater than those from argon based plasmas. The experimental observations of this paper strongly suggest the absence of such plasmas in the keyhole at all pressures.

Considering next the behaviour of the point source, it is clear that the point source strength grows significantly with increasing pressures. The point source strength doubles between atmospheric pressure and a pressure of 0.25 MPa atmospheres after which the point source strength saturates to a constant value. The size of the plume alters with increasing pressure but its behaviour is more complicated. Metal vapour emerging from the keyhole mixes turbulently with the downward directed shielding gas. As stated above radiative losses from metal vapour plasmas such as iron are four orders of magnitude greater than those from rare gases like argon so that small quantities of metal vapour can produce significant radiative losses. These radiative losses increase with increasing pressure.

The experiments conclusively show that the plume ignites producing a visible plasma and experimentally detectable temperature can reach 19000 K. In a study of free burning plasmas with argon similar temperatures and filamentary structures in the plasma were predicted in agreement with the results of experiments [9]. In turn, the plume in general transfers energy to the workpiece by conduction to the mouth of the keyhole and by radiation as well. Convective losses are also likely. Maximum plume temperatures are found to be somewhat insensitive to increasing pressure consistent with plasma analysis in a previous paper [9].

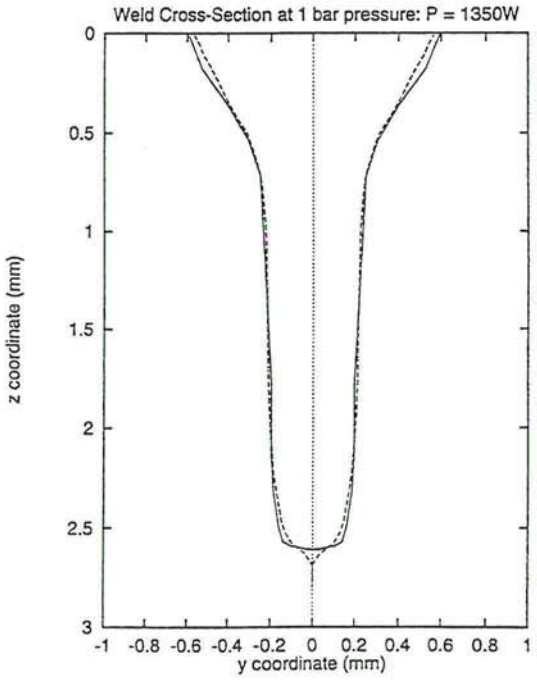

Figure 7. Experimental (solid curve) and computed (dashed curve) weld profiles for 0.1 MPa weld.

5. CONCLUSIONS

A 1.35 kW continuous CO_2 laser has been used to produce welds in steel for a range of pressures between 0.1 and 0.8 MPa. The welding has been carried out at a constant speed of 2.5 m/min and a constant shielding gas delivery rate of 550 g/h so that only the pressure has been allowed to vary. It has been found that the penetration depth falls as the pressure rises according to an almost linear relationship. A calculation of the point and line source strengths corresponding to weld pool profiles obtained for 12 welds has shown that the point source strength increases between 0.1 and 0.25 MPa but then becomes constant at higher pressures. The calculation has also shown that the line source remains approximately constant as the pressure increases but does show a slight overall tendency to decrease in strength.

In explaining these results it has been argued that the plume looses most of its heat through radiation and conduction into the weld piece. The conductive heat losses are responsible for the formation of the nail head structure at the top of the weld and therefore correspond to the point source strength in the calculation. The point source strength levels off at 0.25 MPa but radiation losses keep on increasing as the pressure rises. The total losses from the plume therefore tend to increase with pressure explaining why the penetration depth decreases. The behaviour of the line source as the pressure rises is surprising in the face of plasma based models of the keyhole that predict the absorption per unit depth in the keyhole should increase with the pressure. It has been concluded therefore that the temperature in the keyhole is not as high as these models predict and that inverse Bremsstrahlung is therefore not a dominant absorption mechanism.

6. REFERENCES

1. Steen, W.M., Dowden, J., Davis, M. and Kapdia, P. (1988) A point and line source model of laser keyhole welding. Journal of Physics D: Applied Physics (21). pp. 1255-1260.
2. Akhter, R., David, M., Dowden, J., Kapadia, P., Ley, M. and Steen, W.M. (1989) A method for calculating the fused zone profile of laser keyhole welds. Journal of Physics D: Applied Physics (21). pp. 23-28.
3. Rosenthal, D. (1941) Mathematical Theory of Heat Distribution During Welding and Cutting. Welding Journal (20). pp. 220s-345s.
4. Swift-Hook, D.T. and Gick, A.E.F. (1973) Penetration Welding with Lasers. Welding Journal (52). pp. 492s-499s.

5. Dowden, J., Kapadia, P. and Postacioglu, N. (1988) An analysis of the laser-plasma interaction in laser keyhole welding. Journal of Physics D: Applied Physics (22). pp. 741-749.
6. Ducharme, R., Williams, K., Kapadia, P., Dowden, J., Steen, W.M. and Glowacki, M. (1994) The laser welding of thin metal sheets: an integrated keyhole and weld pool model with supporting experiments. Journal of Physics D: Applied Physics (27). pp. 1619-1627.
7. Tix, C. and Simon, G. (1993) A transport theoretical model of the keyhole plasma in penetration laser welding. Journal of Physics D: Applied Physics (26). pp. 2066-2074.
8. Cram, L.E., Poladiau, L. and Roumeliotis, G. (1988) Departures from equilibrium in a free-burning argon arc. Journal of Physics D: Applied Physics (21). pp. 418-425.
9. Ducharme, R., Glowacki, M., Kapadia, P. and Dowden, J. (1994) Sustained Plasma Burning Using Continuous and Pulsed Lasers Operating at Different Infrared and Optical Frequencies and Various Pulse Repetition Rates. Proceedings of the Laser Materials Processing Conference, ICALEO'93. Oct. 24-28 1993, Orlando FL, USA. pp. 135-144. ISBN: 0 912035501.

Paper IV

Effects of Different Shielding Gas Compositions on the Process of CW CO_2 Laser Welding in the Hyperbaric Range

Effects of Different Shielding Gas Compositions on the Process of CW CO_2 Laser Welding in the Hyperbaric Range

R. Ducharme [*], P. Kapadia [*],
C. Lampa [+], A. Ivarson [+], J. Powell [+#], C. Magnusson [+]

[*] Physics Department
University of Essex, Colchester
Essex CO4 3SQ, UK

[+] Division of Materials Processing
Luleå University of Technology
SE-97187 Luleå, Sweden

[#] Laser Expertise Ltd.
Harrimans Lane, Dunkirk
Nottingham NG7 2TR, UK

ABSTRACT

A continuous CO_2 laser of 1.35 kW has been used to study the welding of 5 mm thick stainless steel for pressures ranging from 0.1 to 0.8 MPa in increments of 0.1 MPa. Experimental data including penetration depths, weld widths and in some cases weld pool profiles has been obtained for each value of the pressure using different mixtures of argon and helium shielding gases. In a previous paper it has been reported that keyhole welding could not be carried out for pressures significantly in excess of atmospheric pressure using pure argon and nitrogen shielding gases, but that the process was possible at pressures up to 0.8 MPa using helium. In the present paper the critical pressure for keyhole welding is determined as a function of the mixed shielding gas composition. The laser material interaction is analysed by solving the heat conduction equation with line and point heat sources representing the keyhole and plume respectively. The line source strength is itself calculated from consideration of the inverse Bremsstrahlung and Fresnel absorption processes in the keyhole. It is concluded that successful laser welding in the hyperbaric range crucially hinges on good plume control through the effective delivery of an appropriate shielding gas mixture.

Keywords: Hyperbaric, laser welding, thermal modelling, shielding gases

1. INTRODUCTION

Laser welding of 5 mm thick sheets of stainless steel has been carried out in a hyperbaric chamber using a CW CO_2 laser. The purpose of this study has been to determine the effects of pressure on the laser material interaction. In a previous paper [1] based on a similar experimental set-up it has been reported that keyhole welding was not possible for pressures significantly in excess of atmospheric pressure using pure argon and nitrogen shielding gases due to the blocking effect of the plume, but that the process was possible at pressures up to 0.8 MPa using helium. In the present paper this existing study has been extended to include mixtures of argon and helium shielding gases. Two further differences from the original paper are as follows. Firstly the F number of the near Gaussian laser beam used in the experiments has been increased from 4.0 to 6.0 and this has been found to produce a marked reduction in the penetration depths of the welds at corresponding pressures. Secondly, the point and line source model employed to analyse the experimental weld pool profiles in the original paper has been extended to include formula for both the strength and length of the line source. These are shown to give good agreement with experiment.

The experimental configuration has been described in detail in our earlier paper. The laser beam is admitted into the hyperbaric chamber through two Zinc-Selenide windows designed to minimise the effects of distortion at the elevated pressures. It is then directed through the shielding gas nozzle and downwards onto the workpiece by a system of reflecting and focusing mirrors. The shielding gas nozzle is situated about 10 mm above the translating workpiece. In the interests of maintaining control over gas dynamic effects in the weld zone the rate of mass flow through the chamber was kept constant for the range of gases and pressures used at a value of 550 g/h. The welding speed throughout the trials was 2.5 m/min and the stainless steel pieces were all of the same dimensions i.e. 160 x 20 x 5 mm.

2. MATHEMATICAL MODEL

One of the simplest method of analysing experimental weld pool cross-sections is to make use of line and point sources [1-3] to represent the thermal influence of the laser generated keyhole and plume respectively. The steady state heat conduction equation is solved using these point and line sources and their strength are adjusted until the calculated weld pool profiles matches the experimental weld. Three constants, the point source strength as well as the strength and length of the line source, are therefore needed in order to calculate the temperature distribution in the workpiece

for each weld. In the present paper the line source strength and length are both calculated from consideration of the absorption processes in the keyhole. The number of arbitrary parameters that need to be fixed for each weld is therefore effectively reduced from three to one.

The formula for the line source strength Q_L (i.e. the power deposition per unit depth in the keyhole) is based on the integrated keyhole and weld pool model of Ducharme [2] et al. The model assumes that Q_L is made up of contributions from inverse Bremsstrahlung absorption in the keyhole plasma and Fresnel absorption on the keyhole wall. For weld translation speeds less than a certain critical value U_c the plasma contribution by itself will be sufficient to maintain a keyhole radius larger than the radius r_0 of the incident laser beam. Under these conditions:

$$Q_L = (LP_0)^{1/2} \qquad (U \le U_c) \tag{1}$$

where P_0 is the incident laser power and L = 8150 W/m^2 is the linking intensity for the action of a CW CO_2 laser beam on steel. At weld speeds greater than U_c, however, the radius of the keyhole will be smaller than r_0 forcing a direct interaction to take place between the laser light and the wall of the keyhole. From analysis of the experimental data [2-4] it appears that the Fresnel contribution arising from this direct interaction is proportional to the weld translation speed but effectively independent of the laser power. This result finds expression in the form:

$$Q_L = (LP_0)^{1/2} + A(U - U_c) \qquad (U > U_c) \tag{2}$$

where $A = 10^7$ J/m^2.

The critical velocity U_c is calculated by equating the line source strength to the power per unit depth needed to maintain a uniform circular keyhole of radius r_0 assuming that the keyhole is at the boiling temperature T_v of the metal being welded. This condition gives:

$$(LP_0)^{1/2} = 2\pi k(T_v - T_0)cyl\left(\frac{U_c r_0}{2\kappa}\right) \tag{3}$$

with:

$$cyl(x) = \frac{I_0(x)}{K_0(x)} + 2\sum_{n=1}^{\infty}(-1)^n \frac{I_n(x)}{K_n(x)} \tag{4}$$

where I_0 and K_0 are modified Bessel functions of the first and second kinds, k and κ denote the thermal conductivity and diffusivity of steel and T_0 is the ambient temperature. This equation is readily solved using a binary chop algorithm.

The line source length d is calculated from the expression:

$$d = \frac{(1-\varepsilon)P_0 - Q_P}{Q_L} \tag{5}$$

where ε is the proportion of the energy in the laser beam which is not absorbed in the workpiece. Typically ε falls in the range 0.1 to 0.3 for partially penetrated keyhole welds, so that $\varepsilon = 0.2$ is usually a good default value.

3. DISCUSSION OF RESULTS

Experimental weld pool cross-sections have been obtained using a near Gaussian CW CO_2 laser beam with F numbers of 4.0 and 6.0. Table 1 lists the focal spot diameters [5], the critical velocities, the line source strengths and the width of the parallel sided stem part of the welds produced using each of these F numbers. Table 2 compares the experimental and calculated values of both the weld width at the top of the workpiece and the penetration depth for 28 different welds. In each case the line source strength has been taken from table 1. The point source strength has been varied until the calculated weld pool profile is reasonably good match to the experimental profile.

Table 1. Laser beam radius and line source strength

F number	beam radius (mm)	critical velocity (mm/s)	line source (W/mm)	stem width (mm)
4.0	0.055	45.0	270	0.38
6.0	0.080	33.0	350	0.53

Welds 1 to 13 have been obtained using pure helium shielding gas and an F number of 4. It can be seen that as the pressure rises the point source strength increases and the weld penetration depth decreases. The increasing strength of the point source is due to the enhanced inverse Bremsstrahlung absorption in the plume with rising pressure. The effect attenuates the available power in the laser beam and is therefore responsible for the reduction in the weld penetration depth. Notice above 0.55 MPa that both the experimental and theoretical top weld widths become insensitive to the point source strength. This is because the weld penetration depth has become significantly shorter than the top weld width. Under these conditions the top weld width asymptotically approaches the maximum possible value of 1.8 mm corresponding to a pure point source of 1080 W.

Welds 14 to 17 show that at atmospheric pressure shielding composition has very little effect on the weld pool profile. It is, however, interesting to compare welds 2 and 14. The only difference in operating conditions between these welds is that the F number has been increased from 4.0 to 6.0. It is clear that this has had little effect on the point source strength but has produced a significant reduction in the penetration depth. This is because the larger diameter laser beam interacts more strongly with the keyhole wall. Since the total power in the laser beam is fixed a greater power dissipation per unit depth in the keyhole leads to a corresponding reduction in its length.

Welds 18 to 21 have been obtained using 10 % argon in helium shielding gas mixture and an F number of 6.0. The results show similar trends to those discussed in connection with welds 1 to 13. The point source strengths are similar at corresponding pressures but the penetration depths are shorter as might be expected given the increase in the F number. It appears that pure helium shielding gas and the 10 % argon in helium mixture behave similarly. The presence of the argon would make a difference, however, if an attempt were being made to use the shielding gas to disrupt the plume. This is usually achieved by delivering a high flow rate of shielding gas from the side rather than from above. The gas mixture containing 10 % argon can be expected to perform better under these circumstances given that this mixture is approximately twice as dense as pure helium and therefore more able to dislodge the plume. It is, of course, the growth of the plume that determines the critical pressure for the failure of keyhole welding. Consequently, disruption of the plume is clearly one method by which the critical pressure for keyhole welding might be increased.

Welds 22 to 28 illustrate the failure of keyhole welding at different critical pressures depending on the absolute pressure. The critical pressure for keyhole welding is less than 0.2 MPa in a pure argon shielding gas environment. This is increased to above 0.3 MPa if the proportion of argon is reduced to 40 %, 0.4 MPa if it is reduced to 20 % and 0.7 MPa if pure helium is used. It is interesting that the failure of keyhole welding involves more than just the disappearance of the line source. In particular, there is also a sudden drop in the top weld width indicating that a much smaller proportion of the laser power is absorbed in the workpiece once keyhole welding fails.

Table 2. Comparison of experimental and predicted weld geometries

weld number	Pressure MPa	% Ar	F number	experimental top width (mm)	experimental penetration depth (mm)	theoretical top width (mm)	theoretical penetration depth (mm)	Q_P (W)
1	0.1	0	4.0	1.2	2.6	1.2	2.8	310
2	0.15	0	4.0	1.3	2.5	1.3	2.7	350
3	0.2	0	4.0	1.3	2.4	1.3	2.5	400
4	0.3	0	4.0	1.4	2.1	1.4	2.3	450
5	0.35	0	4.0	1.4	2.0	1.5	2.1	490
6	0.4	0	4.0	1.5	1.9	1.5	2.0	510
7	0.45	0	4.0	1.5	1.8	1.6	1.9	550
8	0.5	0	4.0	1.6	1.6	1.6	1.7	630
9	0.55	0	4.0	1.7	1.5	1.7	1.5	680
10	0.6	0	4.0	1.7	1.4	1.7	1.4	700
11	0.65	0	4.0	1.7	1.2	1.7	1.2	750
12	0.7	0	4.0	1.7	1.1	1.8	1.1	770
13	0.8	0	4.0	1.7	1.0	1.8	1.0	790
14	0.1	100	6.0	1.4	1.7	1.4	1.9	400
15	0.1	80	6.0	1.4	1.7	1.4	1.9	400
16	0.1	20	6.0	1.3	1.6	1.4	1.9	400
17	0.1	0	6.0	1.4	1.7	1.4	1.9	400
18	0.1	10	6.0	1.4	1.7	1.4	1.9	400
19	0.3	10	6.0	1.6	1.5	1.6	1.5	540
20	0.4	10	6.0	1.7	1.3	1.7	1.2	650
21	0.5	10	6.0	1.8	1.0	1.8	1.0	760
22	0.7	10	6.0	1.8	0.8	1.8	0.9	800
23	0.3	40	6.0	1.8	1.6	1.6	1.7	650
24	0.4	40	6.0	0.8	0.3	-	-	-
25	0.4	20	6.0	1.8	1.2	1.7	1.2	650
26	0.5	20	6.0	0.9	0.4	-	-	-
27	0.7	10	6.0	1.8	0.8	1.8	0.9	770
28	0.8	10	6.0	1.0	0.3	-	-	-

4. REFERENCES

1. Ducharme, R., Kapadia, P., Lampa, C., Ivarson, A., Powell, J. and Magnusson, C. (1996) A Point and Line Source Analysis of the Laser Material Interaction in Hyperbaric Keyhole Laser Welding. Proceedings of the Laser Materials Processing Conference, ICALEO'95. Nov. 13-16 1995, San Diego CA, USA. pp. 1018-1027.
2. Steen, W.M., Dowden, J., Davis, M. and Kapadia, P. (1988) A point and line source model of laser keyhole welding. Journal of Physics D: Applied Physics (21) pp. 1255-1260.
3. Hamoudi, W.K. and Ducharme, R. (1996) Keyhole welding of C/Mn steel using a 10 kW CO_2 laser. International Journal of Joining of Materials (8) pp. 30-36.
4. Ducharme, R., Williams, K., Kapadia, P., Dowden, J., Steen, W.M. and Glowacki, M. (1994) The laser welding of thin metal sheets: an integrated keyhole and weld pool model with supporting experiments. Journal of Physics D: Applied Physics (27) pp. 1619-1627.
5. Steen, W.M. (1991) Laser Materials Processing. (Berlin: Springer). ISBN: 3 540 19670 6.

Paper V

An Analytical Thermodynamic Model of Laser Welding

An Analytical Thermodynamic Model of Laser Welding

C. Lampa [*], A. F. H. Kaplan [#], J. Powell [*+], C. Magnusson [*]

[*] Division of Materials Processing
Luleå University of Technology
SE-97187 Luleå, Sweden

[#] Department of Laser Technology
Vienna University of Technology
Arsenal, Objekt 207
A-1030 Vienna, Austria

[+] Laser Expertise Ltd.
Harrimans Lane, Dunkirk
Nottingham NG7 2TR, UK

ABSTRACT

An earlier model of deep-penetration laser welding has been simplified in order to provide a useful model of process analysis. This work involves the modelling of the various energy-absorption mechanisms which determine the keyhole shape and thus the dimensions of the melt pool. The penetration depth and weld width (top and bottom) predicted by the model are shown to be in close agreement with experimental results. The widening of the top of the weld seam as a result of Marangoni flow is accurately modelled by introducing an artificially enhanced value for the workpiece's thermal conductivity towards the top of the weld. The model allows analysis of the dependence of the weld profile on the process parameters.

1. INTRODUCTION

Over the past decade a substantial amount of theoretical research has been carried out into the subject of deep-penetration laser welding [1-5]. Analysis of a moving line source of energy [6] is the basis of a number of models although the broadening of the top of the weld pool requires an extra calculation device such as the superimposition of a moving point source acting with the line source [3].

In this present work the phenomenon of weld-pool broadening at the top of the weld is accomodated by assuming an artificially high thermal conductivity in the top region of the weld zone. The shape of the keyhole established by the laser beam during welding is central to the discussion of weld pool's cross section and has been investigated in a rotationally symmetrical model [2, 4]. This work was extended to take into account asymmetrical heat flow [1] and the displacement of the laser beam with respect to the centre of the keyhole [7]. Other workers in the field have covered such subjects as the hydrodynamic effects of the metal vapour and melt surface in the keyhole [1, 2, 8], the absorption of energy by the keyhole plasma [1, 2, 4], absorption of energy during multiple reflections [1, 2, 9] and the influence of the energy distribution in the incident beam [10]. Thermocapillary Marangoni flow induced by surface-tension gradients is largely responsible for the broadening of the top of the weld pool [11, 12] and this has been simulated numerically by a number of authors [11, 13].

The most important thing a theoretical model of laser welding can do is to forecast the overall dimensions of the weld cross section for a given set of process parameters. The present authors have found that, by using a simplified version of a model first developed by Kaplan [1], an accurate prediction of weld width and penetration depth can be achieved. While figure 1(a) shows a real laser-weld cross section, figure 1(b) demonstrates the simplified weld cross section geometry assumed in this work and its close relationship to a typical weld profile. The model algorithm is presented schematically in figure 2.

During welding, heat is carried away from the centreline of the weld by two main processes.

(i) thermal conduction and
(ii) thermocapillary (Marangoni) flow.

Towards the bottom of the weld where the melt/solid interfaces are almost parallel (see figure 1(b)) the major thermal transport mechanism is thermal conduction. For this reason the usual value for thermal conductivity (λ_1) is used to calculate the width of the bottom of the weld (w_b). Towards the top of the weld lateral thermal transport is accelerated by thermocapillary flow (see figure 3). The easiest way to account for this effect in the model is to assign the material an artificially high thermal conductivity in this area.

Experimental work and estimates in the literature [2, 11, 14, 15] have suggested that the effective thermal conductivity in the presence of thermocapillary flow is at least twice the stationary melt conductivity. In this work therefore λ_2, the effective thermal conductivity used to calculate the top width (w_t) of the weld, is taken as 2.5 λ_1.

The following sections will explain the model details and the other assumptions made in the calculation of top width (w_t), bottom width (w_b) and penetration depth (d) of the weld.

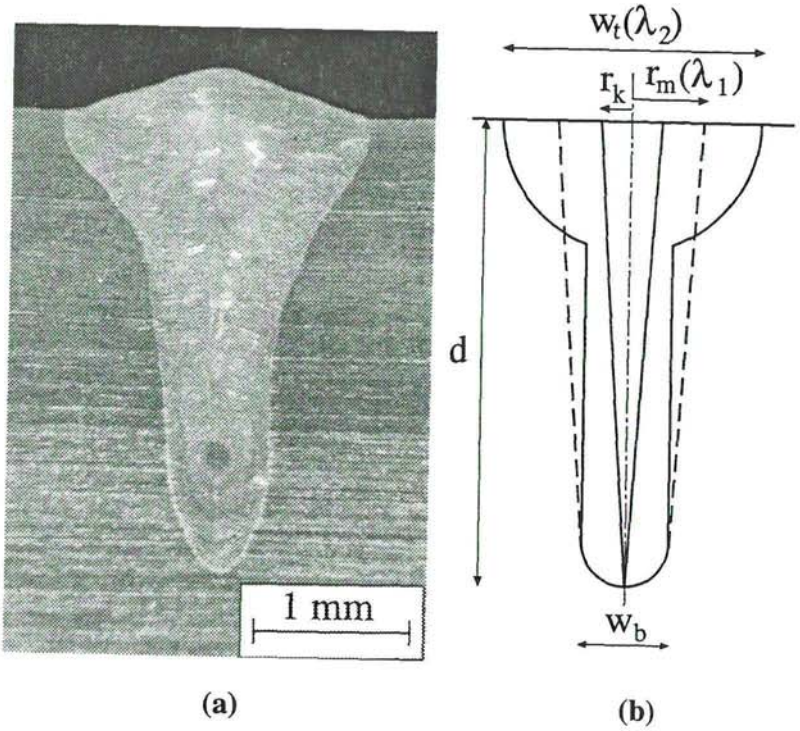

Figure 1. (a) An actual example of a keyhole weld cross section. (b) An idealised keyhole weld cross section showing the three main dimensions to be predicted by the theoretical model.

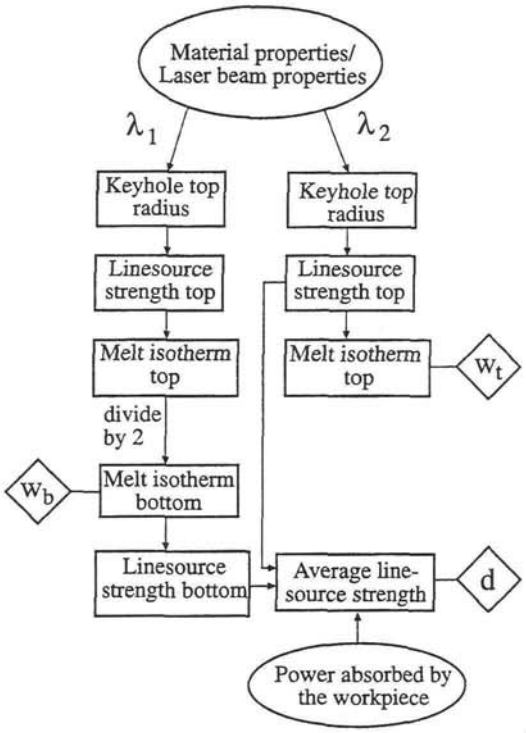

Figure 2. The calculation logic of the model. λ_1, the true thermal conductivity is used to calculate w_b, the width of the bottom of the weld (see figure 1). λ_2, an artificially high thermal conductivity, is used to calculate the width of the top of the weld, w_t.

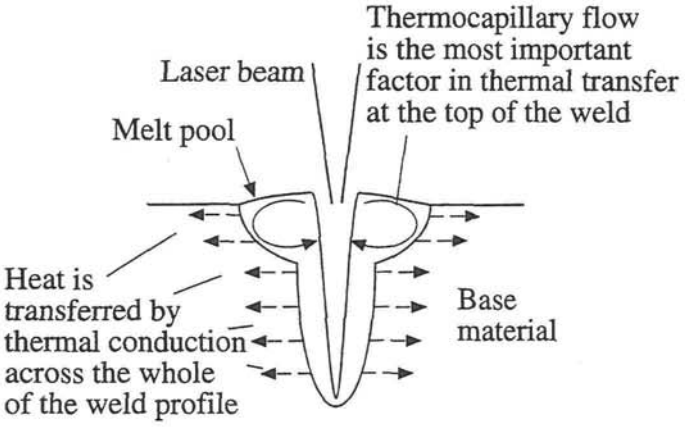

Figure 3. Thermocapillary flow accelerates lateral thermal transport at the top of the weld.

2. THE MODEL

2.1. General considerations

Figure 4 describes the coordinate geometry referred to in the model. The keyhole at the centre of the weld is assumed to be conical and the surrounding melt volume is a hollow truncated cone. The coordinate system is cylindrical (r, φ, z) and the laser is assumed to be a line source of energy acting along the central axis of the conical keyhole. The weld zone is assumed to be moving with a velocity v.

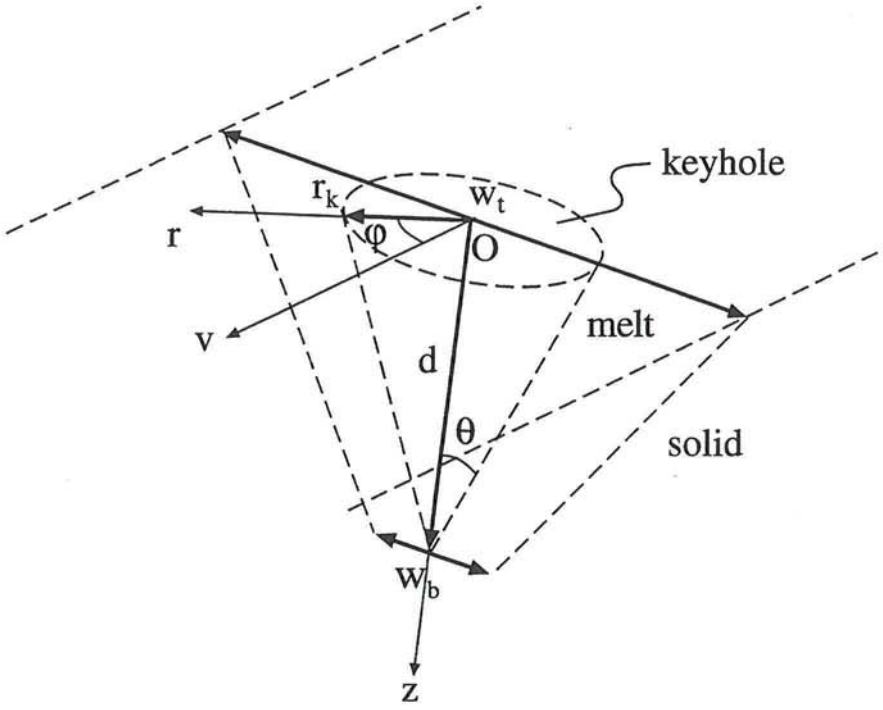

Figure 4. The coordinate system used in the model.

In order to describe the heat flow into the workpiece, the concept of a moving line source [6] is used:

$$P'(r,\varphi) = \left(T(r,\varphi) - T_a\right) 2\pi\lambda_{th} \frac{1}{K_0(\mathrm{Pe})} \mathrm{e}^{\mathrm{Pe}\cos\varphi} \tag{1}$$

with the Péclet number

$$\mathrm{Pe} = rv/(2\kappa) \tag{2}$$

where P' is the line source strength (W m^{-1}), $T(r, \varphi)$ is the temperature field in the workpiece (K), T_a is the ambient temperature (K), λ_{th} is the thermal conductivity (W m^{-1} K^{-1}), $K_0(\ )$ is the modified Bessel function of second kind and zeroth order, v is the welding speed (m s^{-1}) and κ is the thermal diffusivity (m^2 s^{-1}).

By using equation (1) and Fourier's law of heat conduction [16], simplified to consider only the radial component, the heat flow q for an arbitrary point r, φ at any temperature T can be described as [1]

$$q = \frac{1}{r}\left(T - T_a\right)\lambda_{th}\mathrm{Pe}\left(\cos\varphi + \frac{K_1(\mathrm{Pe})}{K_0(\mathrm{Pe})}\right) \tag{3}$$

where q is the heat flow (W m^{-2}), $K_1(\ )$ is the modified Bessel function of second kind and first order and T is the temperature (K). The intensity, I (W m^{-2}) of the incident laser beam is assumed to have a Gaussian distribution [1], [2]:

$$I(r,\varphi) = I_0\left(\frac{r_{f0}}{r_f}\right)^2 \exp\left(-\frac{2r^2}{r_f^2}\right) \tag{4}$$

where I_0 is the beam intensity at the beam's focal point (W m^{-2}), r_{f0} is the beam's focal radius (m), r_f is the beam's radius at depth z (m) and r is the radial distance from the centre of the beam (m).

2.2. The calculation of w_b, the width of the bottom of the weld

In order to calculate w_b the first step must be the identification of r_k, the keyhole entrance radius (see figure 4). This radius is that at which the material reaches its vaporisation point, T_v. From earlier work [1] the inclination of the keyhole wall (θ) is taken as being 45° or $\pi/4$ radians at this radius close to the top surface, see figure 5.

If only Fresnel absorption is considered, as is approximately the case at the top of the keyhole, an energy balance at any point of the keyhole wall could be expressed as

$$I\alpha_{Fr}\tan\theta = q_v \tag{5}$$

where I is the local incoming laser beam intensity (W m^{-2}) (from equation (4)), α_{Fr} is the Fresnel absorption coefficient for the keyhole wall inclination θ and q_v is the heat flow into the material (W m^{-2}), when the surface is at the vaporisation point (T_v) (from equation (3)).

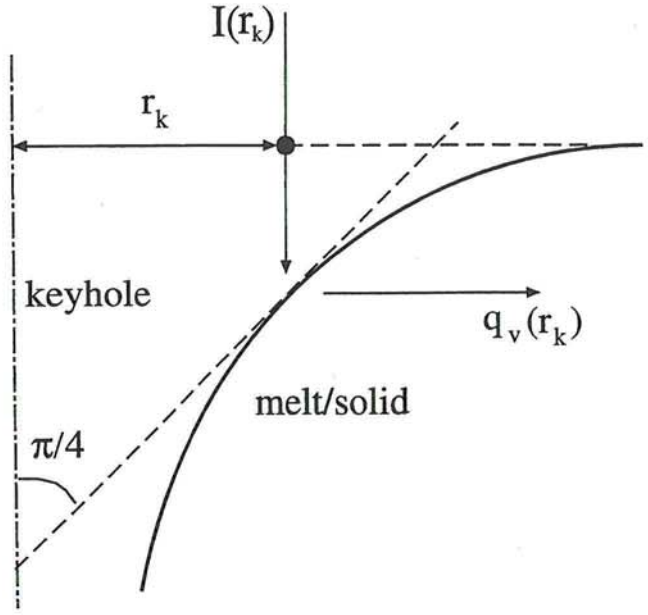

Figure 5. The inclination of the keyhole wall (θ) is taken as being $\pi/4$ radians at the keyhole entrance.

Substituting $\theta = \pi/4$ into equation (5) gives a value for the radius of the top of the keyhole, r_k. This radius can then be used to calculate the line source strength at the top of the keyhole by using equation (1) for $T(r,\varphi) = T_v$ and the Péclet number for r_k (equation (2)).

From this the melt isotherm (r_m) at the top of the keyhole (in the absence of thermocapillary flow) can be estimated by first re-arranging equation (1) to calculate the Péclet number for $T(r, \varphi) = T_m$ and secondly rearranging equation (2) to calculate $r = r_m$.

The melt isotherm at the bottom of the melt is taken as half of the top value in the absence of thermocapillary flow. (This assumption was made after having observed high-speed keyhole weld cross sections, for which thermocapillary flow can be ignored. These weld cross sections are somewhere in between rectangular and triangular in shape and therefore it is a fair assumption that the bottom melt width can be approximated as half the top melt width when thermocapillary flow is ignored.) Identification of this isotherm gives us w_b, the width of the bottom of the weld. In summary, w_b is calculated as follows:

$$w_b = 0.5 \times 2\frac{2\kappa_1 \mathrm{Pe}}{v} \tag{6}$$

where Pe, the Péclet number, is computed from equation (1) in combination with equation (5).

2.3. The calculation of w_t, the width of the top of the weld

Once again equations (1)-(5) are used to calculate the radius of the top of the keyhole, the line-source strength at the top of the keyhole (P'_T) and the melt isotherm. The difference in this case is that an artificially high value for the thermal conductivity λ_2, taken as 2.5 times the value of λ_1 for steel, is employed in the calculations. Estimation of the melt isotherm at the top of the weld naturally gives us a value for w_t:

$$w_t = 2\frac{2\kappa_2 \mathrm{Pe}}{v} \tag{7}$$

where Pe is computed from equation (1).

2.4. The calculation of *d*, the depth of penetration

2.4.1. General

Calculation of the weld depth of penetration (*d*) is perhaps the most useful part of any model of this type insofar as industry is concerned. In this model the penetration depth is calculated as:

$$d = P_{abs} / P'_{av} \tag{8}$$

where P_{abs} is the total power absorbed in the keyhole (W) and P'_{av} is the average line-source strength (W m^{-1}). The average line-source strength P'_{av} is calculated as

$$P'_{av} = \frac{P'_T + P'_B}{2} \tag{9}$$

where P'_B, the line-source strength at the bottom of the weld, is calculated from equations (1) and (2), using $\lambda_{th} = \lambda_1$, $r = w_b/2$ and $T(r,\varphi) = T_m$. P'_T, the line-source strength at the top of the weld, is also calculated from equations (1) and (2), in this case by using $\lambda_{th} = \lambda_2$, $r = w_t/2$ and $T(r, \varphi) = T_m$. The power absorbed in the keyhole (P_{abs}) as well as the power losses will be explained in the following sections.

2.4.2. The power absorbed in the keyhole (P_{abs})

The total power absorbed by the keyhole, which is examined in detail in [1], can be expressed in the following way:

$$P_{abs} = P_{plasma1} + P_{1stFresnel} + P_{2ndFresnel} + P_{plasma2} \tag{10}$$

P_{abs} is, of course, a function of the laser power which enters the keyhole ($P_{keyhole}$):

$$P_{keyhole} = P - P_{plume} - P_{refl} \tag{11}$$

where P is the original laser power (W); P_{plume} is the amount of laser power absorbed by the plume of ionised plasma above the keyhole (W), estimated according to earlier work [1, 17, 18]; and P_{refl} is the amount of power reflected from the liquid and solid material surface surrounding the keyhole (W), calculated by beam integration.

Once $P_{keyhole}$ has been established the various components of equation (10) can be calculated as follows.

(i) $P_{plasma1}$ is the power absorbed by the plasma cloud in the keyhole which is re-radiated and absorbed by the workpiece:

$$P_{plasma1} = P_{keyhole} - P_{keyhole} \exp\left(-\alpha_{ib,plasma} \frac{d^*}{2}\right) \tag{12}$$

where $\alpha_{ib,plasma}$ is the absorption coefficient of the keyhole plasma (m^{-1}) and d^* is the penetration depth (m) (unknown but identified by the model after three or four calculation cycles).

(ii) $P_{1stFresnel}$ is the power absorbed by the keyhole as a result of Fresnel absorption. This absorption is dependent upon the angle of inclination of the keyhole wall, θ see figure 4. For ease of calculation an average value of θ is used by the model:

$$P_{1stFresnel} = \left(P_{keyhole} - P_{plasma1}\right)\alpha_{1stFresnel} \tag{13}$$

where $\alpha_{1stFresnel}$ is the Fresnel absorption coefficient for an average keyhole wall angle inclination of θ . Note that

$$\tan\theta = r_k / d^* \tag{14}$$

(iii) The laser power which impinges directly on the keyhole wall and is not absorbed as a part of the Fresnel absorption is reflected. This reflected energy undergoes multiple reflections in the keyhole, experiencing Fresnel absorption during each reflection. These absorptions are added together to give a value $P_{2ndFresnel}$:

$$P_{2ndFresnel} = \left(P_{keyhole} - P_{plasma1} - P_{1stFresnel}\right)\alpha_{mr,Fr} \tag{15}$$

where

$$\alpha_{mr,Fr} = 1 - \left(1 - \alpha_{Fresnel,\theta=90^\circ}\right)^{(n_{mr}-1)} \tag{16}$$

$$n_{mr} = \pi/(4\theta) \tag{17}$$

That is, the absorption coefficient for each reflection ($\alpha_{2ndFresnel}$) is assumed to be constant and equal to the value for normal incidence (θ = 90°). The average number of reflections experienced by reflected beams before they leave through the keyhole entrance is n_{mr}.

(iv) During the multiple reflections mentioned above the reflected part of the beam repeatedly passes through the plasma and some absorption takes place. The sum of this absorption is $P_{plasma2}$:

$$P_{plasma2} = \left(P_{keyhole} - P_{plasma1} - P_{1stFresnel} - P_{2ndfresnel}\right)\alpha_{mr,ib} \qquad (18)$$

where $\alpha_{mr,ib}$ is the absorption coefficient of the keyhole plasma:

$$\alpha_{mr,ib} = 1 - e^{-\alpha_{ib}s} \qquad (19)$$

where $s = 3d/2$, the mean path length of the reflected light [1].

Solving equations (12), (13), (15) and (18) gives us a value for P_{abs} which can be used in equation (8) to generate a value for d, the penetration depth.

3. RESULTS AND DISCUSSION

3.1. General considerations

In order to verify the model a number of experimental welds were produced using the parameters listed in table 1. The laser beam quality and focusing details are used in the model to calculate the incident beam diameter.

Table 1. Parameters used in the experiments and calculations.

Parameter	Symbol	Value	Unit
Laser power	P	1400	W
Wavelength	λ	10.6	μm
Polarisation	-	unpolarised	
Beam quality	M^2	2.0	
Beam mode	*TEM*	TEM_{00}	
Focal length	f	270	mm
Raw beam diameter	D	18	mm
Focusing number	F	15	-
Focal radius	r_{f0}	0.2	mm
Focal plane	z_0	0	mm
Welding speed	v	0.1 - 4.0	m/min
Material	-	austenitic stainless steel	-
Shielding gas	-	helium	-
Weld type	-	blind	-

3.2 The width of the bottom of the weld (w_b)

Figure 6 demonstrates the accuracy with which the model forecasts the width of the bottom of the weld. The average level of mismatch between the experimental and the theoretical results was only 8 %.

3.3. The width of the top of the weld (w_t)

Figure 7 shows that the model also has a high level of accuracy in forecasting the width of the top of the weld. The average mismatch between experimental and theoretical results is only 9 %. The importance of including a factor to compensate for thermocapillary flow is clearly demonstrated by the difference in accuracy of the two modelled lines. The line which ignores thermocapillary flow has a much larger average mismatch with the experimental results i.e. 37 %.

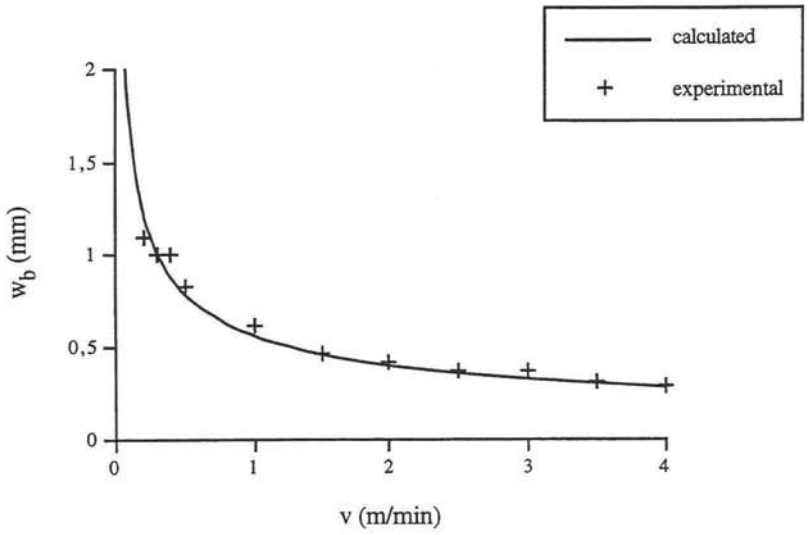

Figure 6. A comparison between the calculated and experimental values for the width of the bottom of the weld.

The use of an artificial thermal conductivity (λ_2) to compensate for thermocapillary flow is clearly supported by the accuracy of weld-width forecasting shown in figure 7. Figure 7 also justifies the choice of $\lambda_2 = 2.5\lambda_1$. The slope of the curve indicates that the effect of Marangoni flow in broadening the top of the weld diminishes as the welding speed increases. This makes sense because at the higher welding speeds there is less time available for thermocapillary stirring. This reduction in the lateral speed of the heat flow means that more energy is available to aid the penetration into the material.

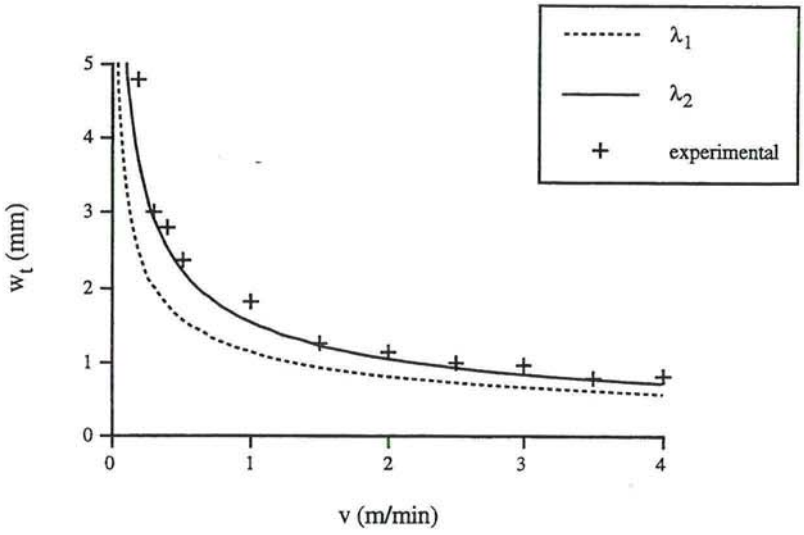

Figure 7. A comparison between the calculated and experimental values for the width of the top of the weld.

3.4. The depth of penetration (*d*)

Once again, there is a high level of agreement between the model and the experimental results (figure 8). The average mismatch between the two was only 7 %. The broken line demonstrates how the accuracy of the model would suffer if thermocapillary flow was ignored. At high welding speeds the two theoretical lines converge because thermocapillary flow has a diminishing influence on the heat distribution in the weld zone as the welding speed is increased. This reduction in lateral thermal flow is compensated for by an increase in vertical thermal flow and this leads to an improvement in the depth of penetration results.

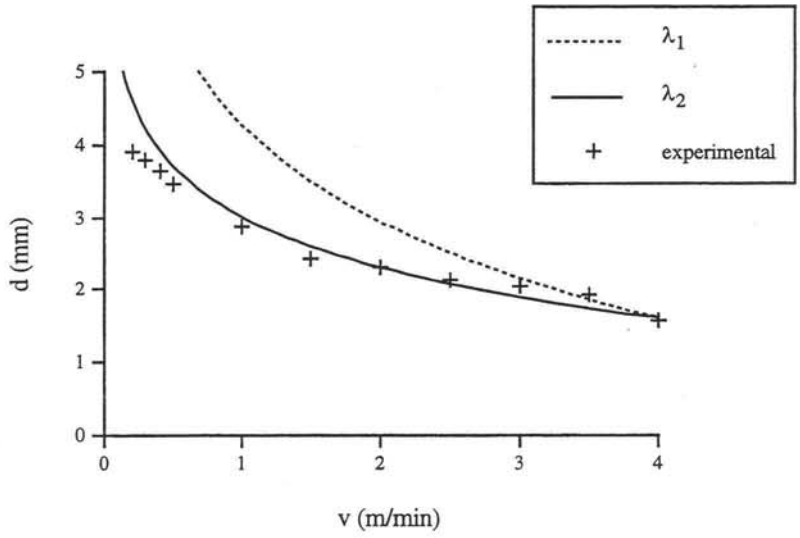

Figure 8. A comparison between the calculated and experimental values of the depth of penetration.

Figure 9 supports this point by showing that, as welding speeds are increased, there is a proportional decrease in the amount of material melted but the depth of penetration falls much more slowly. When the welding speed is increased by a factor of 16 (from 0.25 to 4.0 m min^{-1}) the area of the weld cross section falls by a factor of approximately 12 but the penetration depth is only reduced by a factor of approximately 2.6. This improvement in the efficiency of the process with increasing speed has been discussed in earlier work [12].

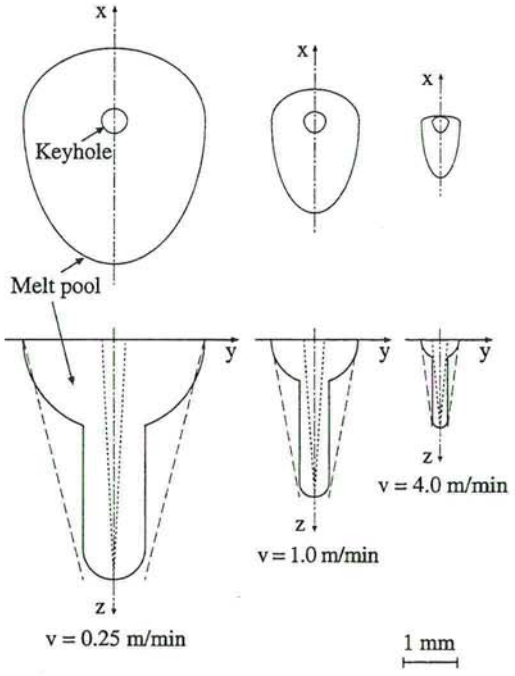

Figure 9. Theoretical weld pool shapes at different welding speeds using the model described in the paper.

4. CONCLUSIONS

A simplified version of an earlier model [1] can predict weld-bead dimensions with an accuracy of greater than 90 %. The width of the bottom of the weld (w_b) is calculated using standard values for the workpiece conductivity, λ_1. The width of the top of the weld (w_t), which is widened by thermocapillary flow, is calculated using an artificially high value for the thermal conductivity, λ_2. A suitable relationship between the two conductivities is $\lambda_2 = 2.5\ \lambda_1$. The penetration depth (d) is calculated by dividing the total power absorbed in the keyhole by the average line-source strength of the incident laser beam.

5. ACKNOWLEDGEMENTS

The authors would like to thank Professor D Schuöcker for his assistance and support. Thanks also to the Faculty Board at Luleå University of Technology for providing funding for travelling. The funding for this work was provided by the Swedish Research Council for Engineering Science (TFR) and by the Austrian Science Foundation (FWF) under grant no. P11384.

6. REFERENCES

1. Kaplan, A. (1994) A model of deep penetration laser welding based on calculation of the keyhole profile. Journal of Physics D: Applied Physics (27). pp. 1805-1814.
2. Beck, M., Dausinger, F. and Hügel, H. (1990) Modelling of Laser Deep Welding Processes. European Scientific Laser Workshop on Mathematical Simulation. Sep. 29-29 1989, Lissabon, Portugal. (Coburg: Sprechsaal).
3. Steen, W.M., Dowden, J., Davis, M. and Kapadia, P. (1988) A point and line source model of laser keyhole welding. Journal of Physics D: Applied Physics (21). pp. 1255-1260.
4. Dowden, J., Postacioglu, N., Davis, M. and Kapadia, P. (1987) A keyhole model in penetration welding with a laser. Journal of Physics D: Applied Physics (20). pp. 36-44.
5. Lankalapalli, K.N., Tu, J.F. and Gartner, M. (1996) A model for estimating penetration depth of laser welding. Journal of Physics D: Applied Physics (29). pp. 1831-1841.
6. Rosenthal, D. (1946) The Theory of Moving Sources of Heat and Its Application to Metal Treatments. Transactions of the A.S.M.E. (48). pp. 848-866.

7. Trappe, J., Kroos, J., Tix, C. and Simon, G. (1994) On the shape and location of the keyhole in penetration laser welding. Journal of Physics D: Applied Physics (27). pp. 2152-2154.
8. Kroos, J., Gratzke, U. and Simon, G. (1993) Towards a self-consistent model of the keyhole in penetration laser beam welding. Journal of Physics D: Applied Physics (26). pp. 474-480.
9. Dowden, J. and Kapadia, P. (1995) A mathematical investigation of the penetration depth in keyhole welding with continuous CO_2 lasers. Journal of Physics D: Applied Physics (28). pp. 2252-2261.
10. Kaplan, A.F.H. (1997) Surface processing with non-Gaussian beams. Applied Physics Letters (70). pp. 1-3.
11. Zacharia, T., David, S.A., Vitek, J.M. and Debroy, T. (1989) Weld Pool Development during GTA and Laser Beam Welding of Type 304 Stainless Steel, Part I - Theoretical Analysis. Welding Journal (68). pp. 499s-509s.
12. Lampa, C., Powell, J., Ivarson, A. and Magnusson, C. (1995) Factors Affecting the Efficiency of Laser Welding. Lasers in Engineering (4). pp. 73-83.
13. Tsai, M.C. and Kou, S. (1989) Marangoni Convection in Weld Pools with a Free Surface. International Journal for Numerical Methods in Fluids (9). pp. 1503-1516.
14. Sudnik, W., Radaj, D. and Erofeev, W. (1996) Computerized simulation of laser beam welding, modelling and verification. Journal of Physics D: Applied Physics (29). pp. 2811-2817.
15. Steen, W.M. (1991) Laser Materials Processing (Berlin: Springer).
16. Kreysig, E. (1988) Advanced Engineering Mathematics (New York: Wiley).
17. Beck, M., Kern, M., Berger, P. and Hügel, H. (1996) Einfluß der Plasmawolke auf Einkopplung und Prozeßstabilität beim Lasertiefschweißen mit CO_2-Lasern. Laser und Optoelektronik (28). pp. 72-78.
18. Beyer, E. (1995) Scweißen mit Laser (Berlin: Springer).

Paper VI

Laser Welding of Copper to Stainless Steel

Laser Welding of Copper to Stainless Steel

C. Lampa [*], J. Powell [*+], C. Magnusson [*]

[*] Division of Materials Processing
Luleå University of Technology
SE-97187 Luleå, Sweden

[+] Laser Expertise Ltd.
Harrimans Lane, Dunkirk
Nottingham NG7 2TR, UK

ABSTRACT

This paper investigates the possibility of CO_2 laser welding austenitic stainless steel to copper. The experimental results show that solidification cracking may be the greatest problem in this application. It is suggested that the cracks are generated in three ways:

- Liquid metal embrittlement, due to the presence of copper in the solidifying steel grain boundaries.
- Stresses generated during solidification due to fixturing and differences in the thermal properties of the materials involved.
- A solidification mode change due to the rapid weld solidification involved in laser welding of austenitic stainless steel.

To overcome these problems the fixturing and specimen edge preparation have to be optimised to minimise the amount of copper in the fusion zone, to reduce the stresses, and to minimise the cooling rate during solidification. These factors were taken into account and the resulting welds were of high integrity with the same strength as the original copper being welded. The role of thermocapillary or Marangoni flow in transferring heat to the copper side of the weld is also discussed.

1. INTRODUCTION

1.1. General

This paper covers the results of an investigation into the laser welding of copper tubes to tubes of austenitic stainless steel. In service, the tubes and the welds have to withstand different kinds of corrosive media at various pressures and dynamic stresses. This means that the welds have to be of a very high quality. The experimental investigation has been divided into two parts. In the first part, plates of copper and stainless steel were welded together, and in the second, tubes of the different metals were joined. To evaluate the quality of the welds a number of different examinations were carried out i.e.: tensile tests, fatigue tests, microhardness measurements, metallographic investigations and leak tests.

Electron beam welding (EBW) of copper to stainless steel has already been shown to be successful [1], but the process needs to be carried out in vacuum or near vacuum conditions, which makes it complicated and expensive, especially for large scale work. Laser welding of copper to stainless steel has briefly been investigated by others [2-4], but there is still a lot to be discovered about the process if it is to be used for industrial applications.

1.2. Solidification cracking when welding austenitic stainless steels

In general, when laser welding austenitic stainless steels, solidification cracks in the fusion zone can be a problem. This is due to the rapid weld solidification, which may change the mode of solidification from duplex ferrite + austenite to fully austenitic. A number of theories have been put forward for this beneficial effect of the presence of ferrite, e.g.:

a) reduced volume contraction on solidification.

b) preferential dissolution of impurity elements in ferrite.

c) increases in phase boundary area which helps to distribute crack promoting elements more widely. This also avoids the formation of liquid regions of very low melting point [5].

It should also be pointed out that ferrite is softer and has a higher ductility than austenite. This in turn may have a positive influence on the crack sensitivity of the material. Predictions of the weld microstructure for conventional welding methods can be made by reference to the Schaeffler diagram [6] or the Welding Research Council (WRC) diagram [7], using the Cr and Ni equivalents for the steels involved. For laser welding these diagrams are no longer valid for predicting the weld microstructure due to the fast cooling rates involved. Work has been carried out to modify the conventional Schaeffler diagram for different cooling rates [8]. Other work [9, 10] shows that a high solidification rate together with a low Cr_{eq}/Ni_{eq} ratio will support a fully austenitic solidification mode and therefore increase the possibility of solidification cracking. From these results the welding speed employed could be used as an upper limit of the solidification rate [9].

According to the WRC [7], the Ni_{eq} is calculated as:

$$Ni_{eq} = Ni + 35C + 20N + 0.25Cu \quad (1)$$

while the Cr_{eq} is calculated as:

$$Cr_{eq} = Cr + Mo + 0.7\ Nb \quad (2)$$

As can be seen from these formulae, the Ni_{eq} is affected by the copper content of the material. This point is obviously important when considering a welded joint between stainless steel and copper alloys.

1.3. The effect of copper on laser welding of stainless steel

In the previous section it was established that solidification cracking is encouraged by reducing the Cr_{eq}/Ni_{eq} ratio or by increasing the weld solidification rate. Unfortunately copper has both of these effects when it is welded to stainless steel. The Cr_{eq}/Ni_{eq} ratio is reduced by an increase in the Ni_{eq} value with the addition of copper (see equation (1)) and the weld solidification rate is increased because copper has a much higher thermal conductivity than stainless steels [11]. The distribution of alloying elements in laser welding is not diffusion controlled. Due to the rapid heating and solidification involved in the process, there is insufficient time for any significant diffusion to take place. The distribution of alloying elements, in this case copper, is strongly related to the material flow within the melt pool. During laser welding the melt is vigorously stirred as a result of thermocapillary or Marangoni flow.

This type of flow is a result of the severe thermal gradients which exist in the melt (i.e. the melt is at its melting point at the solid-liquid boundary and at its boiling temperature in the keyhole which is only one or two millimetres away). These thermal gradients give rise to surface tension gradients which generate the stirring of the pool, see figure 1. It has been suggested [12] that the melt pool rotates approximately five times before it solidifies. When welding stainless steel to copper this Marangoni flow is employed to transfer heat to the interface between the workpiece as the copper is not directly irradiated by the laser beam (see figure 2).

So far, some of the metallurgical factors of weld solidification cracking have been described. However, without stresses acting on the solidifying material, no cracking can occur [13]. Such stresses may arise from thermal contraction or solidification shrinkage or both. The relatively high thermal expansion coefficient of austenitic stainless steel makes it prone to solidification cracking. When two materials with different thermal properties such as copper and stainless steel are joined the stresses may become even larger.

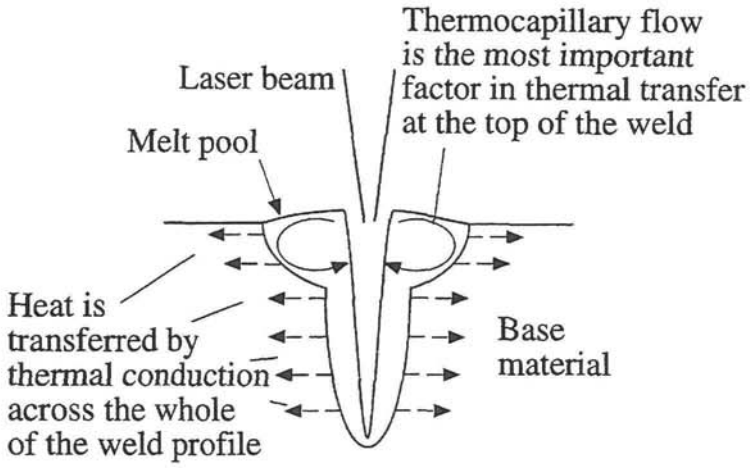

Figure 1. Thermocapillary or Marangoni flow which generates vigorous stirring action in the melt.

2. EXPERIMENTAL PROCEDURE

The experimental program for this work was divided up as follows:

Part I; welding of flat plates
Materials: 1 mm thick copper (SS 5015) welded to 1.5 mm thick austenitic stainless steel (ASTM 304 L). Welding speed: 1 m/min. Laser power: 1300 W. Mirror focal length: 270 mm (focus on surface of material). Shielding gases: Argon, Helium and Nitrogen. The experimental set up is shown in figure 2.

Part II; welding of tubes
Materials: 0.8 mm wall thickness copper tubes welded to 0.7 mm wall thickness stainless steel tubes (ASTM 304 L). Welding speed: 0.5 - 1.0 m/min. Laser power: 600-830 W. Mirror focal length: 127 mm (focus on surface of material). Shielding gases: Argon, Helium and Nitrogen. Two experimental jigs were investigated, these are shown in figures 3 and 4.

General note
Due to the high reflectivity of copper successful welds can only be achieved by focusing the laser on the stainless steel side of the joint. Energy is transferred to the copper by contact with the stainless steel melt pool thus established.

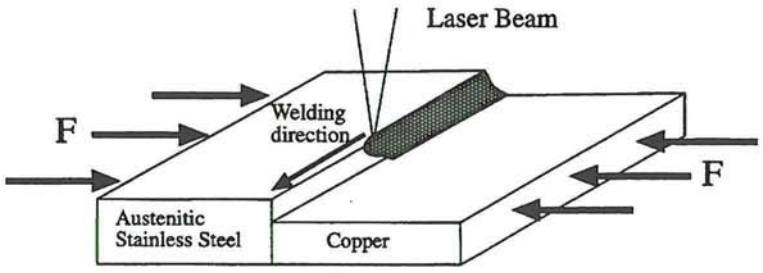

Figure 2. Schematic of the experimental set-up when welding plates. Note that the laser irradiates only the stainless steel side of the interface.

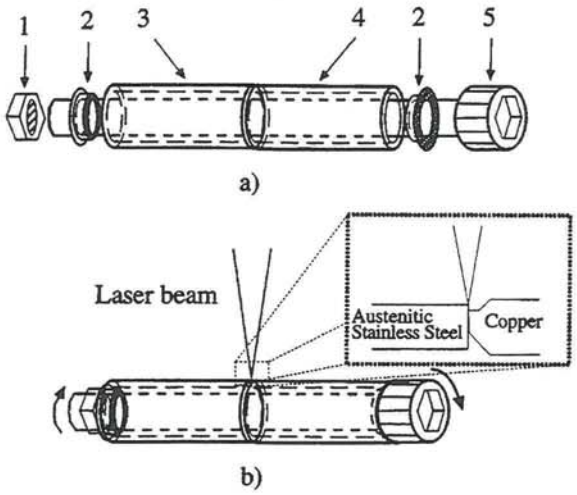

Figure 3. Experimental set-up when welding tubes, run 1. a) Schematic definition of the different parts in the fixture: **1.** Bolt, **2.** Support flanges, **3.** Austenitic stainless steel tube, **4.** Copper tube, **5.** Screw. b) Schematic of the welding procedure and an enlargement of the weld zone. The screw is put through the tube and the support flanges before it is tightened to the bolt. This fixture did not allow the welded parts to contract during solidification.

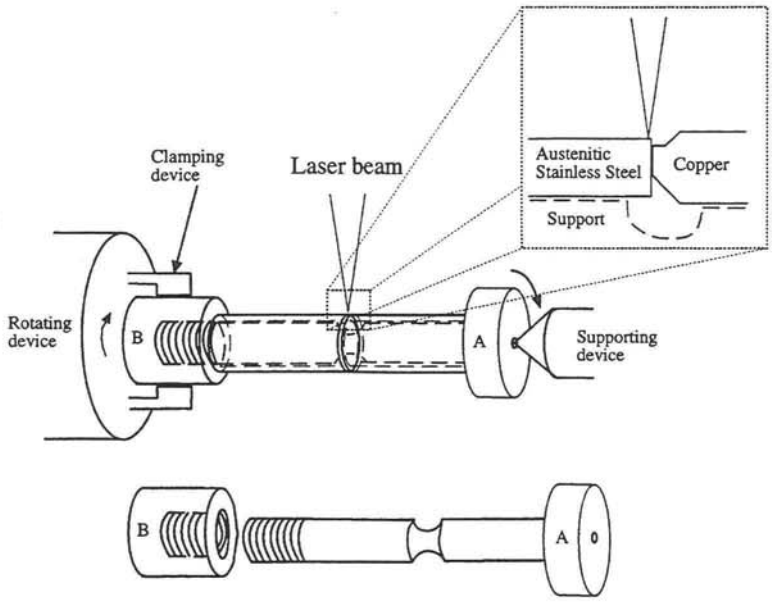

Figure 4. Experimental set-up when welding tubes, run 2. Improved support where part A is put through the tubes to be welded before it is screwed into part B. This fixture allowed the welded parts to contract during solidification

3. EXPERIMENTAL RESULTS

3.1. Plate welding

The first stage of the experimental work involved an investigation into the welding together of stainless steel and copper plate. After welding the samples were subject to metallographic examination, hardness tests and tensile testing. The results are as follows:

3.1.1. Metallographic examination and hardness testing

Figures 5 (a), (b) and (c) show typical weld cross sections together with their hardness profiles for welds completed using each of the shielding gases (helium, nitrogen and argon). The results all show a narrow weld bead ($\approx$ 0.5 mm) with a hardness similar to that of the stainless steel. The micrographs clearly illustrate the stirring effect of thermocapillary flow mentioned earlier. In this case this flow has two major effects:

a) It transports heat from the centre of the weld to the copper-stainless steel interface which produces a molten joint.

b) It distributes the molten copper throughout the weld pool.

During the metallographic examination it was noted that solidification cracks could be avoided if argon or nitrogen were employed as the shielding gas. When helium was used, solidification cracks were apparent in many of the samples. This increase in the presence of cracks could be attributed to the narrower welds which can be achieved by using helium rather than argon or nitrogen. These narrower welds have less melt volume and therefore higher solidification rates which would increase cracking susceptibility. The reasons why narrower welds are produced when using helium as shielding gas are as follows: Above any laser weld pool there is a cloud of vapour and gas which absorbs some of the incident laser energy. This energy is then re-radiated in all directions as if from a point source (see figure 6) whilst the remaining laser energy penetrates into the weld and acts much more like a line source. The ratio of the powers of the two sources determines the width of the eventual weld [14, 15]. If the shielding gas ionises easily it will promote the absorbtivity of the gas cloud above the weld and the point source will become more powerful. In this case (e.g. with nitrogen or argon) a wider weld will be the result. When the shield gas is more difficult to ionise (e.g. helium) the effect of the point source is reduced and narrower welds are the result.

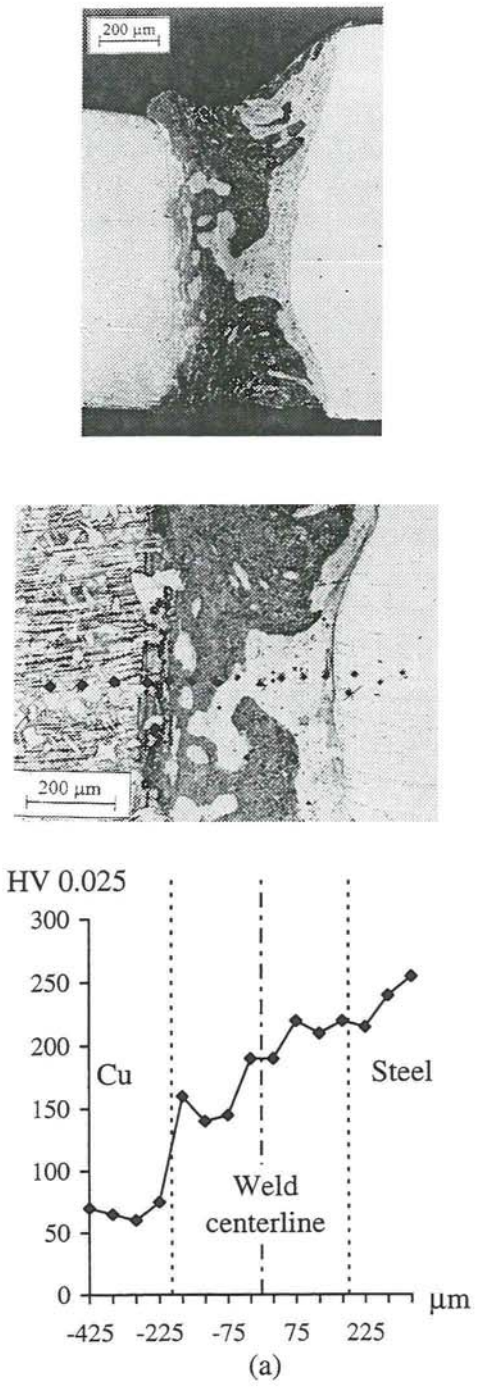

Figure 5 (a). Weld cross sections and hardness profile using helium as shielding gas.

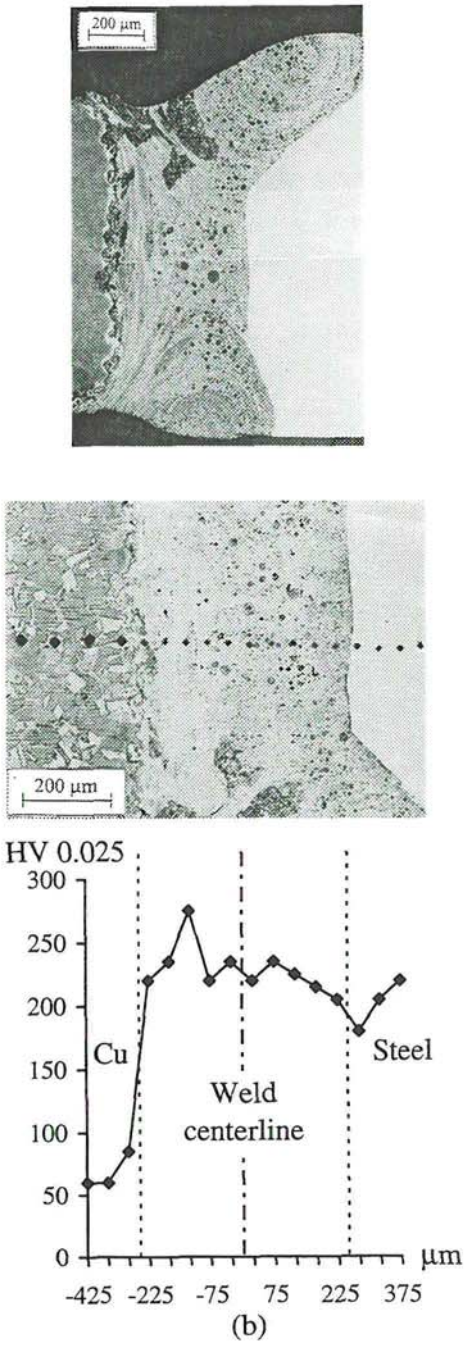

Figure 5 (b). Weld cross sections and hardness profile using nitrogen as shielding gas.

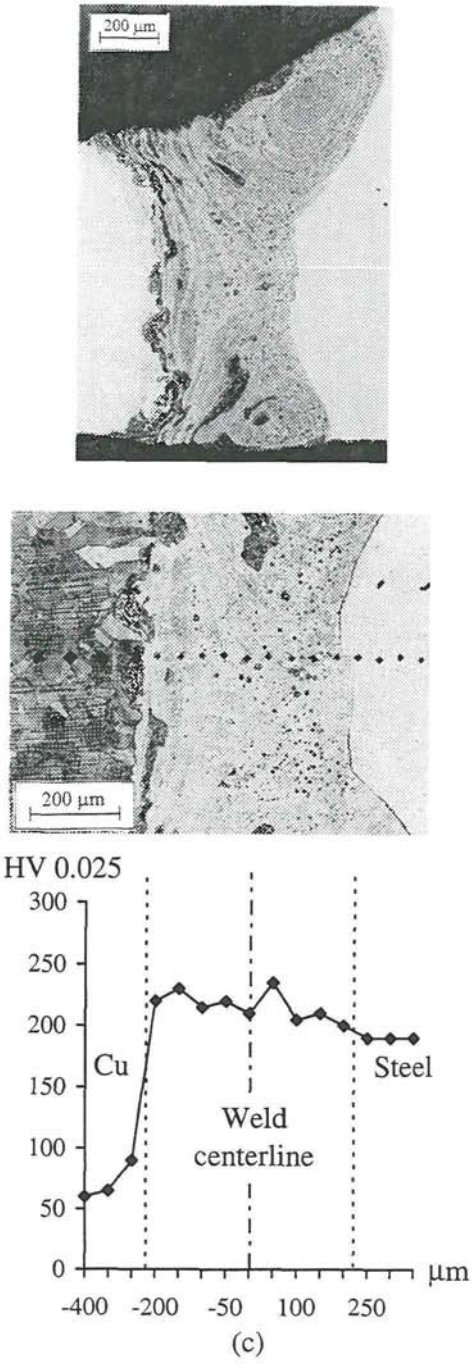

Figure 5 (c). Weld cross sections and hardness profile using argon as shielding gas.

3.1.2. Tensile testing

The tensile test results presented in table 1 demonstrate that in all cases the welds failed in the copper plate rather than in the weld zone. None of the weld strengths were lower than that of the copper alloy.

Table 1. Tensile tests of welded specimens

Specimen	Shield gas	Tensile strength (N/mm^2)	Elongation (%)	Fracture position
A	Argon	249	4.0	in Cu plate
B	Argon	249.8	4.3	in Cu plate
C	Helium	252.6	4.5	in Cu plate
D	Helium	250	4.0	in Cu plate
E	Nitrogen	242.4	6.9	in Cu plate
F	Argon	250.2	3.8	in Cu plate
G	Argon	250.7	4.5	in Cu plate
H	Helium	239.7	6.9	in Cu plate
I	Helium	242.2	8.3	in Cu plate
J	Nitrogen	243.7	3.6	in Cu plate
K	Nitrogen	248.5	5.1	in Cu plate

Note: Tensile strength of stainless steel used: min 460 N/mm^2. Tensile strength of copper used: min 220 N/mm^2

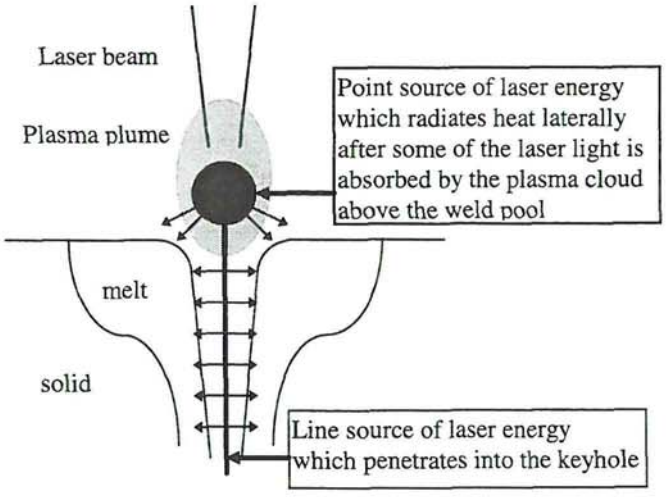

Figure 6. A schematic demonstrating the combined point and line source model of laser welding.

3.2. Tube welding

The first run of welds carried out on the tubes resulted in welds which were extensively cracked. This increase in the level of cracking compared to the plate welds was attributed to a number of factors:

1) The change in grade of stainless steel resulted in a reduction in the Cr_{eq}/Ni_{eq} ratio from 1.9 to 1.7.
2) In the case of the plate welds the thickness of the copper was 67 % of that of the stainless steel. When the tubes were welded the copper thickness was 114 % of that of the stainless steel. This higher proportion of copper substrate adjacent to the weld would result in higher cooling and solidification rates. It also makes it likely that more copper will enter the weld pool.
3) The jig used, see figure 3, did not adequately prevent misalignment of the two tubes. Also the jig did not allow the parts to pull together during solidification which added to the stress implied.

Typical micrographs of a cracked weld are presented in figure 7. The crack shown is intergranular across a copper rich zone. An EDX scan of the area revealed copper contents in the 10-20 wt % range. The successful welds produced in the final experimental run had copper contents below 5 wt %. As this investigation was intended to identify the usefulness of laser welding for tubular copper and stainless steel, leakage tests are of great importance. The limit of leakage allowed was 10^{-5} mbl/s when pressurised with helium at 35 bar. This first batch of welds failed this criterion because the presence of solidification cracks.

A second batch of tubular samples were subsequently welded which had minimal cracks present and leaked at below the limit stipulated above. These welds were successful (see figure 8) because the following steps were taken:

1) Argon was the only shielding gas employed. Helium was rejected because it resulted in narrow welds with their associated higher solidification rates. Nitrogen was also considered inferior because it is reported to reduce the formation of delta ferrite during solidification [16, 17].

2) An improved fixture was produced, see figure 4, which improved the alignment of the tubes and allowed the tubes to move together during solidification (thus minimising stresses).

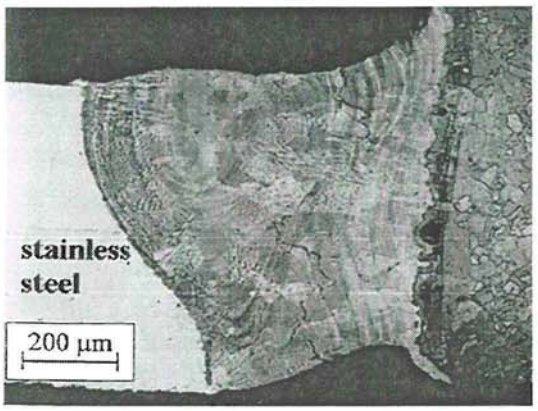

(a)

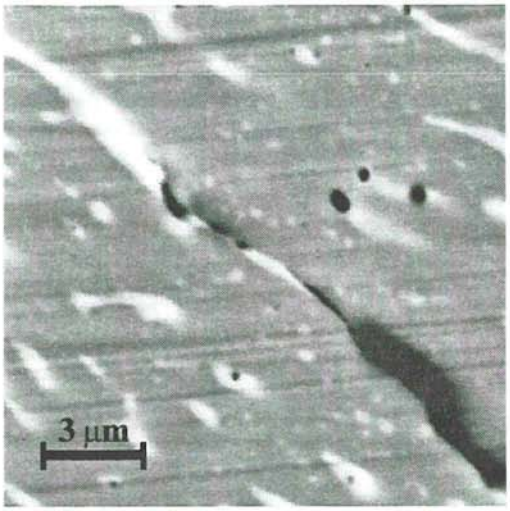

(b)

Figure 7. Micrographs of a cracked weld: (a) weld cross section. (b) bright areas are copper rich.

3) The weld zone was positioned further from the copper-stainless steel interface. In the earlier run the laser interface distance had been 0.1 mm. It was now increased to 0.4 - 0.5 mm. The action of Marangoni flow in distributing heat and molten material in the lateral direction thus became vital for the production of a sound weld. Laser-interface misalignment welding of this type has been successfully utilised when welding other dissimilar metal combinations as a method of tailoring the metals mixture in the weld [18]. Care must be taken when using the technique as it is possible to over-widen the misalignment and produce welds which are incomplete.

Table 2 outlines the range of process parameters which resulted in successful leak free welds. In one case preheating of the workpieces was tried as a method of reducing stresses and solidification rates. Although this could be a useful technique in other, more critical, applications there was no observed benefit in this case.

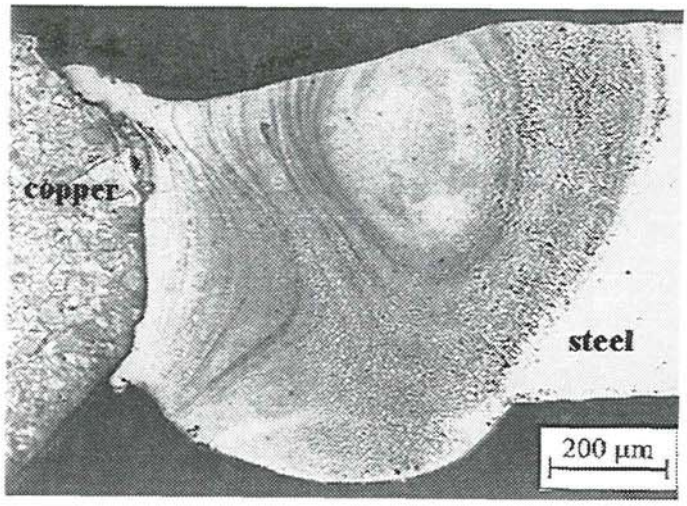

Figure 8. Micrograph of a successful tube weld. Laser power: 830 W (CW), welding speed: 0.5 m/min, shielding gas: argon.

Table 2. Welding parameters for welds passing leakage tests

Power (W)	Welding speed (m/min)	Ar flow (l/min)	Pre-heating (°C)	Pulse frequency (Hz)	Pulse duration time (ms)
830	1.0	24	300	CW	CW
830	1.0	5	-	200	80
830	1.0	5	-	CW	CW
830	0.5	5	-	CW	CW
830	1.0	5	-	50	80

4. CONCLUSIONS

1) Laser welding copper to stainless steel components is technically and commercially feasible.

2) Laser-interface misalignment must be optimised to produce a complete weld without excessive dilution of the melt with copper.

3) Thermocapillary or Marangoni flow is responsible for the lateral spread of the stainless steel melt and the eventual contact melting of the copper.

4) Argon is the preferred weld shroud gas. Helium does not ionise sufficiently in the plasma above the weld and hence aids the production of a narrow weld with insufficient Marangoni flow. Nitrogen may increase the susceptibility to solidification cracking in laser welding of austenitic stainless steels as it suppresses the formation of delta ferrite.

5. ACKNOWLEDGEMENTS

The authors would like to thank Danfoss A/S Nordborg, Denmark for their co-operation in the tube welding part of the project. Thanks also to Mr Johnny Grahn, Luleå University of Technology, for his help with the scanning electron microscopy and to Mrs Elli Grau, Danfoss A/S, for sample preparations.

6. REFERENCES

1. Metzger, G. and Lison, R. (1976) Electron Beam Welding of Dissimilar Metals. Welding Journal (55). pp. 230s-240s.
2. Gopinathan, S., Murthy, J., McCay, T.D. and McCay, M.H. (1994) Microstructural Evaluation of Laser Welded Copper-Stainless Steel Welds. Conf. Proc. of Laser Materials Processing Symposium, ICALEO'93. Oct. 24-28 1993, Orlando FL, USA. pp. 661-671.
3. Dell'Erba, M., Sforza, P., Chita, G. and Cento, L. (1987) Welding Copper to Steel by CO_2 Laser. Conf. Proc. of Laser Materials Processing Symposium, ICALEO'86. Nov. 10-13 1986, Arlington VI, USA. pp. 57-62.
4. Bergmann, H.W., Endres, T. and Müller, D. (1992) High Power Laser Welding of Microstructure Sensitive and Dissimilar Materials. Conf. Proc. of Laser Treatment of Materials, ECLAT'92. Gottingen, Germany. pp. 157-162.
5. Gooch, T.G. (1990) Solidification Cracking of Austenitic Stainless Steels. Conf. Proc. of Materials Weldability Symposium. Oct. 8-12 1990, Detroit MI, USA. pp. 31-40.
6. Schaeffler, A.L. (1949) Constitution Diagram for Stainless Steel Weld Metal. Metal Progress (56). pp. 680-681.
7. Kotecki, D.J. and Sievert, T.A. (1992) WRC-1992 Constitution Diagram for Stainless Steel Weld Metals: A Modification of the WRC-1988 Diagram. Welding Journal (71). pp. 171s-178s.
8. Nakao, Y., Nishimoto, K. and Zhang, W-P. (1988) Effects of Rapid Solidification by Laser Surface Melting on Solidification Modes and Microstructures of Stainless Steels. Transactions of the Japan Welding Society (19). pp. 20-26.
9. Lippold, J.C. (1994) Solidification Behavior and Cracking Susceptibility of Pulsed-Laser Welds in Austenitic Stainless Steels. Welding Journal (73). pp. 129s-139s.
10. David, S.A., Vitek, J.M. and Hebble, T.L. (1987) Effect of Rapid Solidification on Stainless Steel Weld Metal Microstructures and Its Implications on the Schaeffler Diagram. Welding Journal (66). pp. 289s-300s.
11. Pehlke, R.D., Jeyarajan, A. and Wada, H. (1982) Summary of Thermal Properties for Casting Alloys and Mold Materials. National Science Foundation. NSF/MEA-82028.
12. Steen, W.M. (1991) Laser Materials Processing. (Berlin: Springer).
13. Kou, S. (1987) Welding Metallurgy. (New-York: Wiley).

14. Steen, W.M., Dowden, J., Davis, M. and Kapadia, P. (1988) A Point and Line Source Model of Laser Welding. Journal of Physics D: Applied Physics (21). pp. 1255-1260.
15. Ducharme, R., Kapadia, P., Lampa, C., Ivarson, A., Powell, J. and Magnusson, C. (1996) A Point and Line Source Analysis of the Laser Material Interaction in Hyperbaric Keyhole Laser Welding. Proc. of the Laser Materials Processing Conference, ICALEO'95. Nov. 13-16 1995, San Diego CA, USA. pp. 1018-1027.
16. Okagawa, R.K., Dixon, R.D. and Olson, D.L. (1983) The Influence of Nitrogen from Welding on Stainless Steel Weld Metal Microstructures. Welding Journal (62). pp. 204s-209s.
17. Suutala, N. (1982) Effect of Manganese and Nitrogen on the Solidification mode in Austenitic Stainless Steel Welds. Metallurgical Transactions A (13A). pp. 2121-2130.
18. Lampa, C., Sarady, I., Powell, J., Mattson, J. and Magnusson, C. (1993) Laser Welding of Dissimilar Metals. Proceedings of the 4th Conference on Laser Materials Processing in the Nordic Countries, NOLAMP'4. Aug. 16-18, 1993, Sønderborg, Denmark. pp. 215-224.

Paper VII

The Effect of Process Speed on Energy Redistribution in Deep Penetration CO_2 Laser Welding

The Effect of Process Speed on Energy Redistribution in Deep Penetration CO_2 Laser Welding

C. Lampa [+], A.F.H. Kaplan [*], J. Powell [#+], C. Magnusson [+]

[+] Division of Materials Processing
Luleå University of Technology
SE-97187 Luleå, Sweden

[*] Department of Laser Technology
Vienna University of Technology
Arsenal Objekt 207, A-1030 Vienna, Austria

[#] Laser Expertise Ltd.
Harrimans Lane, Dunkirk
Nottingham NG7 2TR,UK

ABSTRACT

This work discusses energy absorption mechanisms in CO_2 laser welding and how they are affected by changes in the process speed. Two main energy absorption processes govern the welding interaction:

(i) Fresnel absorption at the keyhole walls.

(ii) Absorption by the partially ionised metal vapour (or plasma) in the keyhole (laser energy absorbed in this way is re-radiated or conducted to the keyhole walls).

A theoretical model of these absorption mechanisms has been developed and shown to agree closely with experimental results. Fresnel absorption has been identified as being dominant over plasma absorption and becomes even more influential as welding speeds are increased.

1. INTRODUCTION

At high power densities lasers are capable of deep penetration laser welding. During the process the laser acts as a moving line source of energy travelling through the workpiece in the welding direction. The line source welding mechanism is made possible by the generation of a keyhole which

penetrates into the material. This keyhole takes the form of a narrow deep hole of vapour surrounded by molten metal. A schematic of deep penetration laser welding is shown in figure 1.

In the keyhole CO_2 laser radiation is absorbed by one of two mechanisms [1-3]:

(i) Fresnel absorption
(ii) Plasma absorption

These two absorption mechanisms act simultaneously and will be discussed in the following sections.

Earlier theoretical work [1] has indicated a reduction in absorption with increasing welding speed. This model was subsequently developed [4] and the present paper is an extension of that work. The model estimates the heat conduction from a moving line source of heat. An energy balance which takes into account the laser beam intensity distribution is used to calculate the keyhole dimensions.

Not all the incident laser power contributes to the welding process. Non contributing power can be described as losses. These power losses will be discussed in the final part of the following theoretical discussion.

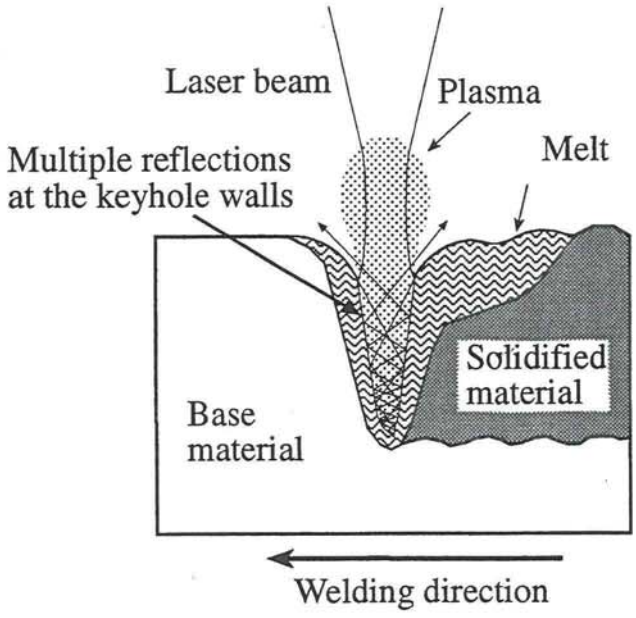

Figure 1. Schematic of the deep penetration laser welding process.

2. THEORETICAL DISCUSSION

2.1. General

Laser energy is absorbed in the keyhole by Fresnel and Plasma absorption. The laser beam experiences multiple reflections off the molten walls of the keyhole and during each of these reflections, part of the beam is absorbed by Fresnel absorption. Throughout the process a portion of the beam is being continuously absorbed by the keyhole plasma, the partially ionised metal vapour which fills the keyhole. Energy absorbed by the plasma is re-radiated and conducted to the keyhole walls.

A proportion of the incident laser power is lost to the welding process by the following routes:

(i) The plasma extends above the top of the keyhole (see figure 1) and some laser energy is absorbed in this zone before it reaches the keyhole.
(ii) Some incident laser light could be reflected off the unmelted workpiece surface just in advance of the weld pool.
(iii) A small proportion of the incident energy completes the cycle of multiple reflections and is eventually reflected out of the keyhole (see figure 1).

These absorption and energy loss mechanisms will now be discussed in detail.

2.2. Fresnel absorption

The Fresnel absorption coefficient is dependent on the angle between the incoming laser light and the absorbing surface, in this case the keyhole wall, see figure 2 for steel.

The Fresnel absorption coefficient for laser light of circular polarisation (α_{Fr}) is a combination of the Fresnel absorption coefficient for laser light of parallel ($\alpha_{Fr,p}$) and perpendicular ($\alpha_{Fr,s}$) polarisation [5]:

$$\alpha_{Fr} = \frac{\alpha_{Fr,p} + \alpha_{Fr,s}}{2} \qquad (1)$$

The absorption coefficients for perpendicular and parallel polarisation to the plane of incidence are calculated as:

$$\alpha_{Fr,p} = \frac{4n\sin\theta}{\left(n^2+k^2\right)\sin^2\theta + 2n\sin\theta + 1} \tag{2}$$

and

$$\alpha_{Fr,s} = \frac{4n\sin\theta}{n^2+k^2+\sin^2\theta+2n\sin\theta} \tag{3}$$

where n is the refractive index of the material, k is the extinction coefficient of the material and θ is the beam-workpiece inclination angle.

The refractive index consists of a real part and a complex part which are both derived from electrical conductivity according to Drude's theory. The refractive index and the extinction coefficient are calculated for CO_2 radiation as [2]:

$$n = k = \sqrt{\frac{\sigma_{el}}{4\pi\varepsilon_0}\cdot\frac{2\pi}{\omega}} = \sqrt{\frac{\sigma_{el}}{2\varepsilon_0\omega}} \tag{4}$$

where σ_{el} is the electric conductivity (A $V^{-1}m^{-1}$) which is temperature dependent, ε_0 is the dielectric constant (As $V^{-1}m^{-1}$) and ω is the angular frequency of the CO_2 laser radiation ($1.78*10^{14}$ rad s^{-1}).

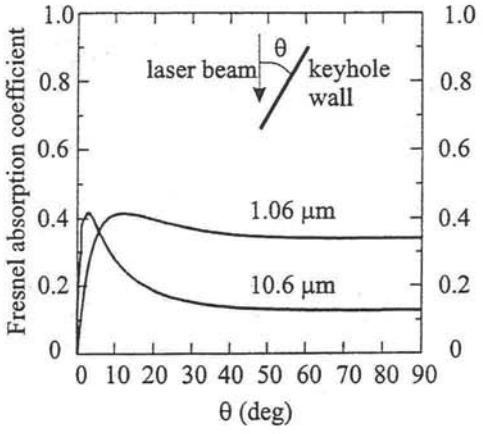

Figure 2. Fresnel absorption as a function of the angle of the keyhole wall. Circular polarised laser light of 10.6 μm and 1.06 μm wavelength. Material: steel [2].

While the absorbtivity for perpendicular polarisation decreases with decreasing inclination angle, the absorbtivity at parallel polarisation shows a strong maximum at the so-called Brewster angle, the angle of incidence where the reflected and refracted rays are perpendicular to each other [6] (see figure 3). In metals the Brewster maximum is found near 0°, however the value of the Brewster angle is also dependent on the wavelength of the incident light. With decreasing wavelength a shift to higher angles of incidence is observed [5] as shown in figure 2.

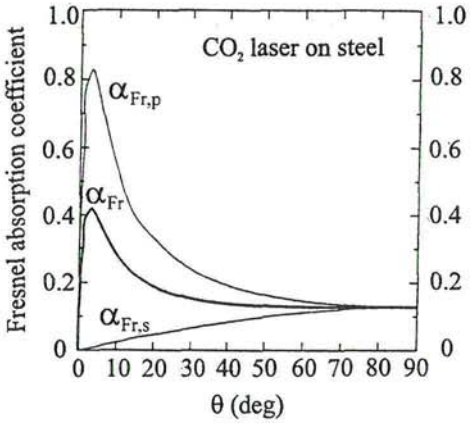

Figure 3. The polarisation dependence of Fresnel absorption [2].

2.3. Plasma absorption

Due to the high temperatures involved in laser processing, the keyhole contains an ionised vapour or plasma which absorbs laser light. This absorption is due to the inverse Bremsstrahlung effect which is significant at wavelengths greater than approximately 5 μm. Plasma absorption is volumetric and can be described by Beer-Lambert's law [7]:

$$P_a = P_0\left(1 - \exp\left(-\alpha_{iB} z\right)\right) \tag{5}$$

where P_a is the laser power (W) absorbed when passing through a path length z (m), P_0 is the incident laser power, α_{iB} is the plasma absorption coefficient due to inverse Bremsstrahlung (m^{-1}) and z is the beam path length (m).

The plasma absorption coefficient, α_{iB} , for welding with CO_2-lasers can be approximated as [3]:

$$\alpha_{iB} \approx 1.5 \cdot 10^{-35} n^2{}_e T_e^{-\frac{3}{2}} \qquad (6)$$

where n_e is the particle density of electrons (m^{-3}) and T_e is the electron temperature in eV (1 eV = 11 600 K).

Equation (6) demonstrates that the plasma absorption coefficient due to inverse Bremsstrahlung, α_{iB}, is temperature dependent and this is shown in figure 4 [8] for various mixtures of iron plasma and a helium shielding gas. For pure iron plasma there is a maximum peak in absorption around 13 000 K which is explained by the following: The laser light interacts mainly with free electrons and the absorption coefficient increases with temperature because of the increased degree of ionisation. However at increasing temperatures, reaching the level of almost complete first ionisation, the overall density of the plasma decreases more rapidly than the electron density increases. Inert gases such as helium reduce the level of ionisation and resultant absorption because they have a high ionisation energy.

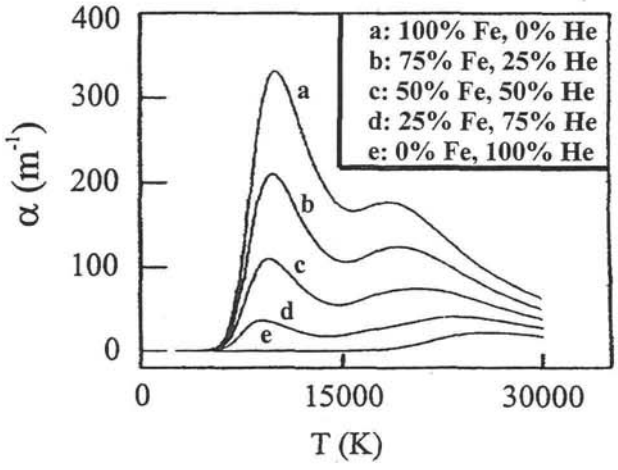

Figure 4. Plasma absorption coefficient as a function of temperature for different iron-helium plasma mixtures: a) 100% Fe, 0 % He, b) 75% Fe, 25% He, c) 50% Fe, 50% He, d) 25% Fe, 75% He, e) 0% Fe, 100% He [8].

The temperature field inside the keyhole has been calculated by Kaplan [1, 2] and shown to experience high temperature gradients. This lead to large variations in local plasma absorption coefficients. The temperature near the keyhole wall is too low to give any detectable absorption. The central zone of the keyhole also has a low absorption coefficient, in this case because of the high temperature and related low overall plasma density. In between these two zones there is a relatively thin layer with a high absorption coefficient. It has been shown [1] that in the keyhole the absorption reaches values in the range of 50-200 m^{-1} for steels interacting with CO_2 laser light, with an average value of the order of $100m^{-1}$.

2.4. Power absorbed by the keyhole

The total power absorbed by the keyhole, P_{abs} , can be expressed in the following way [4]:

$$P_{abs} = P_{plasma1} + P_{1stFresnel} + P_{2yFresnel} + P_{plasma2} \tag{7}$$

The components in (7) are explained by the following:

$P_{plasma1}$: The power absorbed by the plasma cloud in the keyhole which is re-radiated or conducted to the workpiece;

$$P_{plasma1} = P_{keyhole}\left(1 - \exp\left(-\alpha_{iB,plasma}\frac{d^*}{2}\right)\right) \tag{8}$$

where $P_{keyhole}$ is the power that enters the keyhole (W), $\alpha_{iB,plasma}$ is the absorption coefficient of the keyhole plasma (m^{-1}) and d^* is the penetration depth (m).

$P_{1stFresnel}$: The power absorbed by the keyhole as a result of Fresnel absorption. This absorption is dependent upon the angle of inclination of the keyhole wall θ [1, 2, 4]. For ease of calculation an average value of θ is used by this model;

$$P_{1stFresnel} = \left(P_{keyhole} - P_{plasma1}\right)\cdot\alpha_{1stFresnel} \tag{9}$$

where $\alpha_{1stFresnel}$ is the Fresnel absorption coefficient for an average keyhole wall angle inclination of θ .

$P_{2yFresnel}$: Laser power which impinges directly on the keyhole wall and is not absorbed as a part of the Fresnel absorption is reflected. This reflected energy undergoes multiple reflections in the keyhole experiencing Fresnel absorption during each reflection. These absorptions are added together to give a value $P_{2yFresnel}$;

$$P_{2yFresnel} = \left(P_{keyhole} - P_{plasma1} - P_{1stFresnel}\right) \cdot \alpha_{mr,Fr} \tag{10}$$

where:

$$\alpha_{mr,Fr} = 1 - \left(1 - \alpha_{Fresnel,\theta=45^\circ}\right)^{(n_{mr}-1)} \tag{11}$$

and

$$n_{mr} = \frac{\pi/2}{2 \cdot \theta} \tag{12}$$

i.e. the absorption coefficient for each reflection ($\alpha_{2yFresnel}$) is assumed to be constant and equal to the value for $\theta = 45°$. The average number of reflections experienced by the beam before it leaves through the keyhole entrance is n_{mr}.

$P_{plasma2}$: During the multiple reflections mentioned above the reflected part of the beam repeatedly passes through the plasma and some absorption takes place. The sum of this absorption is $P_{plasma2}$;

$$P_{plasma2} = \left(P_{keyhole} - P_{plasma1} - P_{1stFresnel} - P_{2yFresnel}\right) \cdot \alpha_{mr,iB} \tag{13}$$

where $\alpha_{mr,iB}$ is the absorption coefficient of the keyhole plasma:

$$\alpha_{mr,iB} = 1 - e^{-\alpha_{iB} \cdot s} \tag{14}$$

where: $s = 3d^*/2$, the mean path length of the reflected light [1, 2, 4].

Solving equations (8), (9), (10) and (13) gives us a value for P_{abs} (see equation (7)).

2.5. Power losses

Losses can be described as the light incident on the workpiece which does not contribute to the welding process. These are three types of loss to be considered here:

Plasma plume absorption: Above the mouth of the keyhole a plasma plume is formed. This absorbs some of the light before it reaches the workpiece and re-radiates it in all directions. Plasma plume absorption (P_{plume}) is calculated in this model as:

$$P_{plume} = P_{out}\left(1 - \exp\left(-\alpha_{iB,plume} h_{pl}\right)\right) \tag{15}$$

where P_{out} is the total laser output power (W), $\alpha_{iB,plume}$ is the absorption coefficient due to inverse Bremsstrahlung in the plasma plume (m^{-1}), and h_{pl} is the height of the plasma plume (m).

Workpiece surface reflection: There is a proportion of the incident beam which is advance of the melting isotherm and the keyhole (see figure 5). This part of the beam can be reflected off the solid workpiece surface. The calculation for this loss (P_{wsr}) is as follows:

$$P_{wsr} = \left(P_{out} - P_{plume}\right)\alpha_{wsr} \tag{16}$$

where α_{wsr} is the fraction of the incident beam hitting the workpiece outside the keyhole.

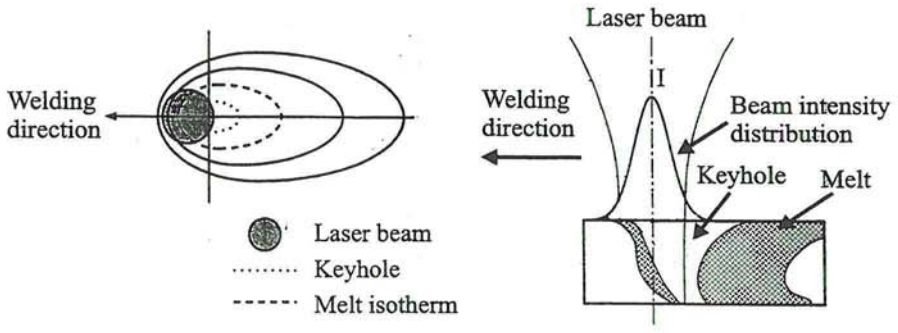

Figure 5. Schematic showing a proportion of the incident beam advance of the melting isotherm and the keyhole [3].

Keyhole reflection: A small percentage of the incident light leaves the keyhole after experiencing multiple reflections. Keyhole reflection for a blind keyhole (P_{kr}) is calculated as follows:

$$P_{kr} = P_{out} - P_{wsr} - P_{abs} \tag{17}$$

where P_{abs} is calculated from equation (7).

3. EXPERIMENTAL VERIFICATION OF THE MODEL

An evaluation of the model was achieved by comparing the theoretical results with experimentally obtained values of power absorbed by the workpiece in deep penetration laser welding [9]. The parameters used in the experiments and calculations are shown in table 1.

A water calorimeter was used to establish how much power was absorbed by the workpieces during welding. A few seconds after completion of the weld the samples were immersed in water. The temperature rise of the water was then measured in order calculate the power absorbed by the workpiece. The experimental and calculated results are shown in figure 6. Figure 7 shows the calculated power losses for different welding speeds and figure 8 shows the variation of the different absorption mechanisms in the keyhole.

Table 1. Parameters used in the experiments and calculations

Parameter	Symbol	Value	Unit
Laser power	P_{out}	1400	W
Wavelength	λ	10.6	μm
Polarisation	-	circular polarisation	
Beam quality	M^2	2.0	
Focusing optic focal length	f	270	mm
Raw beam diameter	D	18	mm
Focusing number	F	15	-
Focal radius	r_{f0}	0.2	mm
Workpiece-focus stand-off	z_0	0	mm
Welding speed	v	0.1 - 4.0	m/min
Material	-	austenitic stainless steel	-
Shielding gas	-	helium	-
Plasma plume height	h_{pl}	1.5	mm
Weld type	-	blind	-

Figure 6 shows a high level of agreement between experimentally measured energy absorption levels and those calculated by using equation (7). The slightly higher values of the calculated curve and the increasing variance between the theoretical and practical results at slower speeds can be explained as a function of the experimental method: After each weld was completed the workpiece was allowed to stand for a few seconds to bring local temperatures down below the boiling point of water before immersion in the calorimeter. During this period heat was lost from the workpiece by radiation and convection. At lower speeds the weld bead would also be losing heat by the same mechanisms whilst the weld was being completed.

Figure 7 demonstrates that, although the importance of the individual energy loss mechanisms changes with increasing welding speed, the combination of them grows gradually from 22 % to 32 % over the range of speeds covered here.

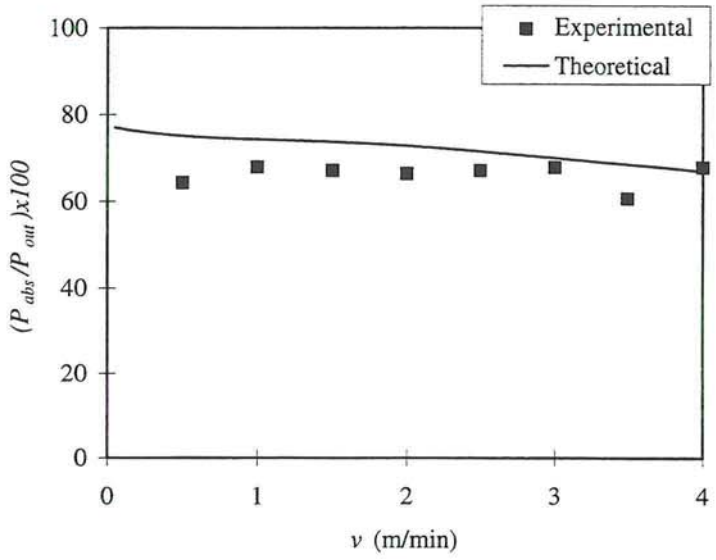

Figure 6. Theoretical values of the laser power absorbed in the keyhole compared to experimental values of the laser power absorbed by the workpiece, as a function of welding speed (see table 1 for parameters used in the calculations).

Workpiece surface reflection increases with welding speed because the lag between the front edge of the beam and the front wall of the weld pool increases. Thus more incident beam is exposed to, and reflected off the solid workpiece surface (see figure 7).

Keyhole reflection increases with welding speed because the keyhole becomes shallower and more elongated at higher speeds (see figure 9). This means that the incident beam will need to experience fewer reflections before it escapes from the keyhole and is lost to the welding process.

Plasma plume absorption is reduced with increasing welding speed because the volume and depth of the plasma above the keyhole is diminished. It has been suggested [3] there is a linear relationship between increasing welding speed and decreasing plasma plume absorption and this is borne out by this model.

Comparisons of figures 6 and 7 shows that the growth in losses over this speed range is matched by a decrease in the calculated energy absorption values.

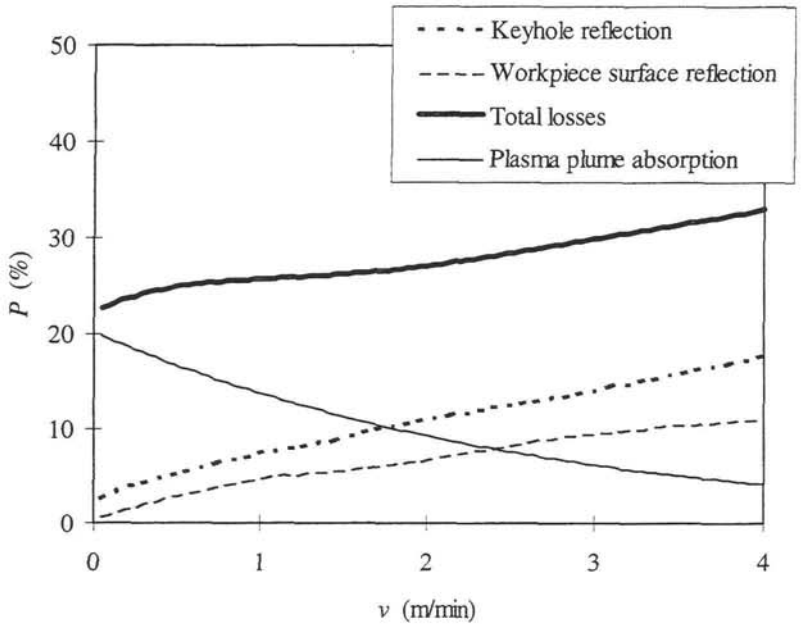

Figure 7. An example of the percentage of laser output power lost by different mechanisms as a function of welding speed (see table 1 for parameters used in the calculations).

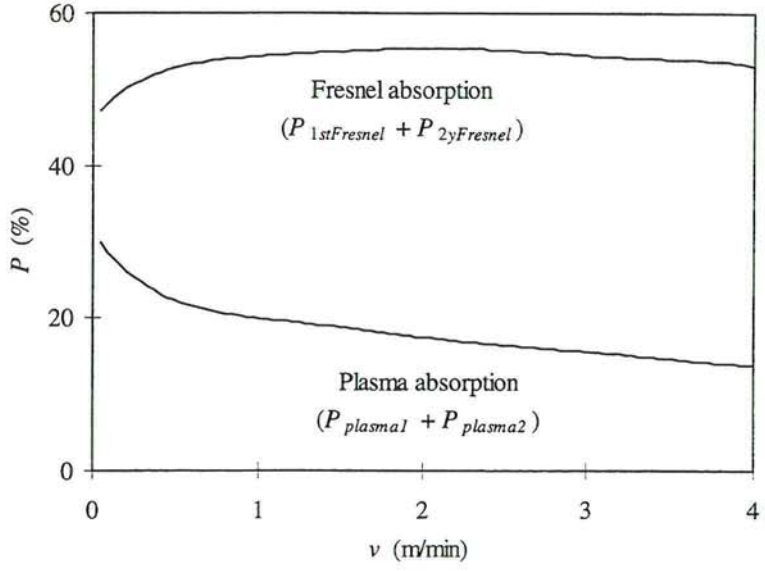

Figure 8. The percentage of laser output power absorbed in the keyhole by different absorption mechanisms as a function of welding speed (see table 1 for parameters used in the calculations).

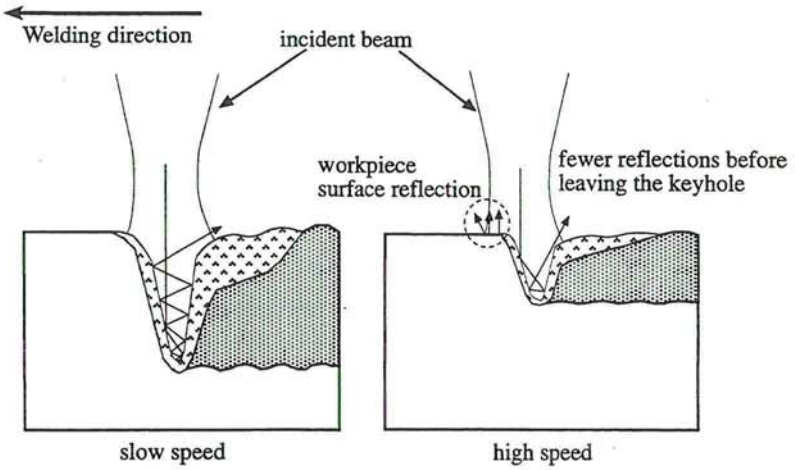

Figure 9. The change of shape of the keyhole and weld pool with increasing speed.

Figure 8 separates the calculated values for Fresnel and plasma absorption which were earlier combined in figure 6. It is clear that Fresnel absorption plays the dominant role in the process. Plasma absorption decreases as welding speed increase because the volume and density of plasma in the keyhole is reduced.

At low speeds such as those shown here the keyhole wall is inclined at a very shallow angle to the incident beam and levels of Fresnel absorption approach the maximum for the laser-material interaction (see figure 2). However at higher speeds the keyhole front wall would become progressively inclined with a subsequent reduction in absorbtivity. Figure 8 demonstrates the beginning of this effect as the speed is increased above 2 m/min.

4. CONCLUSIONS

(i) Fresnel absorption at the walls of the keyhole is the dominant energy transfer mechanism in laser welding. Energy absorption by this method is optimised when the keyhole walls are close to the Brewster angle with respect to the incident beam. As speeds increase the keyhole wall will become more inclined and absorption will be reduced.

(ii) Plasma absorption plays a more minor role which diminishes in importance as welding speeds are increased.

(iii) An increasing amount of incident power is lost to the welding process as speeds are increased. Although plasma plume absorption decreases with speed this is more than compensated for by increases in workpiece surface and keyhole reflection effects.

5. ACKNOWLEDGEMENTS

The funding for this work was provided by the Institute for Computer Integrated Manufacturing (CIM) at Luleå University of Technology and by the Austrian Science Foundation (FWF) Grant No. P11384. The authors are indebted to Professor D Schuöcker for enabling the work.

6. REFERENCES

1. Kaplan, A. (1994) A model of deep penetration laser welding based on calculation of the keyhole profile. Journal of Physics D: Applied Physics (27) pp. 1805-1814.
2. Kaplan, A. (1994) Modellrechnung und numerische Simulation von Absorption, Wärmeleitung und Strömung des Laser-Tiefschweißens Dissertation der Technischen Universität Wien, Austria. 1994
3. Beyer E. Schweißen mit Laser (1995) (Berlin: Springer).
4. Lampa. C., Kaplan, A.F.H., Powell, J. and Magnusson C. (1997) An analytical model of laser welding. Journal of Physics D: Applied Physics (30) pp. 1293-1299.
5. Hügel, H. and Dausinger, F. (1993) Interaction phenomena and energy coupling in laser treatment processes. Module 1: Fundamentals and sources, Euro Laser Academy October 1993, Aachen Germany.
6. Luxon, J.T. and Parker, D.E. (1992) Industrial Lasers and Their Applications 2^{nd} edition (New Jersey: Prentice-Hall).
7. Steen, W.M. (1991) Laser Material Processing (Berlin: Springer).
8. Beck M, Kern M, Berger P and Hügel H. (1996) Einfluß der Plasmawolke auf Einkopplung und Prozeßstabilität beim Lasertiefschweißen mit CO_2-Lasern. Laser und Optoelektronik (28) pp. 72-78.
9. Lampa C, Powell J, Ivarson A and Magnusson C. (1995) Factors affecting the efficiency of laser welding. Lasers in Engineering (4) pp. 73-83.

LULEÅ TEKNISKA UNIVERSITET

NR	1997:33
ISSN	1402-1544
ISRN	LTU-DT--97/33--SE

Institution/Department

Material- och Produktionsteknik

Avdelning/Division

Bearbetningsteknik

Upplaga/Number of copies

300

Datum/Date

97-11-03

Titel/Title

Laser Welding; Energy Redistribution and Weld Geometry

Författare/Author(s)

Conny Lampa

Uppdragsgivare/Commissioned by

Typ/Type

(x) Doktorsavhandling/PhD thesis
() Licentiatuppsats/Licentiate thesis
() Forskningsrapport/Research report
() Teknisk rapport/Technical report
() Examensarbete/Final project report
() Övrig rapport/Other report

Språk/Language

() Svenska/Swedish (x) Engelska/English ()

Sammanfattning, högst 150 ord/Abstract, max 150 words

This work aims to contribute to the understanding of deep penetration laser welding with emphasis on the weld shape and how it is created. The papers which make up the thesis investigate various aspects of the absorption and redistribution of energy during laser welding. Theoretical and experimental methods have been used to analyse the effects of process parameters on the geometry of the resultant welds. Considerable success has been achieved in matching theoretical predictions to actual results. This work has helped to clarify a number of features of the laser welding process including the following;

1. The effect of process parameters on the efficiency of laser welding.
2. The mechanisms of energy absorption in the keyhole which result in a weld.
3. The effect of an increased external pressure on the laser-material interaction.
4. The effect of thermocapillary flow and how it can be taken advantage of in industrial applications.

Nyckelord, högst 8/Keywords, max 8

laser, welding, efficiency, hyperbaric, point-source, line-source, steel, copper.

Underskrift av granskare/handledare / Signature of examinator/supervisor

Claes Magnusson

Claes Magnusson

Universitetstryckeriet, Luleå